Open access • Report • DOI:10.2172/1018470

Hydrocarbon characterization experiments in fully turbulent fires : results and data analysis. — Source link

Jill Marie Suo-Anttila, Thomas K. Blanchat

Published on: 01 Mar 2011

Topics: Liquid fuel

SANDIA REPORT
SAND2010-6377
Unlimited Release
Printed March 2011

Hydrocarbon Characterization Experiments in Fully Turbulent Fires – Results and Data Analysis

Thomas K. Blanchat and Jill Suo-Anttila

Prepared by
Sandia National Laboratories
Albuquerque, New Mexico 87185 and Livermore, California 94550

Sandia National Laboratories is a multi-program laboratory managed and operated by Sandia Corporation, a wholly owned subsidiary of Lockheed Martin Corporation, for the U.S. Department of Energy's National Nuclear Security Administration under contract DE-AC04-94AL85000

Issued by Sandia National Laboratories, operated for the United States Department of Energy by Sandia Corporation.

Available to DOE and DOE contractors from
U.S. Department of Energy
Office of Scientific and Technical Information
P.O. Box 62
Oak Ridge, TN 37831

Telephone: (865) 576-8401
Facsimile: (865) 576-5728
E-Mail: reports@adonis.osti.gov
Online ordering: http://www.osti.gov/bridge

Available to the public from
U.S. Department of Commerce
National Technical Information Service
5285 Port Royal Rd.
Springfield, VA 22161

Telephone: (800) 553-6847
Facsimile: (703) 605-6900
E-Mail: orders@ntis.fedworld.gov
Online order: http://www.ntis.gov/help/ordermethods.asp?loc=7-4-0#online

SAND2010-6377
Unlimited Release
Printed March 2011

Hydrocarbon Characterization Experiments in Fully Turbulent Fires – Results and Data Analysis

Thomas K. Blanchat and Jill Suo-Anttila
Fire and Aerosol Sciences Department
Sandia National Laboratories
PO Box 5800
Albuquerque, NM 87185

Abstract

As the capabilities of numerical simulations increase, decision makers are increasingly relying upon simulations rather than experiments to assess risks across a wide variety of accident scenarios including fires. There are still, however, many aspects of fires that are either not well understood or are difficult to treat from first principles due to the computational expense. For a simulation to be truly predictive and to provide decision makers with information which can be reliably used for risk assessment the remaining physical processes must be studied and suitable models developed for the effects of the physics. The model for the fuel evaporation rate in a liquid fuel pool fire is significant because in well-ventilated fires the evaporation rate largely controls the total heat release rate from the fire.

This report describes a set of fuel regression rates experiments to provide data for the development and validation of models. The experiments were performed with fires in the fully turbulent scale range (> 1 m diameter) and with a number of hydrocarbon fuels ranging from lightly sooting to heavily sooting. The importance of spectral absorption in the liquid fuels and the vapor dome above the pool was investigated and the total heat flux to the pool surface was measured. The importance of convection within the liquid fuel was assessed by restricting large scale liquid motion in some tests. These data sets provide a sound, experimentally proven basis for assessing how much of the liquid fuel needs to be modeled to enable a predictive simulation of a fuel fire given the couplings between evaporation of fuel from the pool and the heat release from the fire which drives the evaporation.

CONTENTS

FIGURES

TABLES

NOMENCLATURE

ASC	Advanced Strategic Computing
CARS	coherent anti-Stokes Raman scattering
CGA	Combustion Gas Analyzer
CRADA	Cooperative Research and Development Agreement
DAQ	Data Acquisition
DAS	Data Acquisition System
DP	Differential Pressure
FLAME	Fire Laboratory for Accreditation of Models and Experiments
FRH	FLAME/Radiant Heat
HP	Hewlett Packard
ID	Inner Diameter
M&S	Modeling and Simulation
MIMS	Mineral-Insulated Metal-Sheathed
MUX	Multiplexer Units
NI	National Instrument
NIST	National Institute of Standards and Technology
OD	Outer Diameter
PIRT	Phenomena Identification and Ranking Table
RSS	Root-Sum-Square
SNL	Sandia National Laboratories
SS	Steady State
TC	Thermocouple
TTC	Thermal Test Complex
UPS	Uninterruptible Power Supply
V&V	Verification and Validation
WSEATC	Weapons Systems Engineering Assessment Technology Campaign
WSECC	Weapons Systems Engineering Certification Campaign

ACKNOWLEDGEMENTS

The author acknowledges and thanks the following individuals; Allen Ricks for working on the test plan and supervising many of the experiments and Jill Suo-Anttila who supervised all aspects of the spectral data collection and performed the extensive post-test spectral analyses.

As always, these experiments could not have been performed without the support of the extremely capable technologists in the Fire and Aerosol Sciences Department and the TMSS support group who assembled the hardware and ran the tests. Especially notable are Dann Jernigan (the TTC manager) who led the setup and conducted every experiment with help from Martin Sanchez and Ciro Ramirez. In addition, Ciro Ramirez developed the macros to analyze the extensive video datasets (162,000 images!). The work reported here could not have been done without them.

This work was part of a Cooperative Research and Development Agreement (CRADA) between Sandia Corporation (the operator of Sandia National Laboratories) and Factory Mutual Insurance Company (FM Global). The author is grateful for the insight and guidance provided by Ben Ditch and John de Ris, the key participants from FM Global.

Lastly, I want to thank those who performed the peer-review of this report, Dr. Walter Gill and Dr. Anay Luketa.

Financial support for this project was provided by the Weapon System Engineering Assessment Technology (WSEAT) Campaign 6 and the Engineering Sciences Research Foundation (ESRF). The authors appreciate management's continued support for diagnostics development and validation quality data sets. Finally, we note that Engineering Sciences has a clear commitment to science in support of our weapons programs and is committed to supporting the research community through publication of its data sets where appropriate.

1. INTRODUCTION

Fuel evaporation rates from large liquid pool fires have been studied for several decades (see Hottel [1959], Babrauskas [1983], Koseki [1989], Koseki and Mulholland [1991], Koseki and Iwata [2000], Chatris et al. [2001], and Muñoz et al. [2004]). Fuel regression rates show a dependence upon fire diameter, fuel type, and ambient conditions including temperature and wind speed. Babrauskas [1983] presented a review of experimental data for large hydrocarbon fires and discussed the effects of pan diameter, pan lip height, and wind speed. Typical scatter in experimental data reported in the review of Babrauskas [1983] for mean, steady-state fuel regression rates for a given fuel under quiescent conditions appears to be approximately ±10% of the measurement.

Among the studies of fuel regression in smaller-scale fires the work of Hamins et al. [1994] is notable because the fuel regression rates were correlated with heat fluxes to the pool. Hamins measured the liquid reflectivity, heat fluxes, and burning rates in concentric rings within a 30 cm fire fueled by methanol, heptane, toluene, or methyl methacrylate. Both the total and the radiative heat fluxes to the pool were studied as a function of both angle and radial location in the pool. The radiation data were not spectrally resolved, and the importance of convection within the pool was not studied.

Fuel regression rate models have recently been incorporated in numerical simulations (see Novozhilov and Koseki [2004], and Prasad et al. [1999]). These modeling efforts have primarily been directed towards relatively small fires (< 1 m diameter) which are not in the fully turbulent regime. Since fire size and intensity are largely controlled by the fuel evaporation rate, improvement in the modeling of fuel evaporation rates in large, fully turbulent fires is a topic of considerable practical interest.

An assessment of the current state of knowledge about physical processes important to predictions of fuel regression rates in pool fires has recently been conducted by Brown et al. [2006]. Several of the physical processes shown in Figure 1 and discussed by Brown et al. were studied in the present work, including convection within the pool and absorptivity in the liquid fuel and fuel vapor. Of these phenomena, the absorptivity in the fuel vapor in a fire stands out because it is believed that the fuel regression rates are strongly dependent upon the radiant heat flux incident on the surface of the pool, and that heat flux is controlled not only by the emission within the fire but also the absorption above the surface of the pool.

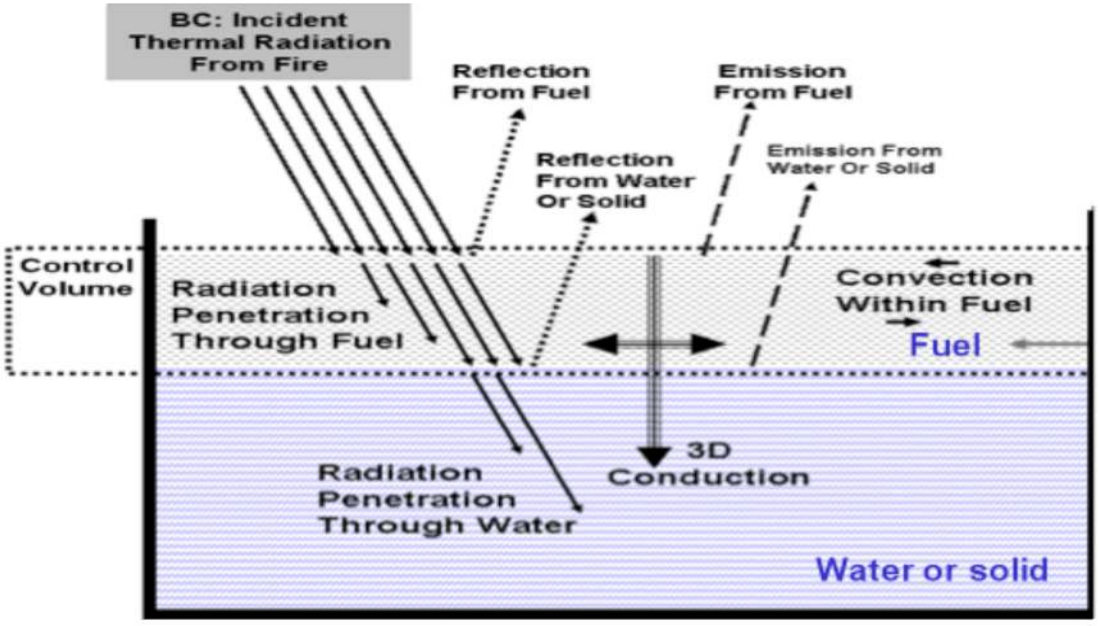

Figure 1 Physical processes important to predictions of fuel regression rates in pool fires.

1.1 Experiment Objective

The objectives of the experiments were to:

1. Measure the spectral reflectivity at the fuel-air interface and the spectral transmissivity in liquid fuels over depths of order millimeters for a range of liquid fuels, including easily simulated, well characterized mixtures of simple fuels as well as fuels in practical use such as JP-8
2. Measure the fuel regression rates for a variety of liquid hydrocarbon fuels in a quiescent environment
3. Measure the spectral absorption coefficients of the fuel/product mixture in the vapor dome above the pool surface
4. Measure the total heat flux (convection and incident radiation) integrated across the surface of the pool to investigate the connection between the integral heat flux and the fuel regression rate
5. Determine the importance of large scale convective transport within the liquid fuel to the fuel regression rate

A brief overview describing how these objectives is presented in the following paragraphs. The measurement techniques and instrumentation used are discussed in greater detail in the measurement section.

The first objective was achieved by testing liquid fuels at room temperature in a laboratory environment. Infrared radiation from a blackbody source at a temperature similar to the effective radiation temperature in a fire [Kearney, 2001] was transmitted through a small amount of liquid fuel and the spectral transmission of the radiation was measured. Infrared spectral transmissivity information is available for a considerable number of compounds (for example, approximately

10,500 spectra are included in Pouchert [1985], and some 50,500 infrared spectra are available online from the National Institute of Advanced Industrial Sciences and Technology (Japan) at http://www.aist.go.jp/RIODB/SDBS/cgi-bin/cre_index.cgi). The thicknesses of the fluid layers are not always reported, however, and the majority of the available data neglects wavelengths smaller than 2.5 micron. Kearney [2001] found that emission from a large JP-8 fire approximated that of a gray body at about 1420 K, for which about 40% of the radiant energy is emitted at wavelengths shorter than 2.5 microns. Laboratory tests were performed to measure the transmissivity of each of the liquid fuels used in this test series in the wavelength range of 1.3 to 4.8 microns, corresponding to the majority of the expected emitted radiation from the fire. The reflectivity of the liquid-air interface was measured in six wavelength bands in the infrared range.

The second objective was achieved by monitoring the rate of change of fuel mass with time for fires burning a number of different hydrocarbon fuel mixtures. A constant level system was used to reduce transient effects due to the fuel level changing over the course of the test.

The third objective was achieved by measuring the spectral radiation intensity from a fire over a very narrow view angle (0.25 degrees). A spectrometer was used to look upward through a pipe which passed through the fuel pan. The spectrometer and pipe were mounted below the pan on a positioning system that moved up and down to investigate the spectral absorption at various heights above the surface of the pool.

The total heat flux at the surface of the fuel was measured by heat flux gauges. The sensing surface of the gauges extended a few millimeters above the surface of the pool. The surface-integrated heat flux to the pool was obtained by integrating the measured heat fluxes across the pool surface. This total, integrated heat flux is believed to be the single most important factor in determining the fuel regression rate.

To meet the final objective small crushed glass pebbles (also called beads or rocks) were placed within the liquid during some tests to restrict large scale liquid motion within the pool and determine the effect of convection on the fuel regression rate.

Uncertainty Analysis

An uncertainty analysis for all measurements was performed. The methodology follows Coleman and Steele [1999]. Bias errors which can be mathematically modeled, such as the bias error in thermocouple measurements in the fire, are algebraically added to the measurement and the uncertainty in the estimation of the bias is treated as a random error [Romero et al., 2005].

2. FACILITY, INSTRUMENTATION, AND PLANNED MEASUREMENTS

2.1 FRH Facility Description

The fuel regression rate experiments with liquid hydrocarbon fuels were performed in the FLAME/Radiant Heat (FRH) test cell in the Thermal Test Complex (TTC) at Sandia National Laboratories (SNL). The main test chamber of the FRH cell is cylindrical in shape, 60 ft (18 m) inner diameter with a height around the perimeter of 40 ft (12 m). The ceiling slopes upwards (~18º) from the perimeter walls to a height of 48 ft (15 m) over the center of the facility. A round hole at the top of the facility 16 ft (4.9 m) diameter transitions to a 10 ft by 12 ft (3.0 m by 3.7 m) chimney duct (see Figure 2). The outer walls are made of steel channel sections and are filled with water that acts as a thermal sink during tests.

The ground level of FRH can be divided into three concentric sections. At the center of the facility is a fuel pan or gas burner. The facility can operate a gas burner (He, H_2, CH_4, etc.) or a liquid fuel pool (JP-8, methanol, etc.) up to 3 m in diameter. This test series utilized a 2 m fuel pan. The second section is a steel spill plate, which extends to a diameter of 40 ft (12.2 m). The floor of the outer section is made of a steel grating, through which air is supplied to the FRH chamber during fire experiments. FRH is designed for flexibility in fuel types and a number of different fuels were used to evaluate spectral radiation fluxes to the fuel surface and regression rates for fuels of varying sooting propensities.

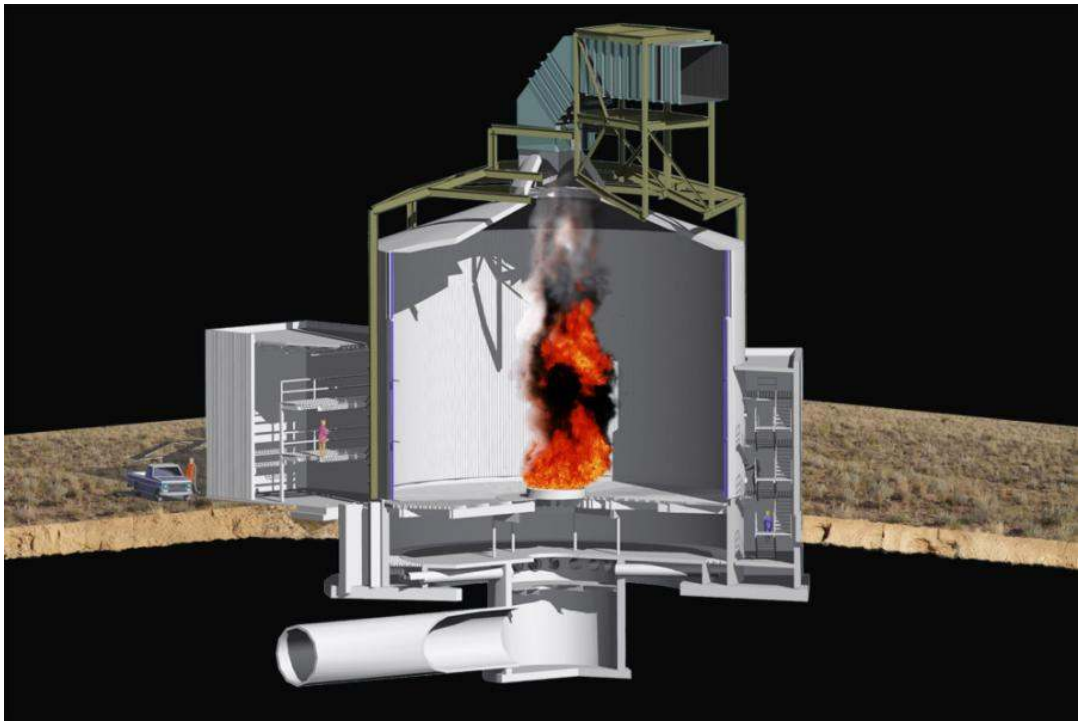

Figure 2 A cutaway view of the FRH facility.

(showing a pool fire at the ground level, pipes supplying air flow through the basement, the chimney, and instrumentation rooms outside the FRH chamber)

The air flow in the FRH chamber combines contributions due to the buoyancy-controlled fire and due to the forced flow of air through the facility. The air flow in the absence of a fire has been characterized experimentally at the air ring in the basement and at the ground level [Ricks, 2006]. The air ring flow field was found to exhibit a pattern (left side of Figure 3) attributable to the 18 supply pipes carrying the air from the diffuser in the center of the facility to the air ring along the outer edges of the facility (refer to Figure 2). The air flow at the ground level was found to be highest in the outer portion of the FRH cell, and exhibited a large recirculation zone in the inner portion of the facility, where mean velocities were in the negative (downward) direction (right side of Figure 3). The presence of a fire at the center of the facility is likely to reduce the recirculation because the air flow will be drawn inwards and entrained into the buoyant fire plume.

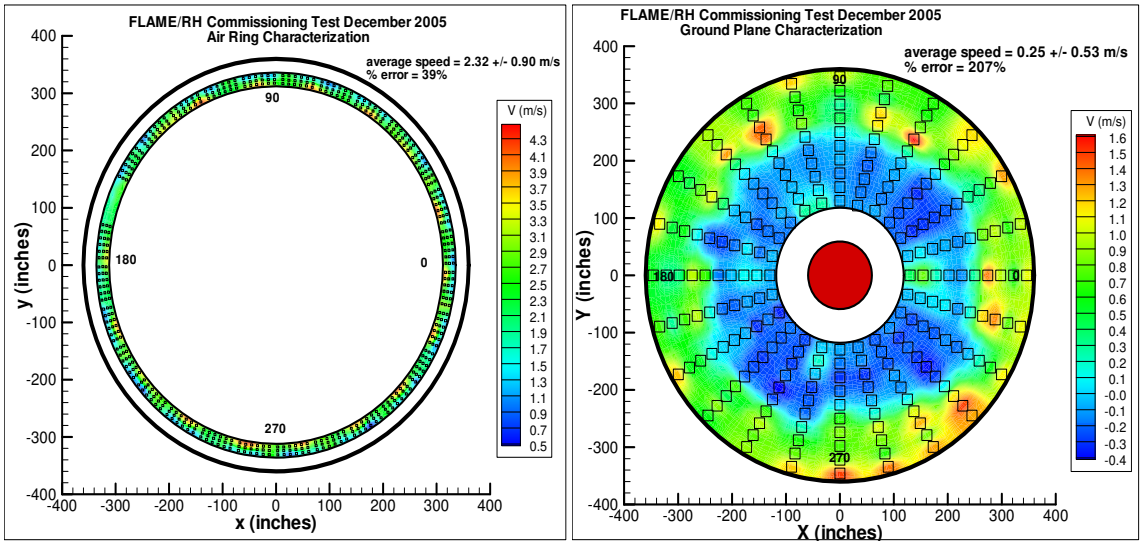

Figure 3 Measured mean velocities at the air ring in the basement of FRH (left) and at the ground level (right).

The test series discussed here were performed with a liquid level control system to maintain a constant level of liquid fuel in the pan. Changes in the fuel level have been shown by Orloff and de Ris (1982) to influence the shape and burning characteristics of a fire, which they attributed to tripped turbulence at the lip of the pan. Maintaining a constant level is also important to prevent changes in radiation or convection interactions with the crushed glass in the fuel pan as the fuel level drops.

The convective transport of energy in the liquid fuel was tested by restricting the large scale motion of the fluid in some tests by introducing a bed of crushed glass in the liquid layer (refer to Figure 8). The crushed glass (opaque black irregularly-shaped pieces from 3 mm to 7 mm in size, Bourget Bros. Building Materials, Santa Monica, CA) rested on a stainless steel screen (12-18 threads per inch) on top of the perforated stainless steel baffle plate in the pool. The depth of the pan was ~¾ inch (19 mm) from the baffle plate to the surface of the pool, and the bed of crushed glass began approximately 3 mm below the surface. The magnitude of the differences in fuel evaporation rate between experiments with and without the crushed glass bed provided a simple means of assessing the importance of convection within the liquid fuel. The fuel pan layout and dimensions are shown in Figures 4 and 5.

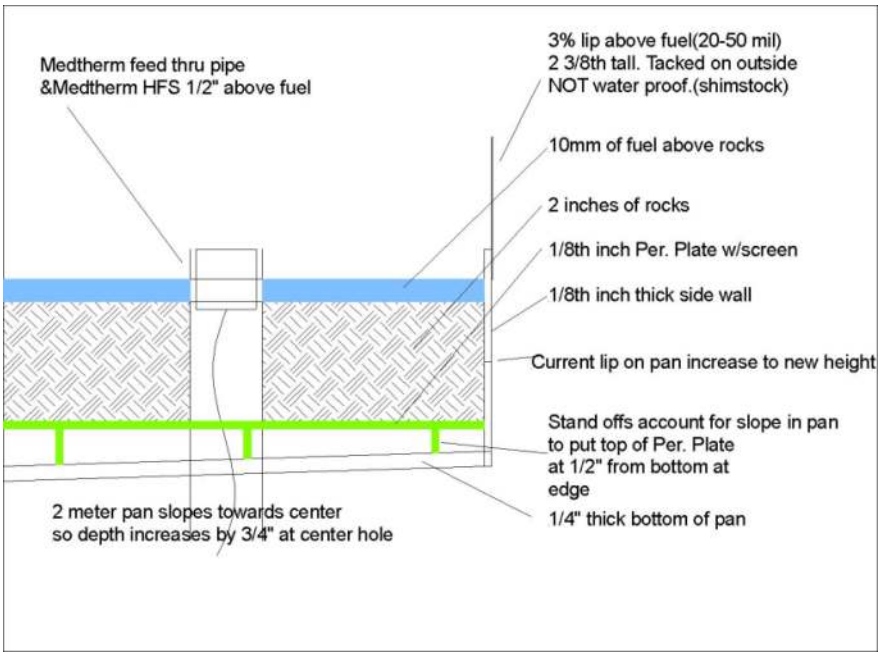

Figure 4 Fuel pan (2 m diameter) layout.

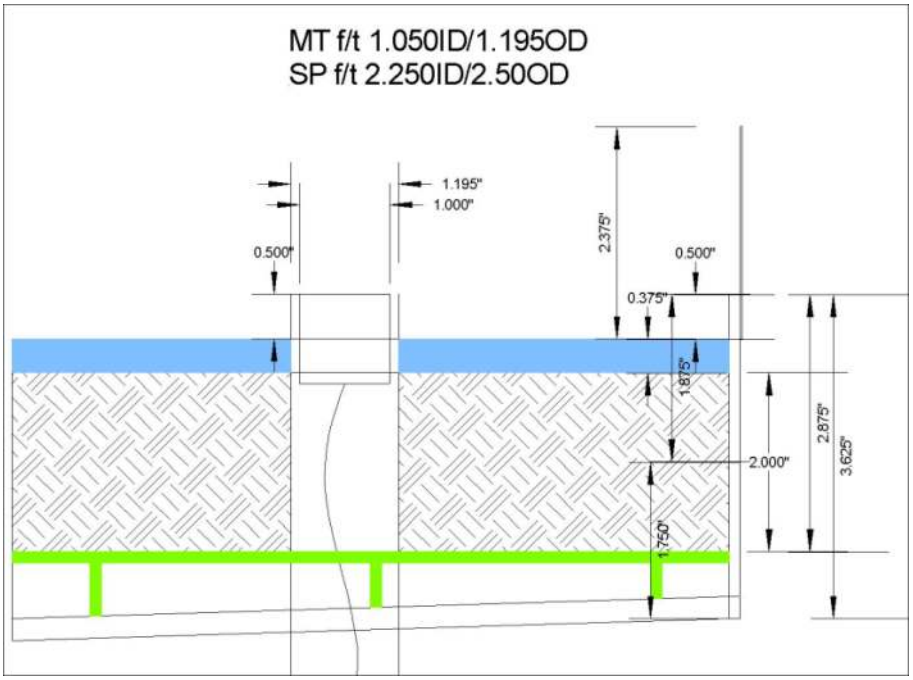

Figure 5 Fuel pan dimensions.

The liquid level control system is shown in Figure 6. Fuel was supplied to the pan from a standard 55 gallon drum located outside the FRH test chamber. The drum sat on a scale (Doran Model XL9000 with a customized 24 in. by 24 in. (61 cm by 61 cm) base to fit inside a spill pallet, manufactured by Doran Scales, Batavia IL). A positive displacement Alsco drum pump (model 2998 with 53 gpm (200 lpm) rated flow) drew fuel continuously out of the supply tank at

a rate that was greater than the burning rate. The fuel that was not needed to maintain a constant amount of fuel in the pan was returned to the supply tank.

The amount of fuel in the pan is inferred from differential pressure measurements made by a Rosemount Model 3051 differential pressure gauge and monitored by a Red Lion programmable controller. When the differential pressure measurement fell below the lower setpoint the controller opened a control valve (ASCO EF8210B054 1 inch solenoid valve) allowing fuel to be fed to the pan through a ¾ in. (inner diameter) fuel rated hose. When the differential pressure reading reached the upper setpoint the controller closed the control valve and the entire flow of fuel drawn out by the pump was simply returned to the supply tank. A second, identical Rosemount 3051 differential pressure gauge was used for data acquisition purposes as it was not affected by minor fluctuation seen by the DP gauge attached to controller.

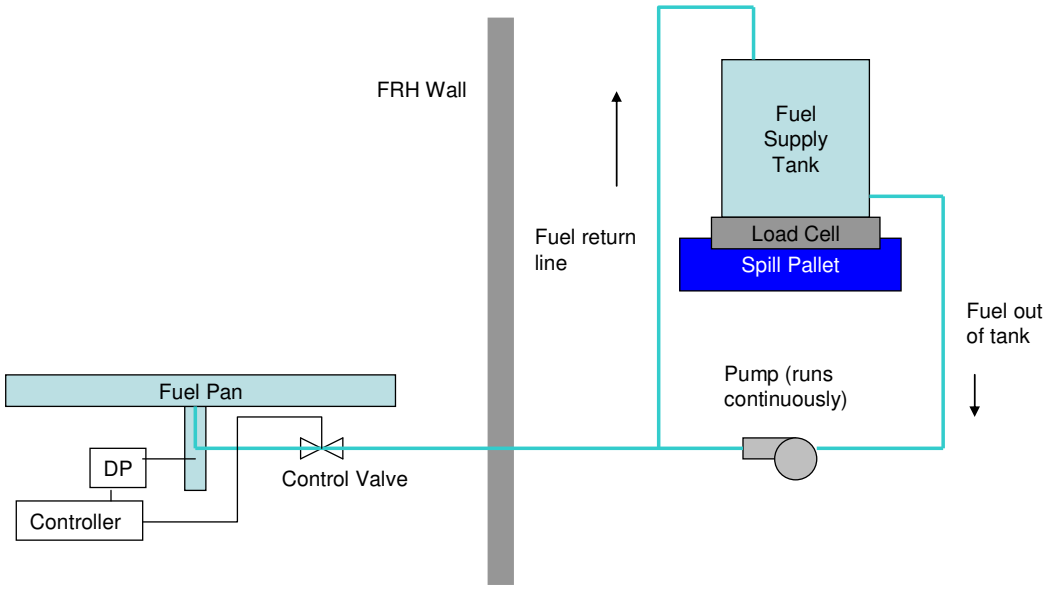

Figure 6 Schematic of the liquid level control system.

To minimize the disturbances to the differential pressure readings caused by the inflow of fuel into the pan, the differential pressure gauges were mounted on the neck of the drain pipe beneath the fuel pan. The fuel was fed up through the neck and then through about 20 ft of perforated tubing to distribute the fuel inflow around the pan (not illustrated).

The liquid level and the temperature distribution across the depth of the pan in the fuel pan were monitored through the use of a thermocouple rake. Thirty (30) thermocouples (type-K, mineral-insulated, metal-sheathed (inconel), 0.040 inch diameter) were mounted on a steel rake with yield positions in the fuel pan as indicated in Figure 7. Note the majority of the spacing was 1 mm, to allow fine control of the fuel level. Figure 7 show that with those tests that used the glass beads (also referred to as rocks) the fuel would start to cover the rocks at the height of TC6 and would completely cover the rocks at TC12 (no tips of the rocks protruding out of the liquid). Figure 7 also shows the position of the faces of the twelve (12) total heat flux gauges (thermopiles) mounted to the fuel pan (between TC26 and TC27).

For each test, the fuel DP controller was set based on the estimated fuel regression rate. After fuel ignition, slight adjustments to the controller setpoint were performed to set the fuel level to the desired level. The liquid level was easily determined by plotting the temperatures from the thermocouple rake; with a temperature gradient for the fuel in the subcooled regime, at the boiling point (the fuel surface), and superheated fuel in the vapor dome above the liquid surface.

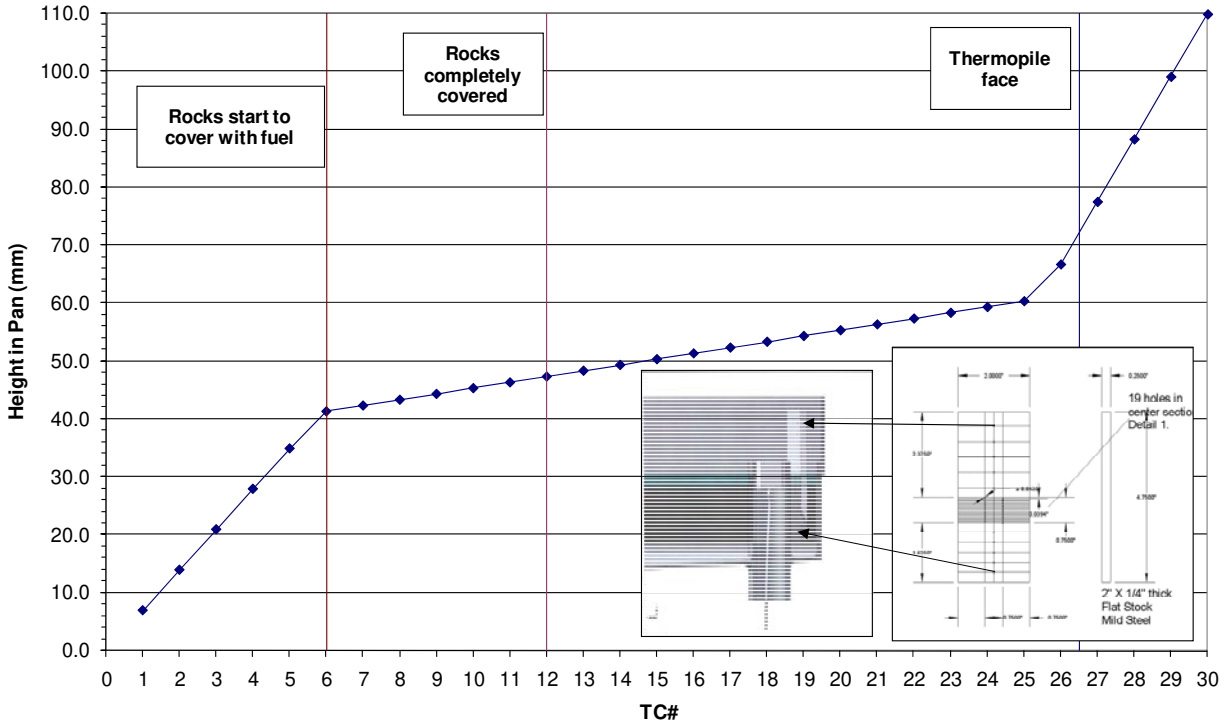

Figure 7 Thermocouple positions in fuel pan.

Figures 8-10 present photographs of the fuel pan configured for as test using glass beads.

Figure 8 Fuel pan configured with glass rocks.

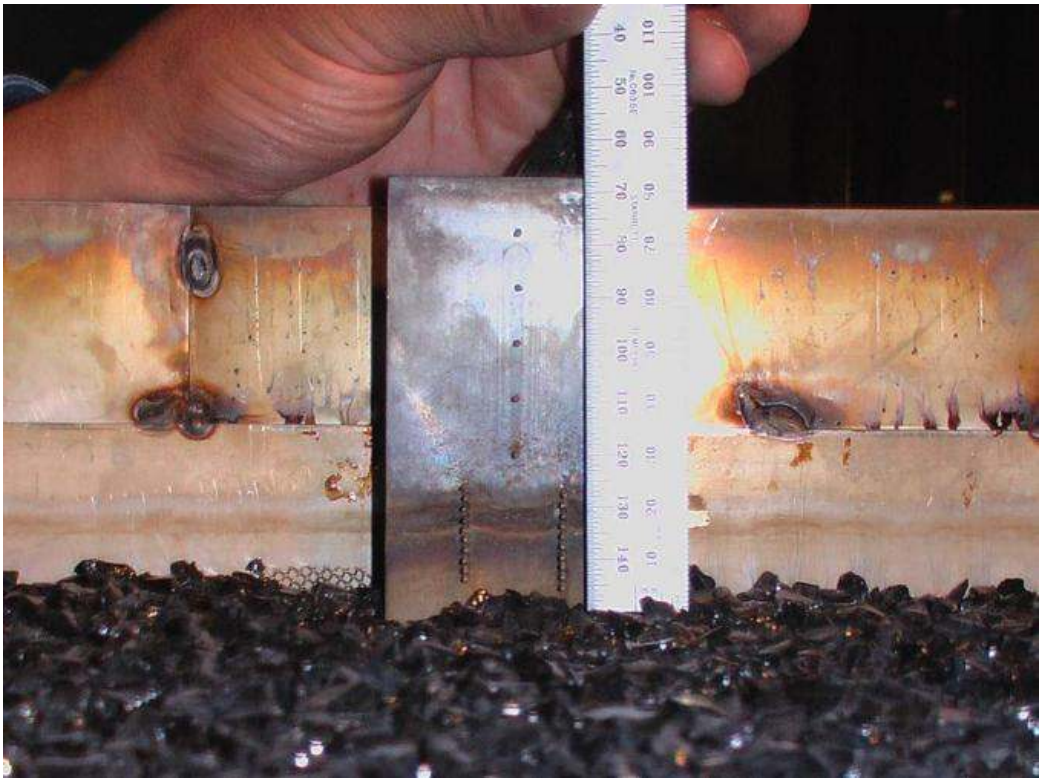

Figure 9 Fuel pan thermocouple rake.

Figure 10 Spectrometer feed through, Medtherm feed through, and TC rake (front to back) in fuel pan.

3. DESIGN OF EXPERIMENTS

A summary of the test matrix describing the boundary conditions and some of the test results is given in Table 1. Table 2 presents a summary of the compiled results, with details of the methodology for analyses given in Sections 4 and 5.

A number of fuels and fuel mixtures have been selected for study in this test series. The assistance of John de Ris and Patricia Beaulieu in selecting the fuel mixtures is gratefully acknowledged (Beaulieu [2005]). All fuel mixtures were tested for their transmittance and reflectance in the laboratory prior to the fire experiments.

For the most part, fuels were selected to cover much of the parameter space for heat of gasification and sooting propensity. The sooting propensity is potentially an important parameter because soot is the primary source (and sink) of radiation in typical hydrocarbon fires. The heat of gasification is a potentially important parameter because it controls the energy that must be absorbed to vaporize the liquid fuel. Tests were also performed for the study of convection effects by placing glass beads within the liquid pool to restrict large scale motion. One fuel in particular, JP8, was chosen due to its role in testing weapon system safety in transportation accidents.

Figure 11 compares the parameter space of heat of gasification and smoke point for the seven fuels comprising the test matrix. All tests were performed in a 2 m diameter fuel pool. Table 3 presents properties of the fuels. Mixture rules (based on mole%) were used to estimate mixture properties.

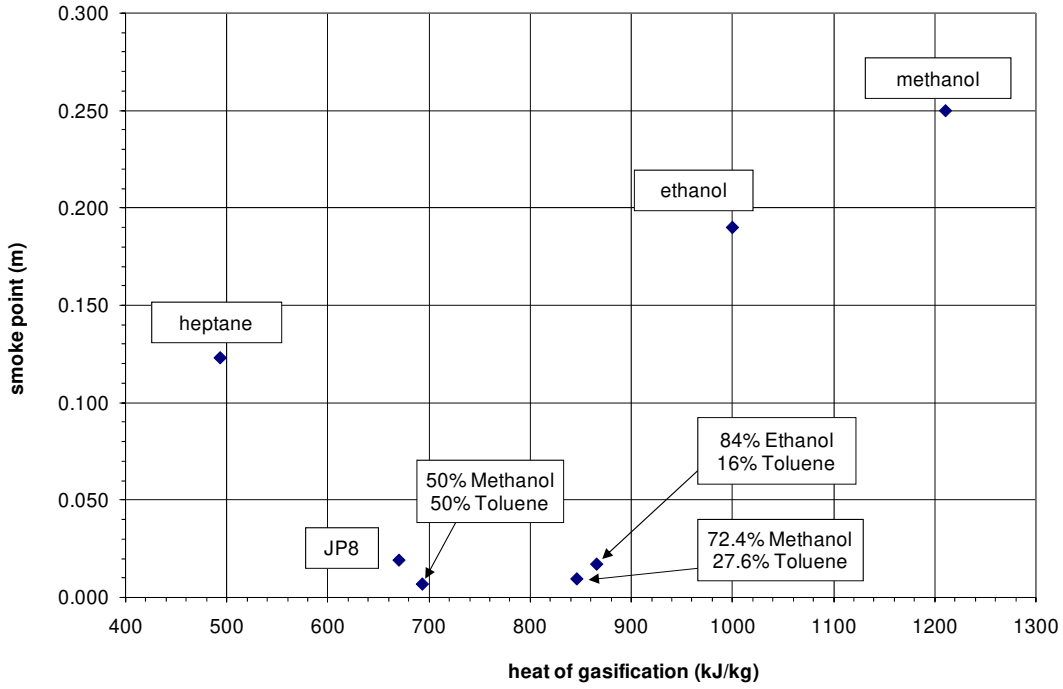

Figure 11 Test parameter space: heat of gasification vs. smoke point.

Table 1 Test Matrix and Data Overview for Fuel Regression Rate Tests

SNL Hydrocarbon Fuel Fire Characterization - TEST DATA OVERVIEW															
Date	Test	Glass Beads	Fuel:	P_{atm} (ABQ at t_0)	T_{atm} (inlet air at t_0)	T_{fuel} (TC1-10 ave at t_0)	T_{wall} (ave at t_0)	ABQ RH (at t_0)	Valid Data Range	Pan HFG (ave)	Wall HFG (ave)	Burn Rate Load Cell (m_b)	Fuel TC (liquid to vapor)	Fan Flow	Soot
-	#	-	-	in. HG	C	C	C	%	min - min	kW/m^2	kW/m^2	g/s	-	scfm	g/s
8/3/2007	SNL **001**	No	100%Methanol	24.72	26	26	26	58	20-35	40.1	0.29	60.5	21-22	57000	-
8/3/2007	SNL **002**	No	100%Methanol	24.58	30	31	27	33	20-35	40.9	0.30	63.0	16-17	57000	-
8/15/2007	SNL **003**	No	100%Methanol	24.52	33	29	29	19	16-40	41.3	0.34	66.4	16-17	57000	-
8/16/2007	SNL **004**	No	100%Methanol	24.56	29	31	29	33	16-41	39.6	0.32	62.3	15-16	57548	-
8/19/2007	SNL **005**	Yes	100%Methanol	24.64	28	29	28	28	36.5-40.5	40.7	0.32	62.6	13-14	57274	-
8/19/2007	SNL **006**	Yes	100%Methanol	24.58	33	34	30	20	20-38	40.6	0.34	62.9	17-18	57631	-
8/20/2007	SNL **007**	Yes	100%Methanol	24.66	27	29	29	35	20-38	40.5	0.31	62.1	18-19	57428	-
8/20/2007	SNL **008**	Yes	100%Ethanol	24.55	34	36	30	18	15-30	43.4	0.66	82.9	18-19	57427	-
8/21/2007	SNL **009**	Yes	100%Ethanol	24.52	34	35	29	9	15-28	45.9	0.71	85.4	12-13	57536	-
8/22/2007	SNL **010**	Yes	100%Ethanol	24.58	30	31	29	31	15-27	44.7	0.66	83.1	10-11	57409	0.5
8/26/2007	SNL **011**	Yes	100%Heptane	24.60	29	33	28	45	10-15.5	29.7	3.42	193.5	10-11	57333	3.7
8/28/2007	SNL **012**	Yes	100%Heptane	24.65	28	32	28	37	8-12	31.6	3.65	201.0	10-11	57322	3.6
8/28/2007	SNL **013**	Yes	84%Ethanol 16%Toluene	24.56	32	35	29	23	10-16	53.2	1.86	146.0	9-10	57415	2.4
8/29/2007	SNL **014**	Yes	84%Ethanol 16%Toluene	24.71	25	33	28	39	10-16	53.4	1.78	146.4	10-11	57373	2.0
8/29/2007	SNL **015**	Yes	72.4%Methanol 27.6%Toluene	24.63	31	34	30	28	10-16	57.9	1.61	144.6	9-10	57518	1.7
8/30/2007	SNL **016**	Yes	72.4%Methanol 27.6%Toluene	24.89	21	26	27	71	10-16	59.5	1.62	148.6	10-11	57453	0.9
8/30/2007	SNL **017**	Yes	50%Methanol 50%Toluene	24.83	25	31	28	46	10-16	59.0	2.25	166.8	10-11	57377	2.9
8/30/2007	SNL **018**	Yes	50%Methanol 50%Toluene	24.75	28	36	28	39	10-16	55.4	2.36	168.1	10-11	57250	2.6
8/31/2007	SNL **019**	Yes	JP8	24.67	29	36	29	40	18-24	44.1	2.56	127.0	15-16	57326	9.1
9/1/2007	SNL **020**	Yes	JP8	24.74	27	32	27	46	18-24	41.0	2.31	116.3	10-11	57634	-
9/1/2007	SNL **021**	Yes	JP8	24.64	26	40	28	37	18-24	41.4	2.31	118.3	10-11	57263	8.6
9/3/2007	SNL **022**	No	JP8	24.78	24	31	26	37	18-24	44.7	2.25	112.1	11-12	57639	11.4
9/3/2007	SNL **023**	No	JP8	24.69	27	39	28	25	18-24	41.6	2.42	117.4	9-10	57585	8.9
9/3/2007	SNL **024**	No	JP8	24.59	29	41	29	19	18-24	48.6	2.49	119.9	9-10	57436	6.7
9/4/2007	SNL **025**	No	100%Ethanol	24.63	26	27	28	38	15-25	40.3	0.64	80.9	10-11	57435	0.2
9/4/2007	SNL **026**	No	100%Ethanol	24.53	29	34	30	25	15-25	42.3	0.65	84.5	10-11	57367	0.3
9/5/2007	SNL **027**	No	72.4%Methanol 27.6%Toluene	24.57	24	26	27	37	10-20	58.2	1.60	144.8	10-11	57468	0.8
9/5/2007	SNL **028**	No	100%Methanol	24.45	30	31	29	27	20-35	36.6	0.33	64.7	11-12	57213	0.1
9/6/2007	SNL **029**	No	100%Heptane	24.59	23	26	28	44	15-17	29.6	3.29	181.3	11-12	58059	2.5

Table 2 Compiled Results Summary for Fuel Regression Rate Tests

SNL Hydrocarbon Fuel Fire Characterization - COMPILED RESULTS												
Date	Test	Glass Beads	Fuel:	Smoke Point	HRR-O2	HRR-CO2	$\chi_{ch} = Q_{chO2}/Q_T$	$\chi_{ch} = Q_{chCO2}/Q_T$	$\chi_r = 4\pi r^2 q''/m_b h_c$ (wall hfg)	$Q_{Total} = m_b * h_c$	Regression Rate	Ψ_{smoke} (smoke yield)
-	#		-	m	MW	MW			-	MW	g/m^2s	g/g
8/3/2007	SNL 001	No	100%Methanol	0.281	1.09	1.65	0.91	1.38	0.23	1.19	19.3	n/a
8/3/2007	SNL 002	No	100%Methanol	0.281	1.13	1.68	0.91	1.35	0.23	1.24	20.0	n/a
8/15/2007	SNL 003	No	100%Methanol	0.281	1.21	1.70	0.92	1.30	0.24	1.31	21.1	n/a
8/16/2007	SNL 004	No	100%Methanol	0.281	1.17	1.72	0.95	1.40	0.25	1.23	19.8	n/a
8/19/2007	SNL 005	Yes	100%Methanol	0.281	1.19	1.71	0.96	1.38	0.25	1.23	19.9	n/a
8/19/2007	SNL 006	Yes	100%Methanol	0.281	1.19	1.73	0.96	1.40	0.26	1.24	20.0	n/a
8/20/2007	SNL 007	Yes	100%Methanol	0.281	1.19	1.74	0.97	1.42	0.24	1.23	19.8	n/a
8/20/2007	SNL 008	Yes	100%Ethanol	0.250	2.03	2.75	0.96	1.30	0.30	2.12	26.4	n/a
8/21/2007	SNL 009	Yes	100%Ethanol	0.250	2.12	2.80	0.97	1.28	0.31	2.19	27.2	n/a
8/22/2007	SNL 010	Yes	100%Ethanol	0.250	2.09	2.66	0.98	1.25	0.30	2.13	26.4	0.006
8/26/2007	SNL 011	Yes	100%Heptane	0.120	7.55	8.72	0.86	0.99	0.37	8.78	61.6	0.019
8/28/2007	SNL 012	Yes	100%Heptane	0.120	7.75	9.05	0.85	0.99	0.38	9.12	64.0	0.018
8/28/2007	SNL 013	Yes	84%Ethanol 16%Toluene	0.095	4.00	5.00	0.92	1.14	0.41	4.37	46.5	0.016
8/29/2007	SNL 014	Yes	84%Ethanol 16%Toluene	0.095	3.94	5.08	0.90	1.16	0.39	4.38	46.6	0.014
8/29/2007	SNL 015	Yes	72.4%Methanol 27.6%Toluene	0.100	3.57	4.46	0.95	1.18	0.41	3.77	46.0	0.012
8/30/2007	SNL 016	Yes	72.4%Methanol 27.6%Toluene	0.100	3.49	4.60	0.90	1.19	0.40	3.88	47.3	0.006
8/30/2007	SNL 017	Yes	50%Methanol 50%Toluene	0.015	4.37	5.42	0.84	1.04	0.41	5.21	53.1	0.017
8/30/2007	SNL 018	Yes	50%Methanol 50%Toluene	0.015	4.56	5.53	0.87	1.05	0.43	5.25	53.5	0.015
8/31/2007	SNL 019	Yes	JP8	0.025	4.65	5.53	0.80	0.95	0.42	5.83	40.4	0.072
9/1/2007	SNL 020	Yes	JP8	0.025	4.33	5.32	0.81	1.00	0.41	5.33	37.0	n/a
9/1/2007	SNL 021	Yes	JP8	0.025	4.48	5.37	0.83	0.99	0.41	5.42	37.6	0.073
9/3/2007	SNL 022	No	JP8	0.025	4.07	5.09	0.79	0.99	0.42	5.14	35.7	0.102
9/3/2007	SNL 023	No	JP8	0.025	4.37	5.29	0.81	0.98	0.43	5.38	37.4	0.076
9/3/2007	SNL 024	No	JP8	0.025	4.31	5.22	0.78	0.95	0.43	5.50	38.2	0.056
9/4/2007	SNL 025	No	100%Ethanol	0.250	1.89	2.70	0.91	1.30	0.29	2.07	25.8	0.002
9/4/2007	SNL 026	No	100%Ethanol	0.250	1.93	2.70	0.89	1.25	0.29	2.16	26.9	0.003
9/5/2007	SNL 027	No	72.4%Methanol 27.6%Toluene	0.100	3.43	4.51	0.91	1.19	0.41	3.78	46.1	0.006
9/5/2007	SNL 028	No	100%Methanol	0.281	1.20	1.71	0.94	1.34	0.25	1.28	20.6	0.002
9/6/2007	SNL 029	No	100%Heptane	0.120	6.90	8.00	0.84	0.97	0.38	8.22	57.7	0.014

Table 3 Properties of Selected Fuels

			Literature Values for Pure Fuels						Calculated Values for Fuel Mixtures *(using mixture rules)*		
Properties	**Properties**	**Units**	**heptane**	**methyl alcohol**	**toluene**	**ethyl alcohol**	**JP8**		**50% Methanol 50% Toluene**	**72.4% Methanol 27.6% Toluene**	**84% Ethanol 16% Toluene**
Name	**Formula**	-	C_7H_{16}	CH_4O	C_7H_8	C_2H_6O	$C_{11.5}H_{22.8}$		CH_4O/C_7H_8	CH_4O/C_7H_8	C_2H_6O/C_7H_8
molecular weight	MW	-	100.2	32.1	92.1	46.1	160.8		48.6	39.7	50.4
Boiling point handbook	T_b	C	98.4	64.8	110.4	78.5	215		77	71	82
smoke point	l_s	m	0.120	0.281	0.005	0.250	0.025		0.015	0.100	0.095
heat of vaporization	hv	kJ/kg	316.0	1101.0	360.0	837.0	280.0		714	883	754
specific heat	c_p	kJ/kg K	2.20	2.37	1.67	2.43	2.01		2.00	2.16	2.30
heat of gasification	hg	kJ/kg	541	1272	520	980	922		879	1050	900
density	ρ	kg/m^3	683.7	791.4	866.9	789.3	808		831	814	803
heat of combustion	Δhc	kJ/kg	45365	19718	41630	25603	45854		31222	26080	29931
carbon monoxide component	Δhc_{CO}	kJ/kg	12800	12900	9000	12700	12200		10861	11751	12060
carbon dioxide component	Δhc_{CO2}	kJ/kg	14500	14500	12100	14500	14100		13245	13793	14085
oxygen component	Δhc_{O2}	kJ/kg	12700	13400	12900	13200	12700		13139	13253	13148
burning rate,	max m"-dot	kg/m^2 s	0.101	0.015	0.075	0.015	0.04		0.046	0.033	0.025
incompleteness of combustion	χ_{ch}	-	0.92	0.95	0.67	0.99			0.80	0.87	0.93
radiant fraction	χ_r	-	0.3	0.14	0.4	0.24	0.32		0.28	0.22	0.27
smoke yield	ψ_s	g/g	0.037	0.002	0.178	0.008	0.06		0.094	0.053	0.037

								Component	**mole%**	**mole%**	**mole%**
								Heptane	-	-	-
Pan Diameter (m)	2.00							**Toluene**	0.28	0.13	0.09
Pan Area (m^2)	3.14							**Methanol**	0.72	0.87	-
*substance in crystalline solid form; $T_b > 25^oC$								**Ethanol**	-	-	0.91
SFPE e.2 Table 3-1 (Taken from NFPA FPH e.17)								**Acetone**	-	-	-
References:								**Component**	**# mole**	**# mole**	**# mole**
Archies new SFPE tables								**Heptane**	-	-	-
SFPE ed. 2, Table 3-4.7								**Toluene**	4.7043	2.5967	1.5054
SFPE ed. 2, Table C-2								**Methanol**	12.3463	17.8775	-
Industrial Fire Protection Engineering, Table 7.4								**Ethanol**	-	-	14.3914
SFPE ed. 2, Table 3-4.19								**Acetone**	-	-	-
Aviation Fuel Properties, Coordinating Research Council, Inc. 1988							177-266				
Distillation Range 177-266 C								**Component**	**mass%**	**mass%**	**mass%**
								Heptane	-	-	-
kerosene	2m complex calorimeter data							**Toluene**	0.52	0.29	0.17
SFPE ed. 3, Table 3-4.10								**Methanol**	0.48	0.71	-
								Ethanol	-	-	0.83
Galbraith Labs								**Acetone**	-	-	-
								Component	**Volume %**	**Volume %**	**Volume %**
								Heptane	-	-	-
								Toluene	0.5	0.276	0.16
								Methanol	0.5	0.724	-
								Ethanol	-	-	0.84
								Acetone	-	-	-

3.1 Test Procedures

The fire was ignited with a propane igniter and allowed to burn to achieve a quasi-steady-state to avoid the initial transient phase of the fire. Data from all instruments except the spectrometer were taken continuously at fixed locations throughout the test. Filling of the pool to maintain a constant fuel level was performed automatically throughout the test. Mean fuel regression rates are found from the time-averaged filling rates.

3.2 Data Acquisition

The data acquisition system (DAS) consisted of a PC with a 16-bit data acquisition card connected to a National Instruments (NI) SCXI-1001 chassis. It had twelve NI SCXI-1102 cards with NI SCXI-1303 blocks for TCs and four NI SCXI-1104 cards with NI SCXI-1300 blocks for analog signals. This provides the ability to increase either analog signals or TC signals. The SCXI-1001 held 12 cards, yielding a total available channel count of 384 channels.

The data acquisition system can acquire temperature, heat flux, and pressure data. The integrity of all thermocouple channels was evaluated prior to the start of the test series with a calibrated Ectron thermocouple simulator, which inputs a controlled signal into each channel at the thermocouple device connection point and provides a check on the integrity of the channel hardware and software.

Data are sampled simultaneously for all channels, typically at 1000 Hz with an average value recorded at a rate of one sample per second, starting at least two minutes prior to the fuel ignition and continuing after burnout of the fire.

A formal checklist for conducting the test was created and used to record actions during the test event. The data from the instrumentation are organized via a Data Channel Summary Sheet and with sketches showing instrumentation location. This summary sheet contains a channel-by-channel listing of the instrumentation with details such as expected range, sampling rate, calibration date and source, instrument location, and the data sample rate. Post-test, all data are collected and converted to electronic format for purposes of archiving and dissemination via PC media (i.e., CD or equivalent).

4. TEST RESULTS AND UNCERTAINTY

Data from Test #24 (see Table 2, JP8, no glass rocks) are plotted in this section to demonstrate the measurement method and data acquisition for the other tests.

4.1.1 Fuel Regression Rates

Figure 12 shows the differential pressure measurement (inches water column x 1000) as JP8 was added to the fuel pan (t = -26 m to t = -13 m). The DP gauges were vented at t = -7 m to remove any trapped air. A fiducial signal and light flash was sent at t = 0 m to set timing on data acquisition computers and camera systems. At t = 2 m, the fuel pool was ignited using the propane burner. Two adjustment were made on the DP controller to set the fuel level, at t = 5 m and t = 7 m. The fire was determined to be at a steady-state condition between 18 and 24 minutes based on wall-mounted radiometers. The fuel DP controller was turned off at t = 28 minutes to allow the fuel in the pan to burn below the glass rocks, and the remaining liquid in the fuel pan was dumped to the drain tank at t = 32 m.

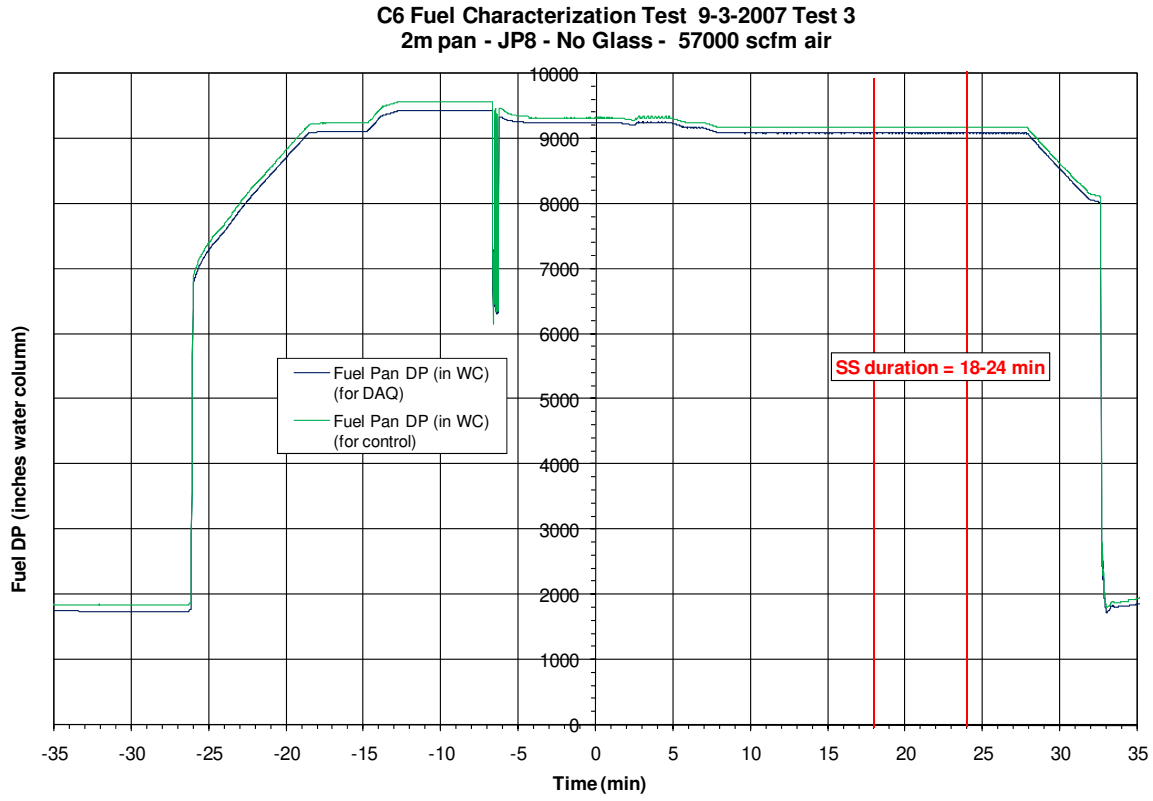

Figure 12 Liquid level measurement in Test #24.

Figure 13 present the fuel pool temperature data. Fuel at ~40 ºC is being added to the pan. At steady-state, the liquid surface is between TC9 and TC10. Thermocouples at and just below the

surface are at the boiling temperature, ~220ºC. Thermocouples above the liquid surface show an increase in temperature with height into the vapor dome.

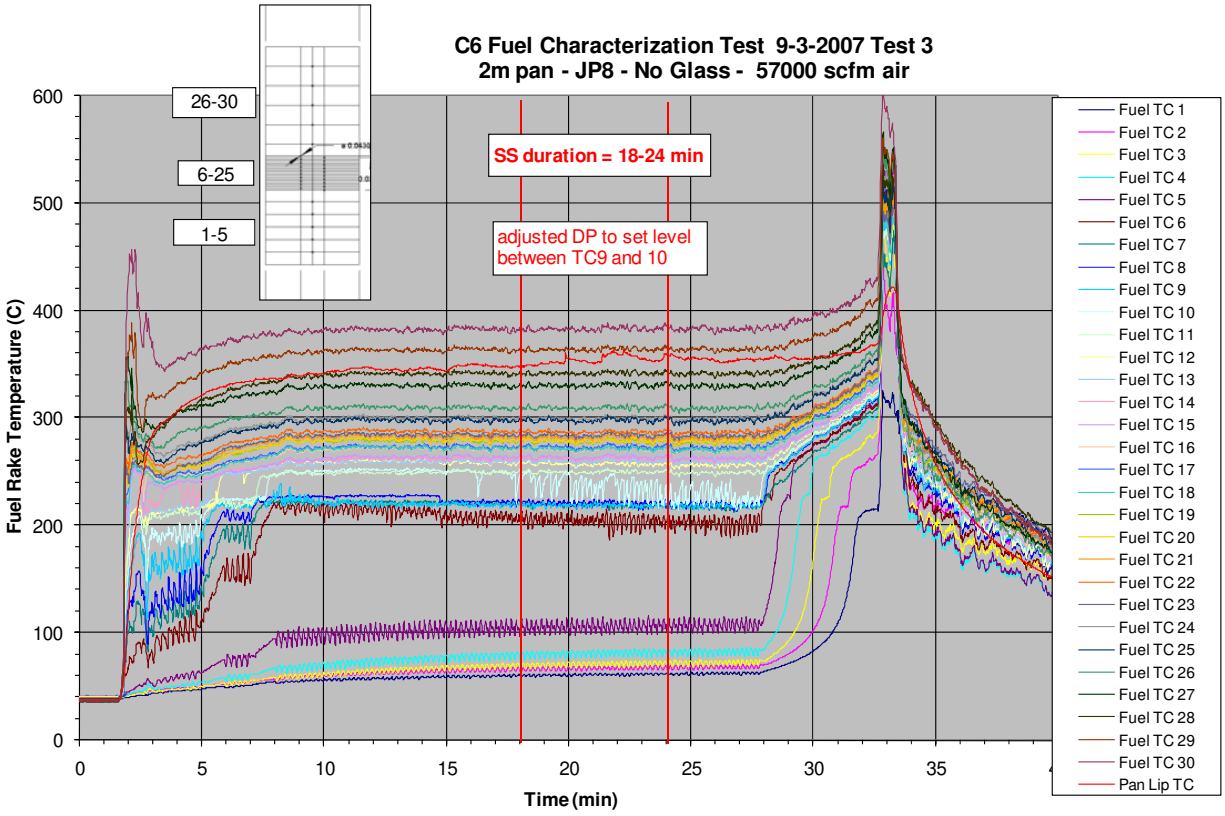

Figure 13 Fuel pool temperature measurements in Test #24.

Uncertainty - Temperature of Liquid Fuel

An uncertainty analysis for thermocouple data acquisition systems in use at Sandia's Radiant Heat facility and the Lurance Canyon burn site has been performed by Nakos [2004]. The analyses apply to Type K, chromel-alumel thermocouples in MIMS thermocouple assemblies and other applications. Several DASs were analyzed, one Hewlett-Packard (HP) 3852A system, and several NI systems. The uncertainty analyses were performed on the entire system from the thermocouple to the DAS output file. Uncertainty sources include thermocouple mounting errors, ANSI standard calibration uncertainty for Type K thermocouple wire, potential errors due to temperature gradients inside connectors, extension wire effects, DAS hardware uncertainties including noise, common mode rejection ratio, digital voltmeter accuracy, mV to temperature conversion, analog to digital conversion, and other possible sources. Typical results for "normal" environments (e.g., maximum of 300 to 400 K) showed the total uncertainty to be about ±1% of the reading in absolute temperature. In high temperature or high heat flux ("abnormal") thermal environments, total uncertainties range up to ±2-3% of the reading (maximum of 1300 K). The higher uncertainties in abnormal thermal environments are caused by increased errors due to the effects of imperfect thermocouple attachment to the test item.

The ANSI standard uncertainty for Type K thermocouple wire is 2.2ºC or 0.75% of reading (in ºC), whichever is greater. This uncertainty applies to the temperature of the thermocouple junction itself. Determination of the actual desired temperature (wall temperatures of an object or fluid temperatures) is subject to additional bias errors due to mounting. These bias uncertainties are very hard to accurately quantify, are application dependent, and are often the largest errors in the measurement system. For the present tests the bias error in the liquid fuel measurements is assumed to be small compared to the thermocouple uncertainty. The thermocouple is in good thermal contact with the liquid, which has a thermal conductivity much greater than that of air. Furthermore, radiation errors, etc. are expected to be small within the liquid. The local liquid temperature is expected to vary slowly compared to the thermal response time of the thermocouple. The overall uncertainty of the liquid fuel temperatures is assumed to be ±3ºC, which adds some conservatism to the ANSI standard uncertainty over the range of temperatures at which the fuel is expected to exist in liquid form.

Figure 14 shows the variance in the fuel pan DP measurements (inches JP8) adjusted to 0 DP at the fiducial. The DP measurements show the two adjustments in the controller set point early in the test. Note that there is essentially no change in DP during the steady-state portion of the test.

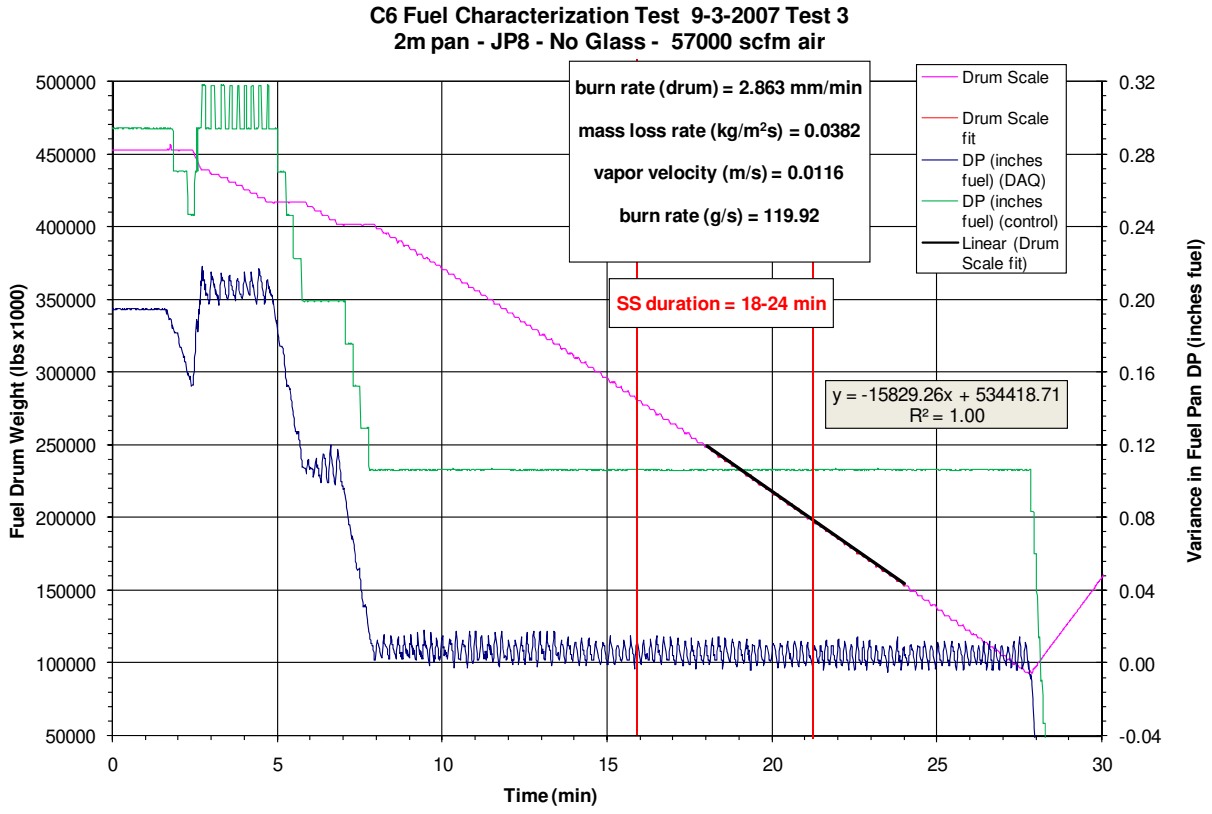

Figure 14 Regression rate measurement in Test #24.

A scale measured the rate of fuel loss from the supply tank over the course of a test. The scale had a range of 0 to 500 lbs (0 to 227 kg) and a resolution of 0.05 lb (0.02 kg). The fuel drum weight measurement (lbs fuel x 1000) is also shown in Figure 14. The fuel regression rate was

determined by dividing the burn rate (the curve fit at steady state shown in Figure 14, ~15.8 lb/min) by the fuel pan area (3.14 m^2) and the fuel density (808 kg/m^3). The mass loss rate from the pool is determined by multiplying the fuel regression rate by the fuel density.

In Test #24, the burn rate was 119.9 g/s (15.83 lbs/min), yielding a mass loss rate of 0.038 kg/m^2s. If not using a constant level fuel system, the fuel regression rate would have been 2.83 mm/min. Equation 1 (with R = 0.0831 bar m^3/kg mol K, T_{boil} = 488K, P = 0.834 bar) was used to determine a vapor velocity (useful for code simulations) of 0.012 m/s.

$$V_{vap} = \frac{\dot{m}'' R T_{boil}}{P} \tag{1}$$

Table 1 lists the burn rate for all tests.

Uncertainty

In the present experiments the fuel regression is determined from the rate of change of mass of a fuel supply tank (previously described). The constant-level control system matches the averaged rate of mass loss from the supply tank to the averaged mass loss rate from the pool, but fuel is supplied to the pan at a rate greater than the regression rate when the control valve is open and is not supplied to the pan when the control valve is closed. The nature of the control system dictates that fuel regression measurements should be averaged over periods much larger than the typical cycle time between commanded signals to open the control valve. A cycling rate of about 2.9 cycles per minute was observed in methanol tests that were run during development of the constant level system.

The scale used for measuring the rate of change of fuel mass during the course of a test is resolved to 0.05 lb (0.02 kg) with an uncertainty of ±0.06 kg. Uncertainty in the averaged fuel regression rate decreases as a function of the time over which the results are averaged. For a 2 m pool of JP8, density 808 kg/m^3, with a fuel regression rate of 2.86 mm/min the total mass loss from the fuel over a 6 minute span is 43.6 kg. Since fuel is not supplied to the pan continuously, the uncertainty in the actual amount of fuel added to the pan is assumed to be half the average mass added per cycle. If the fuel fill cycle rate is 4.3 cycles per minute, the uncertainty due to the unsteady fill rate is ±0.84 kg. If the uncertainty in the pan area, fuel density, and time between measurements are neglected, the total RSS combined uncertainty in the fuel regression rate measurement is ±0.06 mm/min or 1.9%.

4.1.2 Radiative Heat Transport to Pool

The total heat transfer from the fire to the pool was measured by an array of heat flux gauges (Model 64-20SB-18-5MGO-120-20970K Schmidt-Boelter type water-cooled thermopile gauges measuring total heat flux with a range of 0 to 120 kW/m^2, Medtherm Corporation, Huntsville, AL). The sensing surface of each gauge was placed at a nominal height approximately 26 mm above the surface of the liquid fuel (with the glass beads completely covered). The gauges were placed at radial locations spaced such that each gauge was in the center of a concentric ring of

equal area to minimize uncertainty in integrating the total heat flux over the surface of the pool (Table 4 and Figure 15). Duplicate gauges at the same radial distance from the pan center were used to assess the degree of symmetry in the radial direction.

The gauges were "cooled" using a hot oil recirculation bath to prevent soot collecting on the sensor surface caused by thermophorisis. The bath temperature was maintained a few degree above the measured boiling temperature of each fuel (listed in Table 12) with the exception of JP8 (the maximum operating temperature was ~140ºC). The gauge temperatures were typically ~10º hotter than the bath during the course of the fire. Inspection of the gauges before and after each test was performed to verify clean sensor surface conditions. Very little soot was seen on the gauges after each test.

Table 4 Location of pan heat flux gauge rings.

ring number	inner radius (m)	outer radius (m)	area (m^2)
1	0.000	0.408	0.524
2	0.408	0.577	0.524
3	0.577	0.707	0.524
4	0.707	0.816	0.524
5	0.816	0.913	0.524
6	0.913	1.000	0.524

position #	ring #	Medtherm #	theta	radius (m)	x (m)	y (m)
1	1	7	-90	0.289	0.000	-0.289
7	1	11	135	0.289	-0.204	0.204
2	2	10	-150	0.500	-0.433	-0.250
8	2	9	75	0.500	0.129	0.483
3	3	2	150	0.645	-0.559	0.323
9	3	12	15	0.645	0.624	0.167
4	4	1	90	0.764	0.000	0.764
10	4	5	-45	0.764	0.540	-0.540
5	5	6	30	0.866	0.750	0.433
11	5	3	-105	0.866	-0.224	-0.837
6	6	8	-30	0.957	0.829	-0.479
12	6	4	-165	0.957	-0.925	-0.248
	1	spec 1	15	0.183	0.178	0.044
	1	**spec 2**	1	0.387	0.390	0.012
	3	spec 3	-110	0.675	-0.221	-0.640

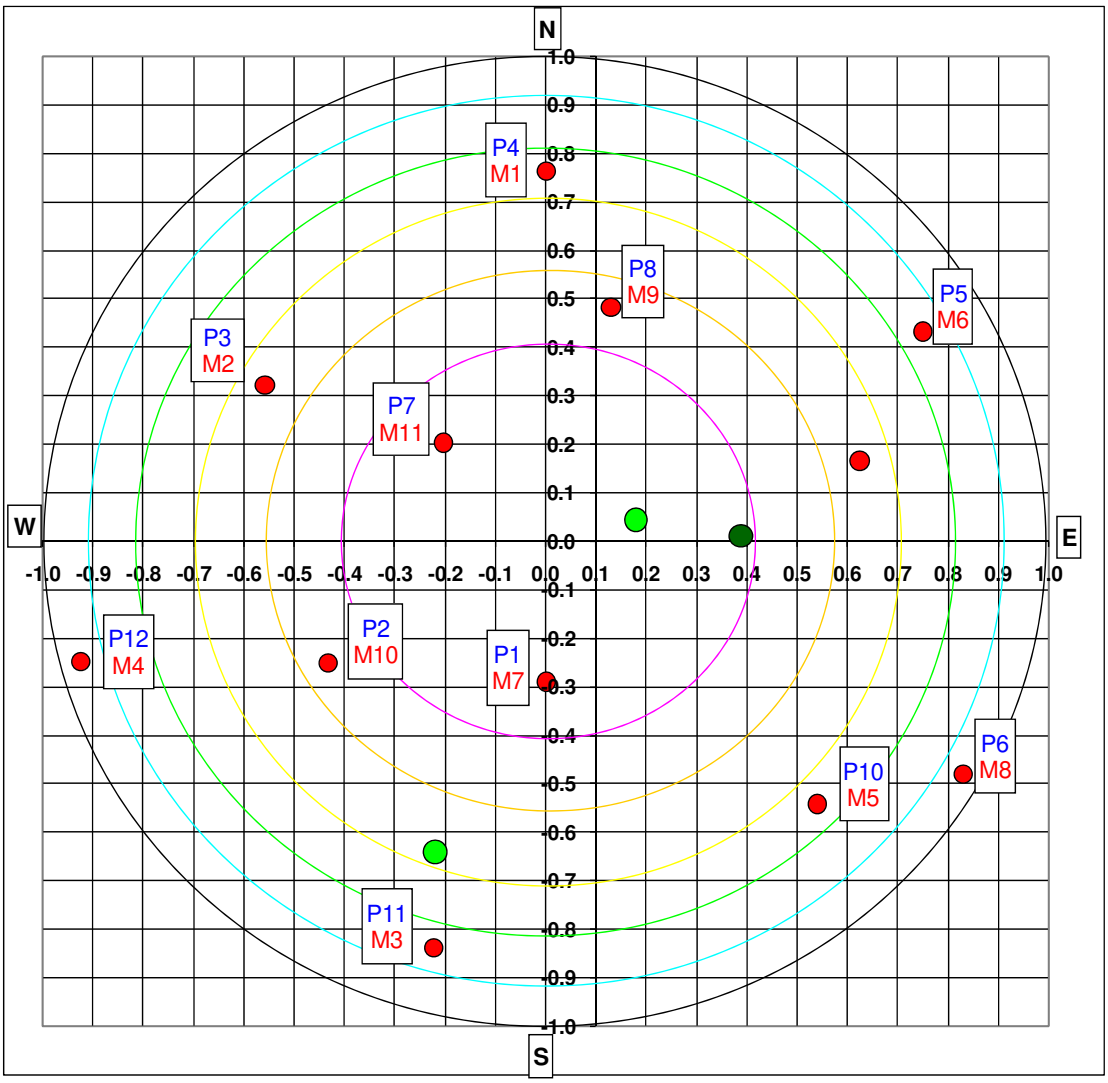

Figure 15 Locations of heat flux gauges and spectrometer viewing ports.

Figure 15 also shows the three locations where the mid-infrared spectral radiation intensity measurements could be obtained (green circles, discussed later in the report); however, only the spec 2 position listed in Table 4 was utilized.

Figure 16 presents the time-dependent heat flux data in test #24 as measured by the pool gauges. Note that the gauge at position 3 (Medtherm #2) in ring 3 was determined to be bad (for all tests). At steady-state (determined to be between 18-24 minutes for this JP8 test), the heat flux ranged from a 30 kW/m^2 to 60 kW/m^2 (depending on gauge location), with an pan average of ~49 kW/m^2.

The peak in heat flux at the start of the fire is caused by the propane burner. Increases in the flux during the initial 5-10 minutes (fuel-dependent) were due to the system coming to thermal equilibrium. The start and stop times for the steady-state analyses are given in Table 1 (valid data range). At the completion of the test, the drum pump would be turned off and the fuel in the pan would be allowed to burn down into the glass beads (after which it would be dumped to the

fuel drum). The increase in the flux seen in Figure 16 (and also the thermocouple temperatures in 13) at the end of the test was due to the decrease in fuel level and effectively changing the location of the vapor dome.

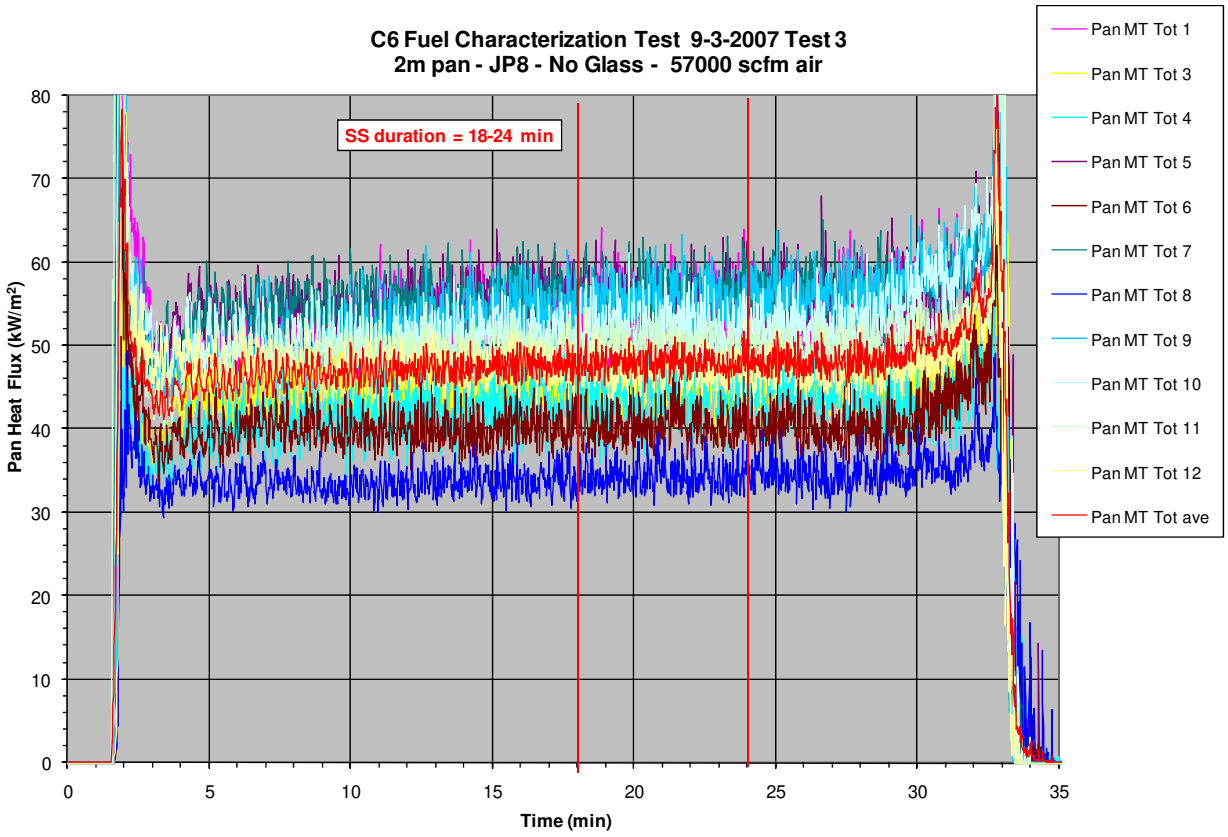

Figure 16 Heat flux to fuel surface in Test#24.

Tables 5 and 6 present the time-averaged and standard deviation of the time-averaged heat flux data, respectively, from all of the pool gauges over the times listed for the valid data ranges (see Table 1) and for all tests. Note the fluctuations in the flux, largely due to the puffing of the fires at their natural frequency.

Table 5 Pool Heat Flux Data (time-average, all position and all tests)

Date	Test	Glass Beads	Fuel:	M-1	M-2	M-3	M-4	M-5	M-6	M-7	M-8	M-9	M-10	M-11	M-12
-	-	-	-	kW/m^2	kW/m^2	kW/m^2	kW/m^2	kW/m^2	kW/m^2	kW/m^2	kW/m^2	kW/m^2	kW/m^2	kW/m^2	kW/m^2
8/3/2007	SNL **001**	No	100%Methanol	41.2	n/a	32.8	29.1	36.2	34.4	50.9	24.4	52.9	47.9	48.3	41.7
8/3/2007	SNL **002**	No	100%Methanol	41.9	n/a	33.7	29.7	37.1	35.8	50.9	26.3	52.0	47.1	49.8	43.4
8/15/2007	SNL **003**	No	100%Methanol	42.4	n/a	34.7	29.7	38.2	36.1	49.6	29.3	48.7	46.0	50.3	45.2
8/16/2007	SNL **004**	No	100%Methanol	41.0	n/a	32.7	30.6	36.7	33.1	49.1	26.6	48.6	47.0	46.9	41.6
8/19/2007	SNL **005**	Yes	100%Methanol	42.4	n/a	34.3	31.7	35.8	35.1	50.2	29.7	50.0	46.5	49.3	41.9
8/19/2007	SNL **006**	Yes	100%Methanol	42.2	n/a	33.6	30.7	36.0	34.5	49.4	28.7	50.1	47.5	48.4	42.7
8/20/2007	SNL **007**	Yes	100%Methanol	42.0	n/a	34.7	30.3	36.1	34.1	50.1	28.0	50.3	47.5	47.9	42.6
8/20/2007	SNL **008**	Yes	100%Ethanol	47.7	n/a	37.3	28.1	42.3	36.8	44.0	25.0	54.0	56.6	43.9	52.5
8/21/2007	SNL **009**	Yes	100%Ethanol	50.7	n/a	39.7	30.0	44.9	40.6	46.8	27.6	55.4	57.7	46.1	55.5
8/22/2007	SNL **010**	Yes	100%Ethanol	48.6	n/a	41.0	29.3	44.7	38.5	45.9	26.7	54.7	57.2	44.4	52.9
8/26/2007	SNL **011**	Yes	100%Heptane	29.2	n/a	27.0	26.0	28.9	26.8	32.1	23.9	31.3	33.5	31.9	33.3
8/28/2007	SNL **012**	Yes	100%Heptane	31.1	n/a	31.0	27.9	30.6	26.9	33.9	25.9	34.5	36.3	34.5	33.6
8/28/2007	SNL **013**	Yes	84%Ethanol 16%Toluene	65.8	n/a	51.9	34.5	62.7	48.8	44.5	36.1	55.2	57.2	46.5	67.4
8/29/2007	SNL **014**	Yes	84%Ethanol 16%Toluene	66.7	n/a	49.7	34.3	63.0	46.5	45.0	35.8	56.9	58.4	47.5	68.3
8/29/2007	SNL **015**	Yes	72.4%Methanol 27.6%Toluene	67.5	n/a	53.1	35.3	65.2	49.2	52.1	36.0	67.3	68.1	54.0	73.7
8/30/2007	SNL **016**	Yes	72.4%Methanol 27.6%Toluene	69.5	n/a	53.6	36.2	66.4	49.5	53.7	37.0	70.0	69.0	56.0	76.8
8/30/2007	SNL **017**	Yes	50%Methanol 50%Toluene	70.0	n/a	55.7	35.9	65.3	53.8	52.3	39.2	66.4	65.1	54.2	75.0
8/30/2007	SNL **018**	Yes	50%Methanol 50%Toluene	63.3	n/a	52.6	34.8	61.5	50.2	49.7	37.4	61.8	61.5	52.1	69.7
8/31/2007	SNL **019**	Yes	JP8	41.9	n/a	42.6	47.3	45.3	36.1	44.7	29.1	46.8	47.5	44.4	51.4
9/1/2007	SNL **020**	Yes	JP8	45.1	n/a	40.4	36.4	47.9	31.5	43.7	32.3	37.0	42.2	47.3	44.4
9/1/2007	SNL **021**	Yes	JP8	46.5	n/a	35.3	38.5	47.6	34.8	43.9	32.8	37.9	41.6	48.6	45.0
9/3/2007	SNL **022**	No	JP8	50.7	n/a	38.4	40.2	53.4	34.1	48.0	33.7	46.6	43.1	52.2	48.3
9/3/2007	SNL **023**	No	JP8	48.8	n/a	37.0	37.9	49.5	33.4	45.5	31.9	42.8	45.5	45.4	41.0
9/3/2007	SNL **024**	No	JP8	55.4	n/a	44.4	44.0	56.1	40.6	56.5	34.4	55.4	52.5	50.1	47.2
9/4/2007	SNL **025**	No	100%Ethanol	36.3	n/a	37.4	23.0	42.1	35.4	42.5	23.8	50.9	50.7	44.0	48.7
9/4/2007	SNL **026**	No	100%Ethanol	46.0	n/a	39.0	25.3	42.7	37.2	42.8	26.2	52.5	51.4	44.2	50.2
9/5/2007	SNL **027**	No	72.4%Methanol 27.6%Toluene	68.7	n/a	52.9	29.6	67.7	48.9	51.9	30.5	71.5	68.7	54.8	76.9
9/5/2007	SNL **028**	No	100%Methanol	38.4	n/a	33.7	17.9	36.3	33.7	43.6	19.1	44.2	42.2	45.2	42.3
9/6/2007	SNL **029**	No	100%Heptane	27.0	n/a	27.4	22.9	28.9	27.1	31.3	22.7	34.1	33.8	33.7	33.2
9/6/2007	SNL **030**	No	100%Heptane	29.1	n/a	26.1	24.4	28.0	26.2	30.9	23.9	32.6	32.5	32.6	32.9

Table 6 Pool Heat Flux Data (standard deviation, all position and all tests)

Date	Test	Glass Beads	Fuel:	M-1	M-2	M-3	M-4	M-5	M-6	M-7	M-8	M-9	M-10	M-11	M-12
-	-	-	-	kW/m^2	kW/m^2	kW/m^2	kW/m^2	kW/m^2	kW/m^2	kW/m^2	kW/m^2	kW/m^2	kW/m^2	kW/m^2	kW/m^2
8/3/2007	SNL **001**	No	100%Methanol	6.1	n/a	6.6	4.0	6.2	6.4	8.2	7.1	8.5	9.5	8.8	7.5
8/3/2007	SNL **002**	No	100%Methanol	6.1	n/a	6.2	3.7	6.1	6.3	7.9	8.0	8.2	9.7	8.6	7.7
8/15/2007	SNL **003**	No	100%Methanol	5.9	n/a	6.0	3.9	6.3	6.2	7.6	8.0	7.5	9.5	8.3	7.4
8/16/2007	SNL **004**	No	100%Methanol	6.0	n/a	6.6	4.2	6.3	6.6	8.2	6.2	6.9	8.8	9.0	8.0
8/19/2007	SNL **005**	Yes	100%Methanol	6.2	n/a	5.7	4.2	6.4	6.9	8.1	6.9	7.1	9.0	8.3	8.1
8/19/2007	SNL **006**	Yes	100%Methanol	6.3	n/a	6.2	4.3	6.1	6.4	7.9	7.4	6.7	8.8	8.4	8.0
8/20/2007	SNL **007**	Yes	100%Methanol	6.4	n/a	6.4	4.2	6.3	6.7	8.3	7.3	7.0	9.1	8.2	7.5
8/20/2007	SNL **008**	Yes	100%Ethanol	5.8	n/a	6.5	3.5	6.1	6.6	9.4	4.6	7.4	8.6	9.1	7.1
8/21/2007	SNL **009**	Yes	100%Ethanol	5.8	n/a	6.4	4.1	6.2	6.2	9.2	5.5	6.5	8.4	9.3	7.0
8/22/2007	SNL **010**	Yes	100%Ethanol	6.0	n/a	6.5	3.7	6.4	6.1	9.3	4.6	6.4	8.3	8.5	7.4
8/26/2007	SNL **011**	Yes	100%Heptane	1.5	n/a	1.5	1.4	2.0	1.6	1.8	1.3	1.7	2.4	1.9	2.1
8/28/2007	SNL **012**	Yes	100%Heptane	1.9	n/a	1.6	1.5	2.1	1.9	2.0	1.7	2.3	2.5	2.1	2.2
8/28/2007	SNL **013**	Yes	84%Ethanol 16%Toluene	6.6	n/a	8.3	3.2	8.2	8.4	4.0	3.6	6.0	8.7	5.0	8.4
8/29/2007	SNL **014**	Yes	84%Ethanol 16%Toluene	6.4	n/a	7.2	2.9	7.7	7.8	3.9	3.5	6.5	7.6	4.7	8.3
8/29/2007	SNL **015**	Yes	72.4%Methanol 27.6%Toluene	6.5	n/a	7.9	3.0	7.7	8.1	5.3	3.3	8.2	8.5	5.9	7.3
8/30/2007	SNL **016**	Yes	72.4%Methanol 27.6%Toluene	6.3	n/a	7.9	3.0	7.7	8.3	5.0	3.7	8.1	8.7	5.4	7.7
8/30/2007	SNL **017**	Yes	50%Methanol 50%Toluene	7.1	n/a	8.5	3.2	9.0	8.4	4.5	4.0	8.3	8.4	4.9	8.8
8/30/2007	SNL **018**	Yes	50%Methanol 50%Toluene	6.7	n/a	7.9	3.4	8.0	7.9	4.0	3.8	6.5	7.0	4.7	8.2
8/31/2007	SNL **019**	Yes	JP8	1.6	n/a	1.4	2.8	1.8	1.5	1.8	1.5	2.1	2.0	1.9	2.1
9/1/2007	SNL **020**	Yes	JP8	2.2	n/a	2.1	1.9	2.1	1.5	1.8	1.6	1.8	2.0	2.1	1.7
9/1/2007	SNL **021**	Yes	JP8	2.3	n/a	1.9	2.5	2.7	1.9	1.9	1.7	2.1	2.1	2.3	2.1
9/3/2007	SNL **022**	No	JP8	2.3	n/a	1.8	2.4	2.5	1.7	1.9	1.6	2.0	1.9	2.2	1.8
9/3/2007	SNL **023**	No	JP8	2.5	n/a	1.9	2.6	2.6	1.7	2.2	1.9	2.3	2.4	2.2	1.8
9/3/2007	SNL **024**	No	JP8	2.6	n/a	2.3	2.8	2.4	2.0	2.3	1.8	2.5	2.5	1.8	1.8
9/4/2007	SNL **025**	No	100%Ethanol	1.5	n/a	5.3	2.1	6.1	5.5	7.2	2.6	5.6	5.9	7.5	6.3
9/4/2007	SNL **026**	No	100%Ethanol	4.8	n/a	5.8	2.6	6.0	6.1	7.1	3.5	5.4	5.9	8.1	5.5
9/5/2007	SNL **027**	No	72.4%Methanol 27.6%Toluene	6.2	n/a	7.9	1.7	7.7	7.7	5.7	1.9	8.6	8.7	6.5	7.4
9/5/2007	SNL **028**	No	100%Methanol	5.0	n/a	5.3	2.1	5.7	6.2	5.5	2.5	6.2	6.7	6.3	5.7
9/6/2007	SNL **029**	No	100%Heptane	1.6	n/a	2.0	1.4	2.1	2.5	1.7	1.4	2.6	2.8	2.4	2.5
9/6/2007	SNL **030**	No	100%Heptane	3.0	n/a	1.9	2.6	2.6	2.4	2.1	3.2	2.8	3.0	3.1	2.0

Table 7 presents the difference between the two gauges located in the same ring, calculated as (Gage1 - Gage2) / Gage1. Note that the differences between gauges are small, with the exception for the JP8 tests. The 21% difference at ring 6 for JP8 is considered acceptable because the measurement is made at the pan edge for a fuel with a puffing tendency

Table 8 presents the ring-averaged heat flux, with the values plotted in Figure 17. To allow the plotting of heat flux across pan diameter, the data in the "negative" radial direction is a replicate of the "positive" radial average data. Figure 18 presents the pan average heat flux and compares that to the burn rate (average of all tests with identical fuel). The fuel averaged boundary condition summary table (Table 12) also presents the fuel averaged heat flux and burn rates.

Table 7 Ring Gauge Comparisons

	Ring 1		Ring 2		Ring 3		Ring 4		Ring 5		Ring 6	
Fuel:	**M-7**	**M-11**	**M-9**	**M-10**	**M-2**	**M-12**	**M-1**	**M-5**	**M-3**	**M-6**	**M-4**	**M-8**
-	**kW/m²**	**kW/m²**	**kW/m²**	**kW/m²**	**kW/m²**	**kW/m²**	**kW/m²**	**kW/m²**	**kW/m²**	**kW/m²**	**kW/m²**	**kW/m²**
100%Methanol	50.9	48.3	52.9	47.9		41.7	41.2	36.2	32.8	34.4	29.1	24.4
100%Methanol	50.9	49.8	52.0	47.1		43.4	41.9	37.1	33.7	35.8	29.7	26.3
100%Methanol	49.6	50.3	48.7	46.0		45.2	42.4	38.2	34.7	36.1	29.7	29.3
100%Methanol	49.1	46.9	48.6	47.0		41.6	41.0	36.7	32.7	33.1	30.6	26.6
100%Methanol	50.2	49.3	50.0	46.5		41.9	42.4	35.8	34.3	35.1	31.7	29.7
100%Methanol	49.4	48.4	50.1	47.5		42.7	42.2	36.0	33.6	34.5	30.7	28.7
100%Methanol	50.1	47.9	50.3	47.5		42.6	42.0	36.1	34.7	34.1	30.3	28.0
100%Methanol	43.6	45.2	44.2	42.2		42.3	38.4	36.3	33.7	33.7	17.9	19.1
Average:	49.2	48.3	49.6	46.5		42.7	41.4	36.6	33.8	34.6	28.7	26.5
Norm STDEV:	0.05	0.03	0.05	0.04		0.03	0.03	0.02	0.02	0.03	0.15	0.13
Difference:	2%		6%		n/a		12%		-2%		8%	
100%Ethanol	44.0	43.9	54.0	56.6		52.5	47.7	42.3	37.3	36.8	28.1	25.0
100%Ethanol	46.8	46.1	55.4	57.7		55.5	50.7	44.9	39.7	40.6	30.0	27.6
100%Ethanol	45.9	44.4	54.7	57.2		52.9	48.6	44.7	41.0	38.5	29.3	26.7
100%Ethanol	42.5	44.0	50.9	50.7		48.7	36.3	42.1	37.4	35.4	23.0	23.8
100%Ethanol	42.8	44.2	52.5	51.4		50.2	46.0	42.7	39.0	37.2	25.3	26.2
Average:	44.4	44.5	53.5	54.7		52.0	45.9	43.3	38.9	37.7	27.2	25.8
Norm STDEV:	0.04	0.02	0.03	0.06		0.05	0.12	0.03	0.04	0.05	0.11	0.06
Difference:	0%		-2%		n/a		6%		3%		5%	
100%Heptane	32.1	31.9	31.3	33.5		33.3	29.2	28.9	27.0	26.8	26.0	23.9
100%Heptane	33.9	34.5	34.5	36.3		33.6	31.1	30.6	31.0	26.9	27.9	25.9
100%Heptane	31.3	33.7	34.1	33.8		33.2	27.0	28.9	27.4	27.1	22.9	22.7
100%Heptane	30.9	32.6	32.6	32.5		32.9	29.1	28.0	26.1	26.2	24.4	23.9
Average:	32.0	33.2	33.1	34.0		33.3	29.1	29.1	27.9	26.7	25.3	24.1
Norm STDEV:	0.04	0.04	0.04	0.05		0.01	0.06	0.04	0.08	0.01	0.08	0.06
Difference:	-4%		-3%		n/a		0%		4%		5%	
72.4%Methanol 27.6%Toluene	52.1	54.0	67.3	68.1		73.7	67.5	65.2	53.1	49.2	35.3	36.0
72.4%Methanol 27.6%Toluene	53.7	56.0	70.0	69.0		76.8	69.5	66.4	53.6	49.5	36.2	37.0
72.4%Methanol 27.6%Toluene	51.9	54.8	71.5	68.7		76.9	68.7	67.7	52.9	48.9	29.6	30.5
Average:	52.6	54.9	69.6	68.6		75.8	68.6	66.4	53.2	49.2	33.7	34.5
Norm STDEV:	0.02	0.02	0.03	0.01		0.02	0.01	0.02	0.01	0.01	0.11	0.10
Difference:	-4%		1%		n/a		3%		8%		-2%	
84%Ethanol 16%Toluene	44.5	46.5	55.2	57.2		67.4	65.8	62.7	51.9	48.8	34.5	36.1
84%Ethanol 16%Toluene	45.0	47.5	56.9	58.4		68.3	66.7	63.0	49.7	46.5	34.3	35.8
Average:	44.7	47.0	56.1	57.8		67.9	66.3	62.8	50.8	47.7	34.4	35.9
Norm STDEV:	-	-	-	-		-	-	-	-	-	-	-
Difference:	-5%		-3%		n/a		5%		6%		-4%	
JP8	44.7	44.4	46.8	47.5		51.4	41.9	45.3	42.6	36.1	47.3	29.1
JP8	43.7	47.3	37.0	42.2		44.4	45.1	47.9	40.4	31.5	36.4	32.3
JP8	43.9	48.6	37.9	41.6		45.0	46.5	47.6	35.3	34.8	38.5	32.8
JP8	48.0	52.2	46.6	43.1		48.3	50.7	53.4	38.4	34.1	40.2	33.7
JP8	45.5	45.4	42.8	45.5		41.0	48.8	49.5	37.0	33.4	37.9	31.9
JP8	56.5	50.1	55.4	52.5		47.2	55.4	56.1	44.4	40.6	44.0	34.4
Average:	47.0	48.0	44.4	45.4		46.2	48.1	50.0	39.7	35.1	40.7	32.4
Norm STDEV:	0.10	0.06	0.15	0.09		0.08	0.10	0.08	0.09	0.09	0.10	0.06
Difference:	-2%		-2%		n/a		-4%		12%		**21%**	
50%Methanol 50%Toluene	52.3	54.2	66.4	65.1		75.0	70.0	65.3	55.7	53.8	35.9	39.2
50%Methanol 50%Toluene	49.7	52.1	61.8	61.5		69.7	63.3	61.5	52.6	50.2	34.8	37.4
Average:	51.0	53.1	64.1	63.3		72.3	66.7	63.4	54.2	52.0	35.4	38.3
Norm STDEV:	-	-	-	-		-	-	-	-	-	-	-
Difference:	-4%		1%		n/a		5%		4%		-8%	

Table 8 Ring Average Heat Flux

Date	Test	Glass Beads	Fuel/Radius(m)	Ring 1 (M7,11) 0.289	Ring 2 (M9,10) 0.5	Ring 3 (M12) 0.645	Ring 4 (M1,5) 0.764	Ring 5 (M3,6) 0.866	Ring 6 (M4,8) 0.957	Average
-	-	-	-	kW/m^2	kW/m^2	kW/m^2	kW/m^2	kW/m^2	kW/m^2	kW/m^2
8/3/07	SNL 001	No	100%Methanol	49.6	50.4	41.7	38.7	33.6	26.8	40.1
8/3/07	SNL 002	No	100%Methanol	50.4	49.5	43.4	39.5	34.7	28.0	40.9
8/15/07	SNL 003	No	100%Methanol	49.9	47.4	45.2	40.3	35.4	29.5	41.3
8/16/07	SNL 004	No	100%Methanol	48.0	47.8	41.6	38.8	32.9	28.6	39.6
8/19/07	SNL 005	Yes	100%Methanol	49.8	48.2	41.9	39.1	34.7	30.7	40.7
8/19/07	SNL 006	Yes	100%Methanol	48.9	48.8	42.7	39.1	34.1	29.7	40.6
8/20/07	SNL 007	Yes	100%Methanol	49.0	48.9	42.6	39.0	34.4	29.1	40.5
9/5/07	SNL 028	No	100%Methanol	44.4	43.2	42.3	37.4	33.7	18.5	36.6
			Average:	48.8	48.0	42.7	39.0	34.2	27.6	40.0
			STDEV:	1.9	2.2	1.2	0.8	0.8	3.9	1.5
8/20/07	SNL 008	Yes	100%Ethanol	44.0	55.3	52.5	45.0	37.0	26.5	43.4
8/21/07	SNL 009	Yes	100%Ethanol	46.4	56.5	55.5	47.8	40.2	28.8	45.9
8/22/07	SNL 010	Yes	100%Ethanol	45.1	55.9	52.9	46.6	39.8	28.0	44.7
9/4/07	SNL 025	No	100%Ethanol	43.2	50.8	48.7	39.2	36.4	23.4	40.3
9/4/07	SNL 026	No	100%Ethanol	43.5	52.0	50.2	44.3	38.1	25.7	42.3
			Average:	44.5	54.1	52.0	44.6	38.3	26.5	43.3
			STDEV:	1.3	2.6	2.6	3.3	1.6	2.1	2.2
8/26/07	SNL 011	Yes	100%Heptane	32.0	32.4	33.3	29.0	26.9	24.9	29.7
8/28/07	SNL 012	Yes	100%Heptane	34.2	35.4	33.6	30.9	28.9	26.9	31.6
9/6/07	SNL 029	No	100%Heptane	32.5	33.9	33.2	28.0	27.3	22.8	29.6
9/6/07	SNL 030	No	100%Heptane	31.8	32.5	32.9	28.6	26.1	24.1	29.3
			Average:	32.6	33.6	33.3	29.1	27.3	24.7	30.1
			STDEV:	1.1	1.4	0.3	1.3	1.2	1.7	1.1
8/29/07	SNL 015	Yes	72.4%Methanol 27.6%Toluene	53.1	67.7	73.7	66.4	51.1	35.7	57.9
8/30/07	SNL 016	Yes	72.4%Methanol 27.6%Toluene	54.9	69.5	76.8	67.9	51.5	36.6	59.5
9/5/07	SNL 027	No	72.4%Methanol 27.6%Toluene	53.3	70.1	76.9	68.2	50.9	30.0	58.2
			Average:	53.7	69.1	75.8	67.5	51.2	34.1	58.6
			STDEV:	1.0	1.3	1.8	1.0	0.3	3.5	0.8
8/28/07	SNL 013	Yes	84%Ethanol 16%Toluene	45.5	56.2	67.4	64.3	50.4	35.3	53.2
8/29/07	SNL 014	Yes	84%Ethanol 16%Toluene	46.2	57.7	68.3	64.9	48.1	35.0	53.4
			Average:	45.9	56.9	67.9	64.6	49.2	35.2	53.3
			STDEV:	-	-	-	-	-	-	-
8/31/07	SNL 019	Yes	JP8	44.6	47.1	51.4	43.6	39.4	38.2	44.1
9/1/07	SNL 020	Yes	JP8	45.5	39.6	44.4	46.5	35.9	34.4	41.0
9/1/07	SNL 021	Yes	JP8	46.2	39.8	45.0	47.0	35.0	35.7	41.4
9/3/07	SNL 022	No	JP8	50.1	44.8	48.3	52.1	36.2	36.9	44.7
9/3/07	SNL 023	No	JP8	45.4	44.1	41.0	49.2	35.2	34.9	41.6
9/3/07	SNL 024	No	JP8	53.3	53.9	47.2	55.7	42.5	39.2	48.6
			Average:	47.5	44.9	46.2	49.0	37.4	36.5	43.6
			STDEV:	3.4	5.3	3.6	4.3	3.0	1.9	2.9
8/30/07	SNL 017	Yes	50%Methanol 50%Toluene	53.3	65.7	75.0	67.6	54.8	37.6	59.0
8/30/07	SNL 018	Yes	50%Methanol 50%Toluene	50.9	61.7	69.7	62.4	51.4	36.1	55.4
			Average:	52.1	63.7	72.3	65.0	53.1	36.8	57.2
			STDEV:	-	-	-	-	-	-	-

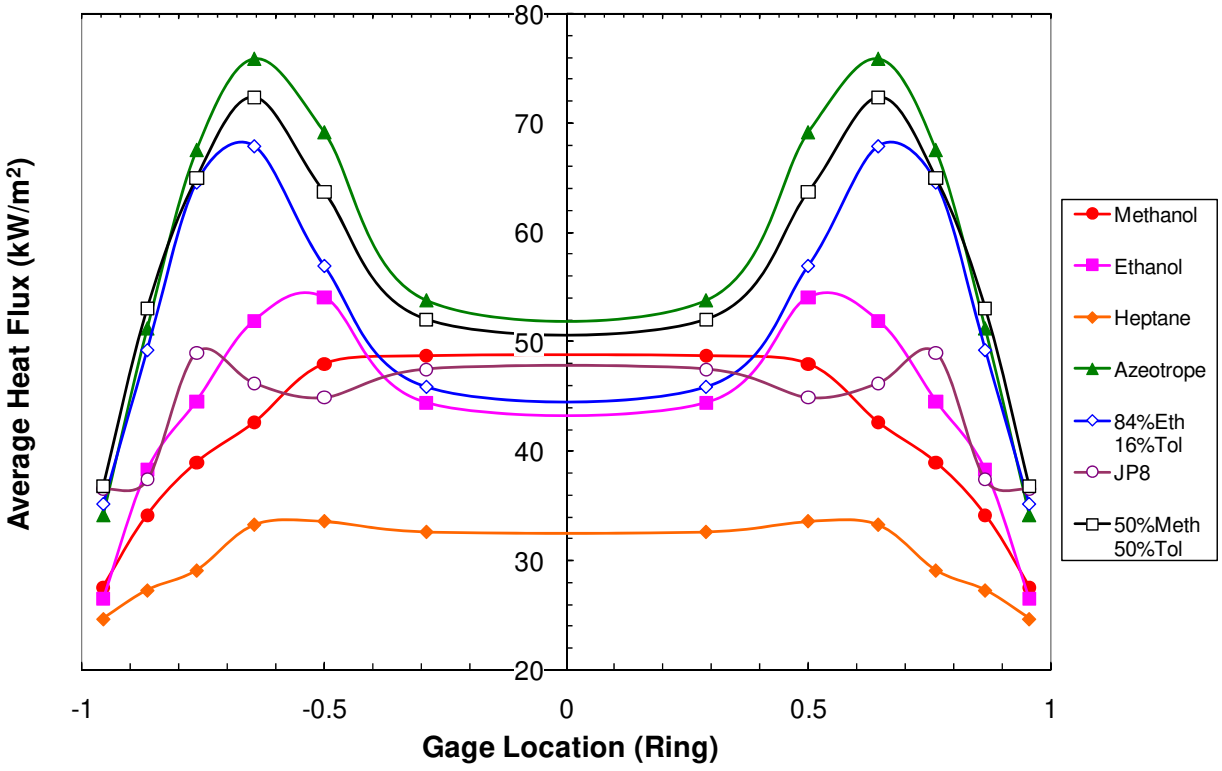

Figure 17 Ring averaged heat flux to fuel surface.

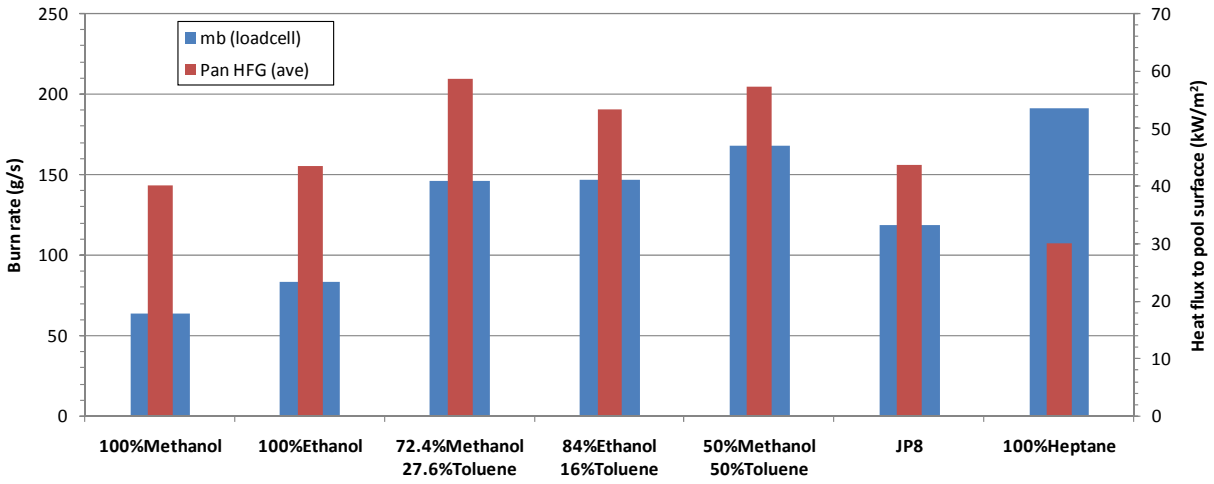

Figure 18 Fuel average burn rate compared to the pan heat flux.

Uncertainty - Total Heat Flux to Fuel Surface

The manufacturer's stated uncertainty for the heat flux gauges used to measure the incident heat flux at the pool surface is ±3%. Nakos [2005] estimated that uncertainties in fire applications can be much larger (±20% to ±40%), largely due to uncertainties in the convective component of

heat transfer. The uncertainty in the measurement of heat flux to the fuel includes the gauge measurement uncertainty, the uncertainty in the net heat flux due to differences in temperature and reflectivity between the fuel and the gauge, and the uncertainty in the integration of heat flux over the pool surface area based on measured heat fluxes at a finite number of measurement locations.

4.1.3 Absorption of Radiation by the Gaseous Fuel

A mid-infrared spectrometer (model ES-200, Spectraline, Inc., West Lafayette, IN was used to measure the thermal radiation spectra within the turbulent flame brush and vapor dome in a few of the fire tests in listed in Table 1. Fuels used included ethanol, an ethanol/toluene blend, JP-8, and heptane. These unique data provide insight into the relative contributions of soot and gas species emissions to the overall emission. They further assess the impact of absorption of thermal radiation from within the flame zone and the fuel rich region on the incident flux to the fuel pool.

The ES-200 measures spectral radiation intensity in the 1.3 to 4.8 micron wavelength range (~22 nm resolution) at 390 Hz. This wavelength range accounts for 75% of the emitted radiation energy from a blackbody source at 1420 K, which is approximately the effective radiation temperature from a large hydrocarbon fuel fire as determined by Kearney (2001).

The spectrometer was mounted underneath the fuel pan (Figure 19), looking vertically upwards through a stainless steel pipe (~1.6 m long, 3.5 cm diameter) which passed through a hole cut in the base of the pan (the spec 2 location, Table 4 and Figure 15). The view angle of the spectrometer is approximately 0.25 degrees. A small flow of nitrogen through the spectrometer and pipe kept the optics clean and eliminated the contaminating effects of changes in gas composition within the pipe. The inside surface of the pipe was painted with black Pyromark paint to minimize any reflections. Emissions from the hot tube were determined to be negligible. The spectrometer and pipe were mounted on a positioning system which traversed in the vertical direction to shift the viewing location from a height of 1 m above the pool surface down to the pool surface with a resolution of 25 mm.

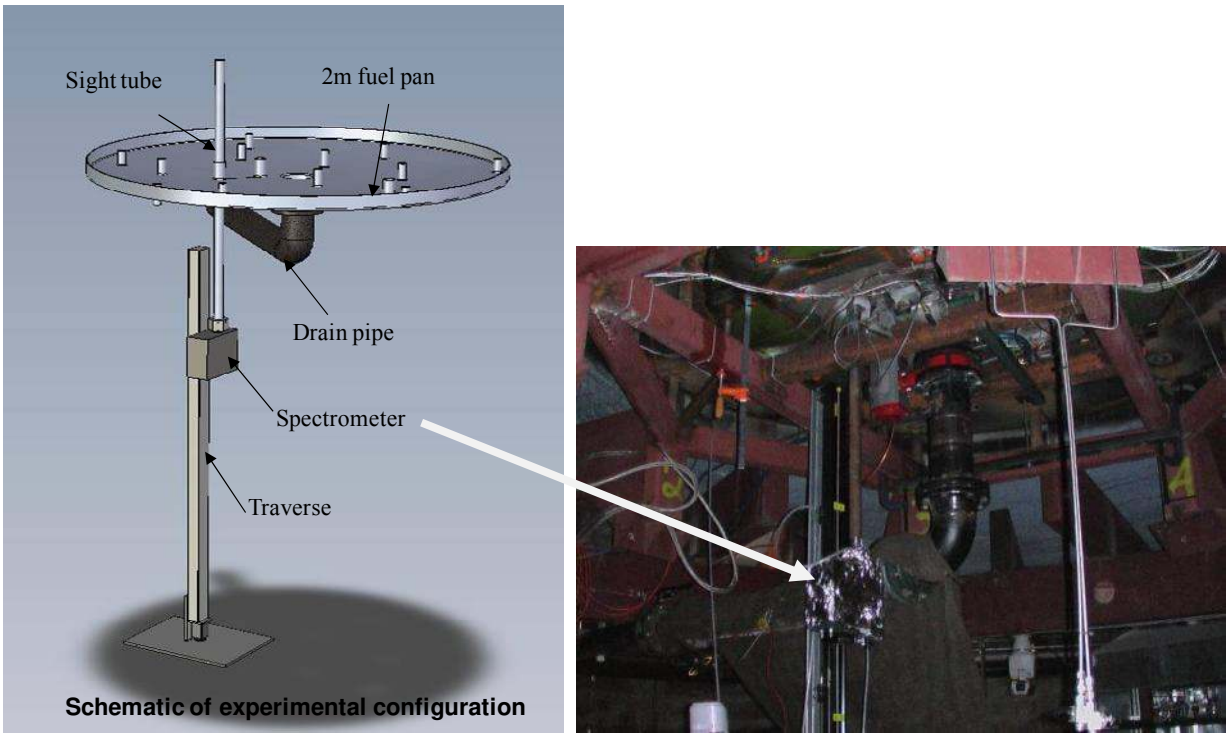

19 Schematic of instrumentation near pool for heat flux measurements.

Data were obtained from 15 - 20 minutes after ignition. At each position (25 mm increments), 2000 spectra (5 seconds) of data were obtained and were averaged to provide quasi-steady results despite the ~1Hz puffing frequency. It was determined that increasing the time averaging period to 15 seconds did not alter the results; thus, 5 seconds was used to conserve fuel. The acquired voltages were converted to intensities using a blackbody calibration file. The manufacturer's stated random error uncertainty is ±0.5% of full range of the signal (0-10 volts), which translates to approximately +0.2 kW/m2/μm/sr for typical measurements.

Suo-Anttila et al. [2008] presents a complete description and analyses of the dataset. An overview of those results is presented here. Figure 20 presents the complete spectra from four tests using ethanol, an ethanol (84%) / toluene (16%) blend, JP-8, and heptane. The plots present intensity as a function of both wavelength and height above the fuel surface.

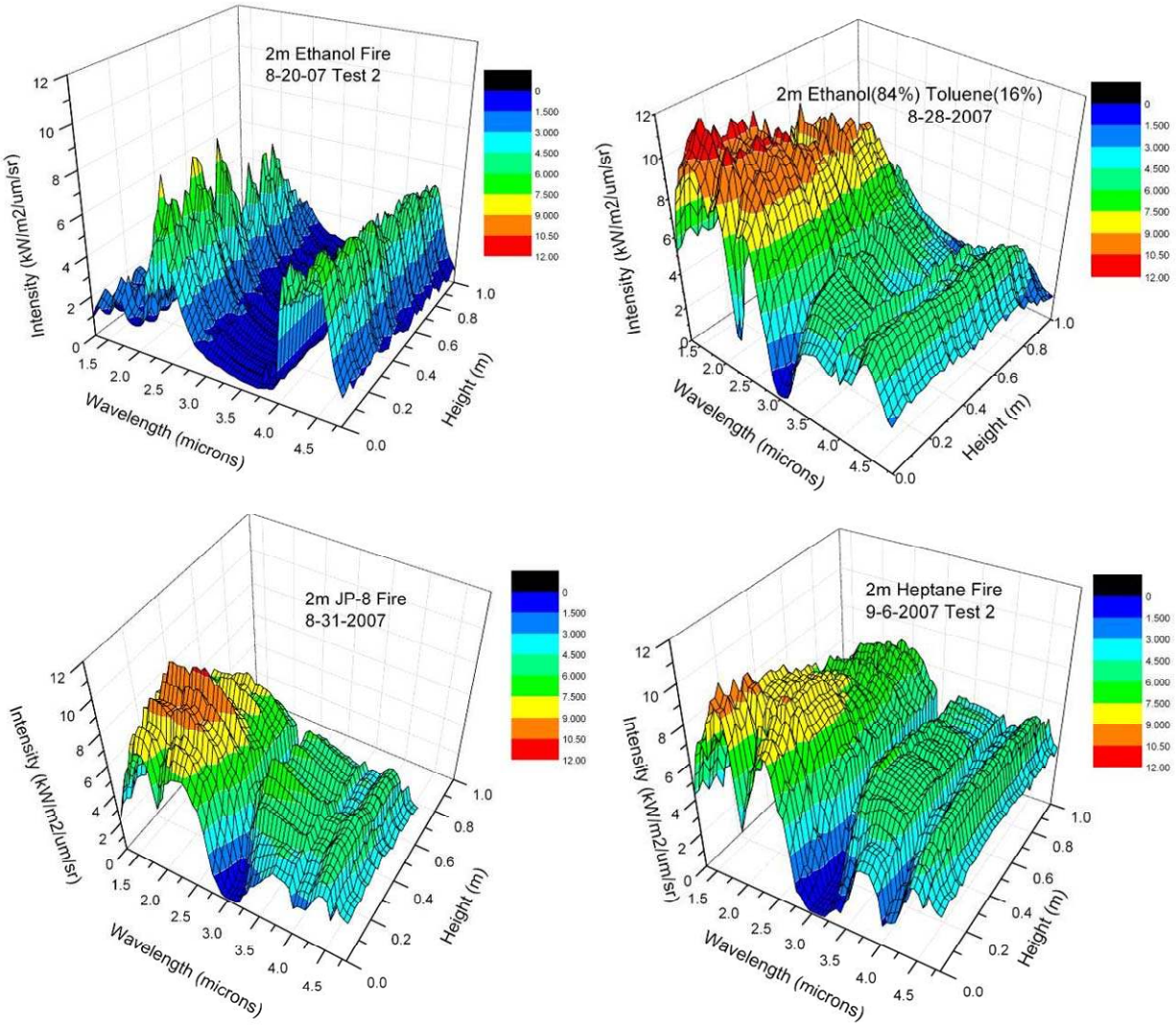

Figure 20 Thermal radiation spectra results (function of fuel type, height, and wavelength).

Analysis of the ethanol thermal radiation spectra (Figure 21) determined that the thermal radiation was dominated by gas band emission from the combustion products; H_2O at 1.85 µm, 2.0 µm, 2.4 µm, and 2.8 µm and CO_2 at 2.7 µm and 4.5 µm. Peak intensities observed were 7 kW/m^2/µm/sr in the 2.8 µm H_2O band and the 2.7 µm / 4.5 µm CO_2 bands.

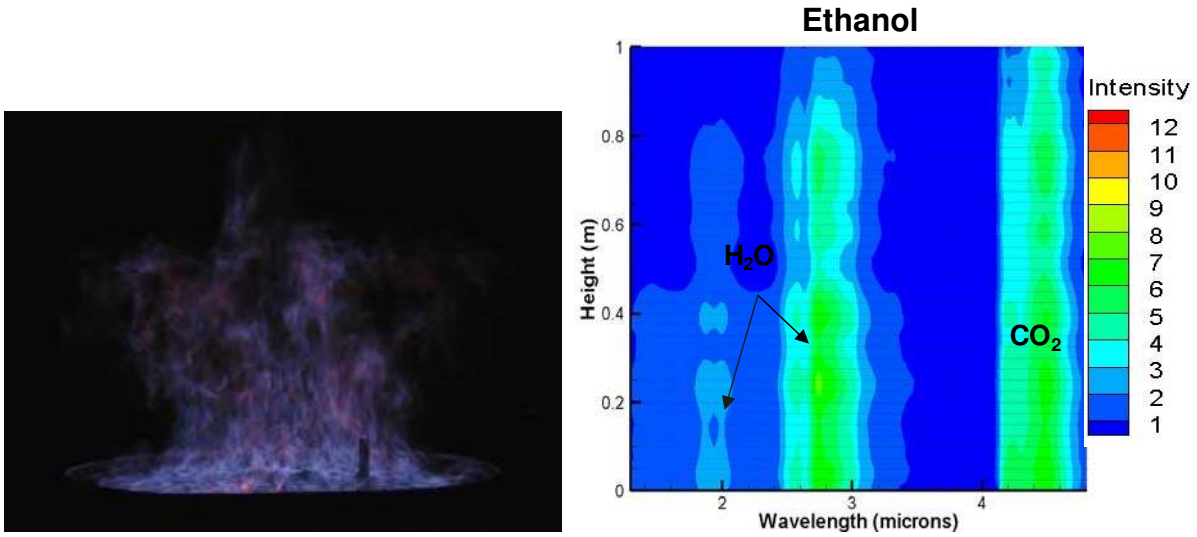

Figure 21 Ethanol 2m fire and thermal radiation spectra.

Analysis of the JP-8 thermal radiation spectra (Figure 22) determined that JP-8 fuel creates luminous, high intensity fires dominated by broadband soot emission for $\lambda < 3.2$ μm with peak intensities of ~10 kW/m^2/μm/sr. The fuel vapor absorption at 3.3 - 3.6 μm is due to C-H bond stretching that suggests the fuel rich region (vapor dome) persists to ~0.2 m. Other weak absorption bands include CO_2 at 4.2 - 4.4 μm and H_2O at 2.4 μm (exists in a region of the spectrum where a significant amount of soot emission occurs). This absorption serves to decrease the amount of energy reaching the fuel surface.

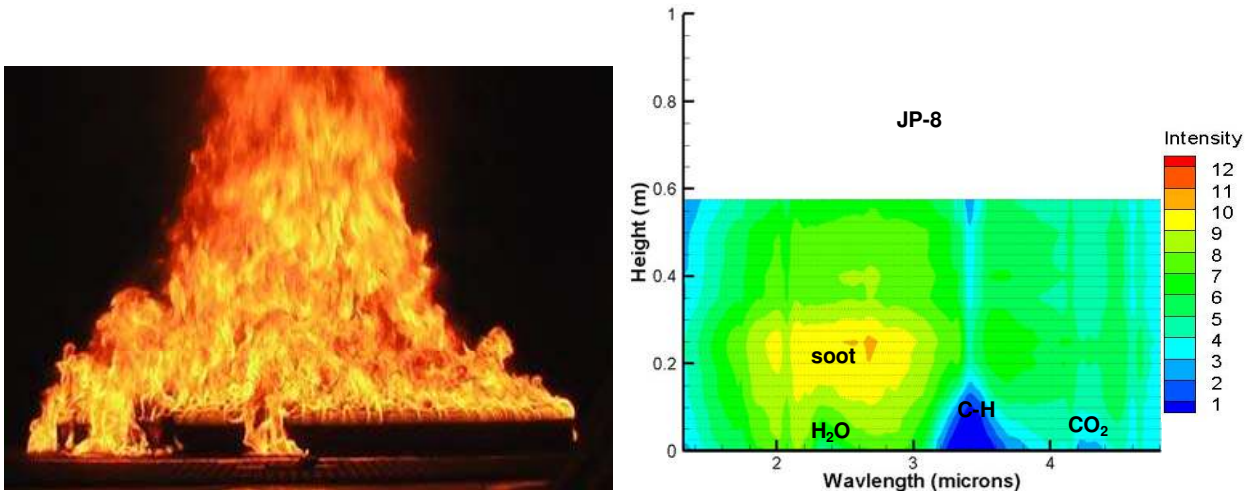

Figure 22 JP-8 2m fire and thermal radiation spectra.

Analysis of the heptanes thermal radiation spectra (Figure 23) determined that peak intensities are from broadband soot emission. The fuel vapor absorption at 3.3 - 3.6 μm was due to C-H

bond stretching. This suggests there is a very large fuel rich region that persists to 1 m and likely beyond. Other weak absorption bands include CO_2 at 4.2 - 4.4 μm and H_2O at 2.4 μm.

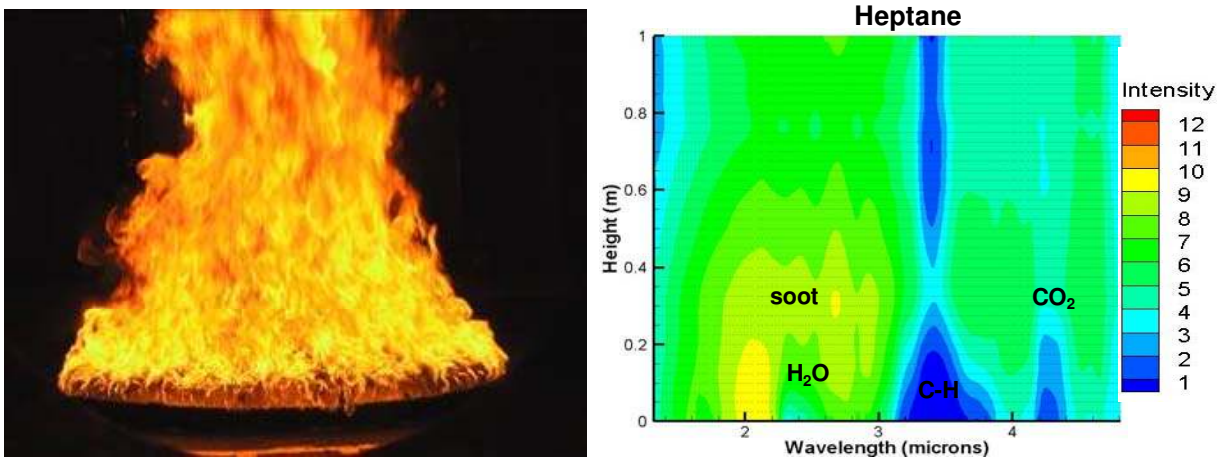

Figure 23 Heptane fire and thermal radiation spectra.

Analysis of the ethanol/toluene blend thermal radiation spectra (Figure 24) determined that the addition of toluene to the ethanol greatly impacted the thermal radiation spectra. The spectra were dominated by broadband soot emission with produced peak intensities of 12 $kW/m^2/\mu m/sr$. The CO_2 emission was found at 4.5 μm and CO_2 / H_2O were seen at 2.7-2.8 μm (with absorption low in the flame zone and emission high in the flame zone). The fuel vapor absorption at 3.3 - 3.6 μm was due to C-H bond stretching which suggests the fuel rich region (vapor dome) persists to ~0.15 m.

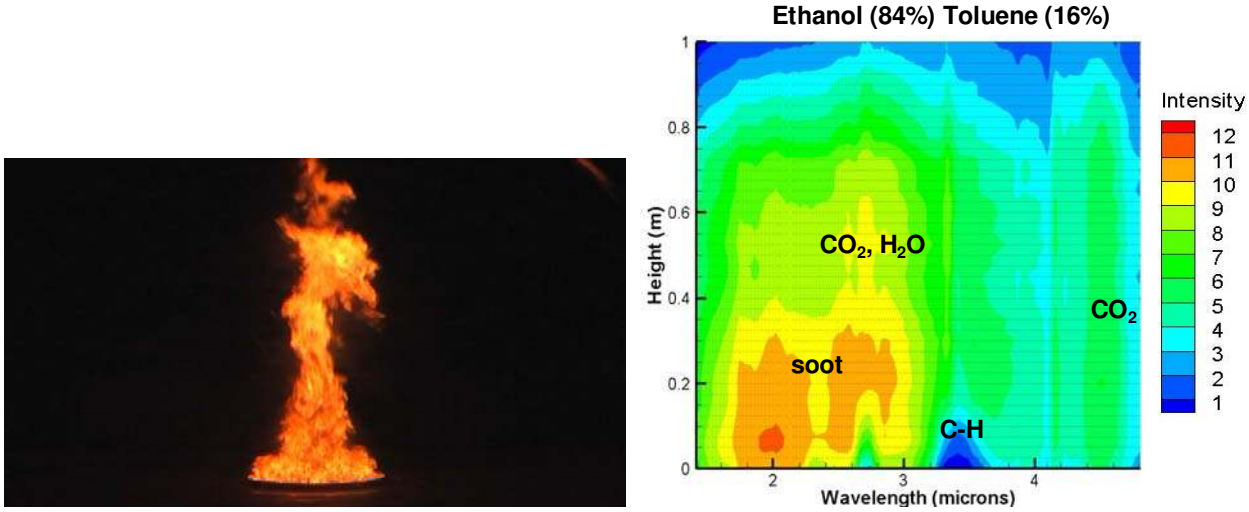

Figure 24 Ethanol/toluene blend thermal radiation spectra.

Summarizing, the thermal radiation incident upon the fuel pool varies greatly with the type of fuel. The reduction in the peak emission for heavily sooting fuels is attributed to the presence of cold soot near the fuel surface. A theoretical gray body intensity at T=1450 K and ε=0.4 is shown in Figure 25. The observed spectra (at 1.27 cm above the pool surface) differ from the gray approximation due to emission and absorption by combustion products as previously described.

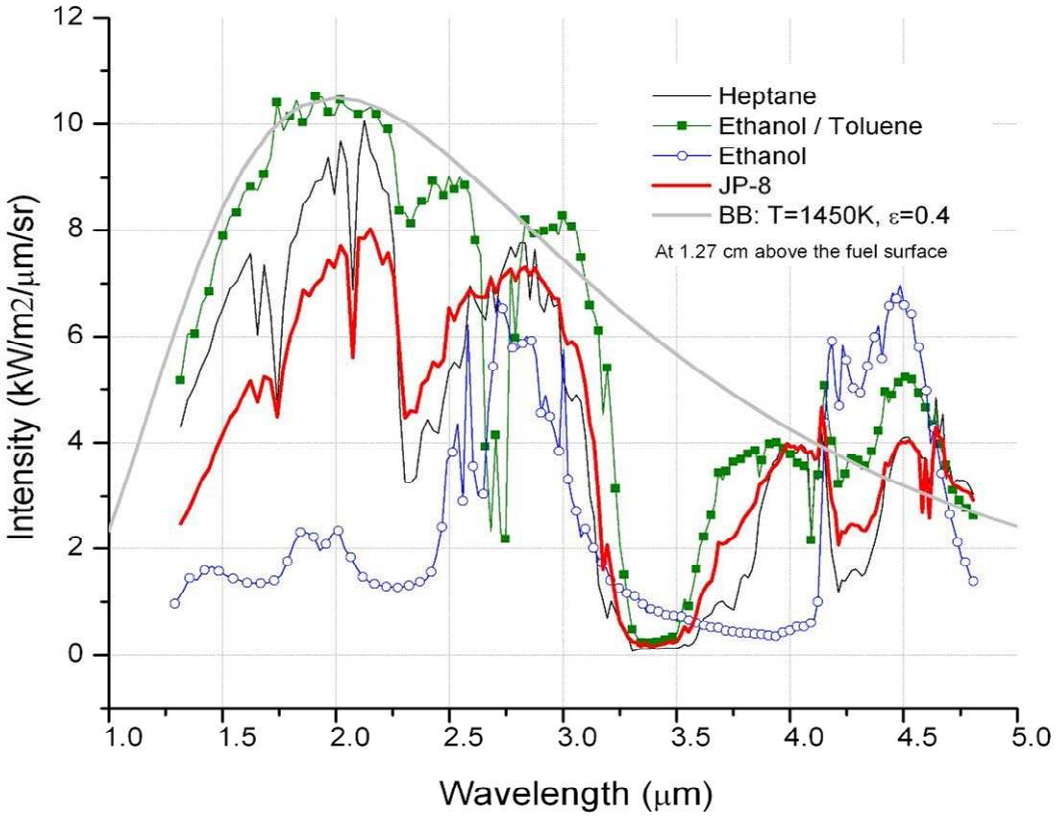

Figure 25 Comparing gray body to fire intensity near the fuel pool surface.

Uncertainty - Spectral Transmission Coefficients in Fuel Vapor in Fires

The manufacturer's stated uncertainty for the Spectraline ES-200 spectrometer is ±0.5% of full range of the signal (0 to 10 Volts), which corresponds to the random error in the measurement. The accuracy of the intensity or the transmission coefficient measurement is then a function of the accuracy and appropriateness of the calibration. For transmission measurements the average voltage measured at the top of the vapor dome is used as a reference, and the ratio of the measured voltage lower in the vapor dome to the reference voltage is taken to be the transmissivity. With a baseline intensity appropriate for a fire, the maximum and minimum reference voltages are estimated for the present analysis to be 1.5 V and 0.5 V. The uncertainty in the transmissivity due to the random error in the recorded voltage is then ±0.03 transmissivity units at the maximum intensity and ±0.10 transmissivity units at the minimum intensity. If the uncertainty in the reference voltage is assumed to be ±15%, the overall uncertainties rise to ±0.15 and ±0.18 transmissivity units.

4.1.4 Transmissivity in Liquid Fuel

The absorption of thermal radiation within various liquid fuels was investigated in a laboratory setting. The measurement setup is shown in Figure 26. The diagnostic used to acquire the spectrally-resolved absorption was a Spectraline ES-100 NIR spectrometer. An Infrared Systems IR-364 blackbody source, operating at 1000ºC, was positioned on the side of the absorption cell opposite the spectrometer. Thermal radiation from the blackbody was transmitted through the absorption cell and the intensity was recorded by the spectrometer. The magnitude of the signal passing through the fuel, relative to the empty cell reference signal, provided the spectrally-resolved transmission of the fuel for that particular thickness. A variable path length absorption cell, with a diameter of 8 mm, was attached to the spectrometer. The path length was variable from 0-3.125 mm using a micrometer with a resolution of +0.005 mm.

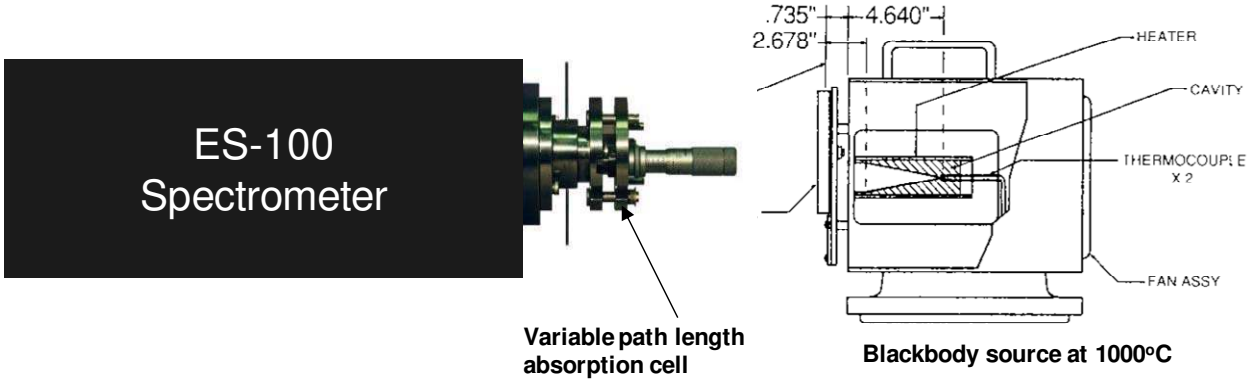

Figure 26 Setup for the fuel absorption measurements.

The selected fuels (ethanol, ethanol(84%) / toluene(16%) blend, JP-8, and heptane) were introduced into the cell via a 1.6 mm tube. The cell was filled until fluid spilled out the exit port to ensure that air bubbles within the cell were eliminated. After each fuel type, the cell was cleaned with acetone and dried with inert gas to ensure that the reference signal was reproduced. Fuels within the absorption cell were not heated during the experiments (i.e., all measurements were performed with the fuels at ambient temperature).

Figure 27 shows the wavelength-dependent magnitude of the thermal radiation transmitted through various depths of selected liquid fuels. The data were obtained by taking the ratio of the spectral blackbody intensities through the fuel thickness to the reference spectral blackbody intensities. For all fuels, the liquid is opaque for wavelengths between ~3.2-3.6 μm (C-H bond stretching). The impact of C-H absorption is minimal since incident thermal radiation in this band has already been absorbed by the fuel rich region low in the fire. Note that ethanol and the ethanol/toluene blend absorb most of the energy in very thin layers. Note large absorption bands for JP-8 and heptane 1.7 and 2.4 μm and large transmission bands for JP-8 and heptane at <1.6 μm and 1.85-2.1 μm (high energy bands). In highly transmissive regions, the reference spectra could have been higher than the measured spectra due to increased sensitivity to reflection from the empty cell.

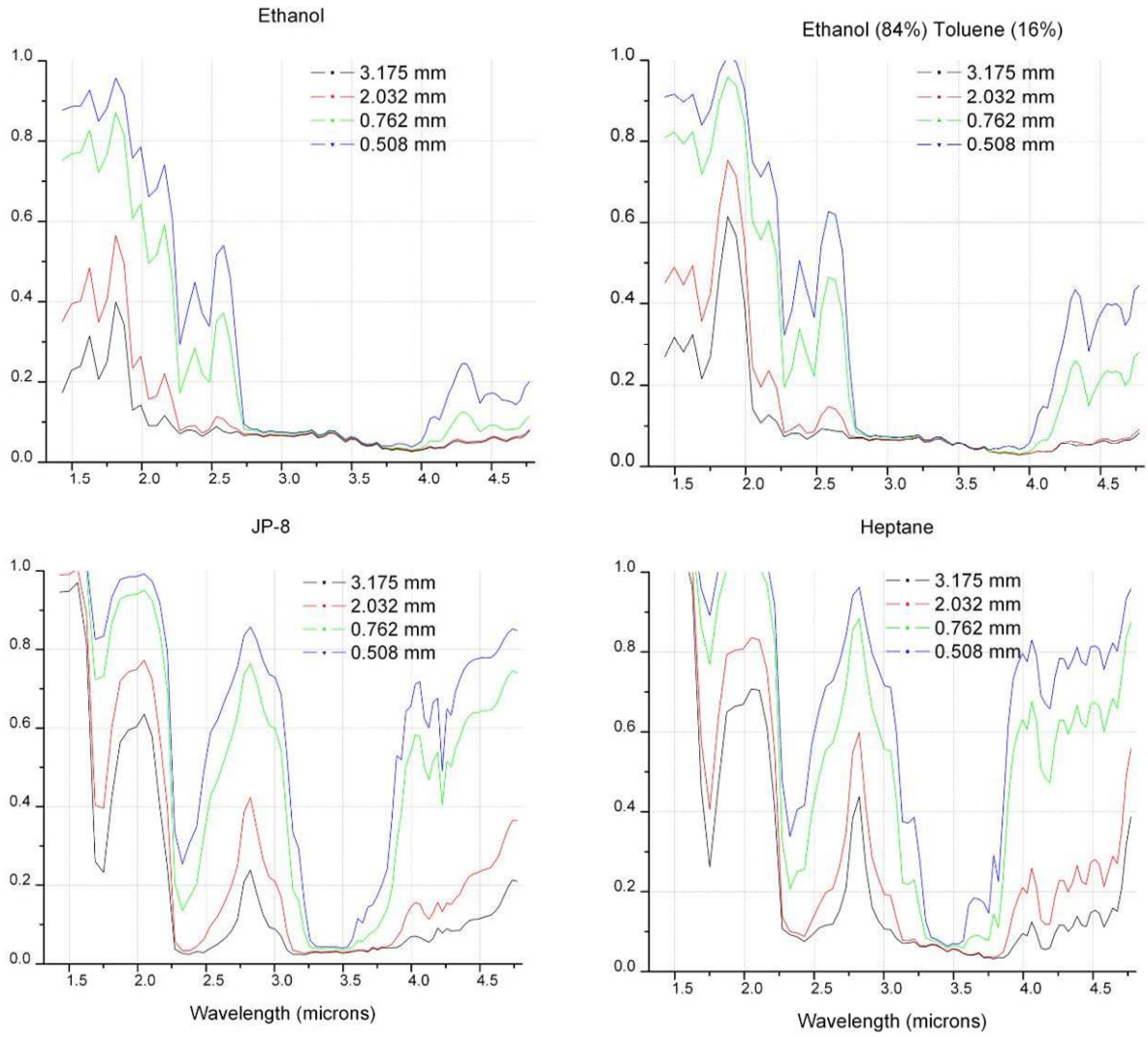

Figure 27 Thermal radiation transmission in liquid fuel.

In order to quantify the fraction of the thermal radiation being transmitted through various fuel thicknesses, the incident thermal radiation spectra for each fuel (Figure 26) was multiplied by the fractional spectral transmission for each thickness (Figure 27). The resulting thermal radiation being transmitted through that thickness of fuel was integrated and compared with the integrated value of the incident thermal radiation. The fraction of energy transmitted for each fuel as a function of the fuel thickness is shown in Figure 28 for the different fuels. Ethanol and methanol are least transmissive (90% absorbed in the first 3 mm). Heptane is the most transmissive with 65% absorbed in the first 3 mm. JP-8 has ~75% of the energy absorbed in the first 3 mm.

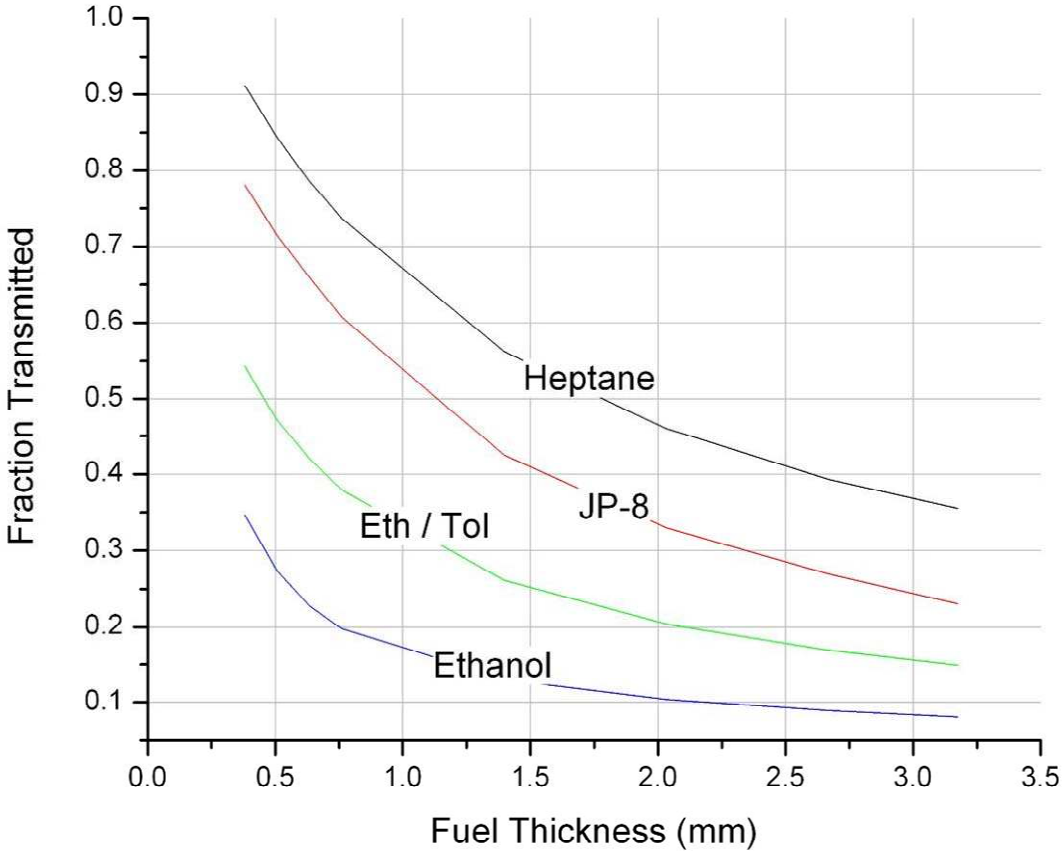

Figure 28 Fraction of the incident thermal radiation transmitted.

Uncertainty - Spectral Transmission Coefficients in Liquid Fuels

The same spectrometer is used for spectral transmission in the liquid fuel as in the fuel vapor. The absorption of the liquid test cell without any fuel in it can be measured independently in a steady environment, reducing the uncertainty in the determination of the reference voltage as compared to the study of the absorption in the vapor dome. If a blackbody source at 1200ºC is assumed to provide the spectral energy, the maximum and minimum voltages are assumed to be 6.5 V and 0.3 V. The uncertainty due to the random error in the voltage measurement then ranges from ±0.01 to ±0.17 transmissivity units. If the uncertainty in the reference voltage is assumed to be ±5%, the overall uncertainties rise to ±0.05 transmissivity units at the maximum intensity and ±0.17 transmissivity units at the minimum.

4.1.5 Reflectivity of Liquid Fuel

The reflectivity of the liquid fuel surface was measured with an SOC 410 reflectometer (Surface Optics Corporation, San Diego, CA) in a laboratory environment prior to the fire tests. This handheld device measures the reflectivity of a surface at two different viewing angles in six

wavelength bands, from which the total, hemispherical reflectivity may be estimated. The reflectivity measurements were taken with a test setup designed to reliably position and align the reflectometer within 1 mm of the liquid surface.

Figures 29 and 30 present the reflectivity data for 20 degree and 60 degree measurement angles, respectively. Each fuel was measured three times. All fuels had a low reflectance. JP-8, toluene, and heptane had the highest reflectance (~0.1) at a wavelength of ~1 µm and incident angle of 20 degrees, with reflectance reducing to ~0.04 at the same wavelength and an angle of 60 degrees. At higher wavelengths, reflectance was nominally zero for all fuels.

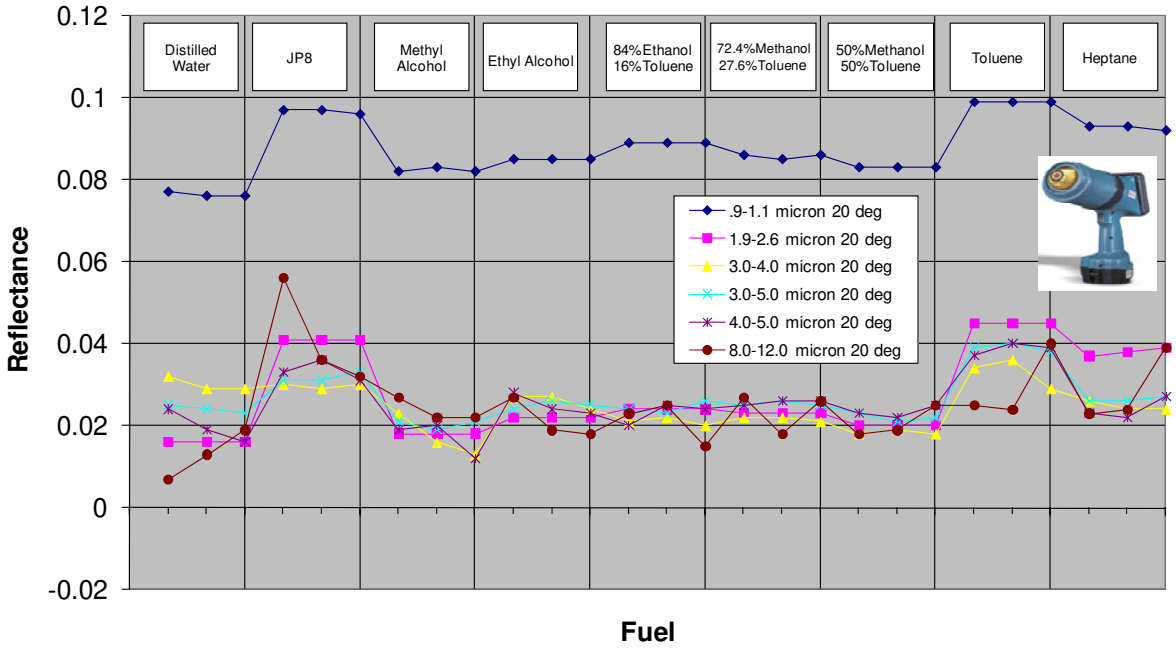

Figure 29 Reflectance of fuels at 20 degree incident angle.

Uncertainty - Reflectivity of Liquid Fuel

The uncertainty of the reflectivity measurements taken by the SOC 410 is ±0.03 reflectivity units for temperatures in the range 0ºC to 40ºC. The measurement applies to the interface between the liquid fuel and air at room temperature. The reflectivity of the interface between the liquid fuel and the gaseous mixture in the actual fire is assumed to be similar, so the overall uncertainty in the reflectivity is assumed to be ±0.05 reflectivity units.

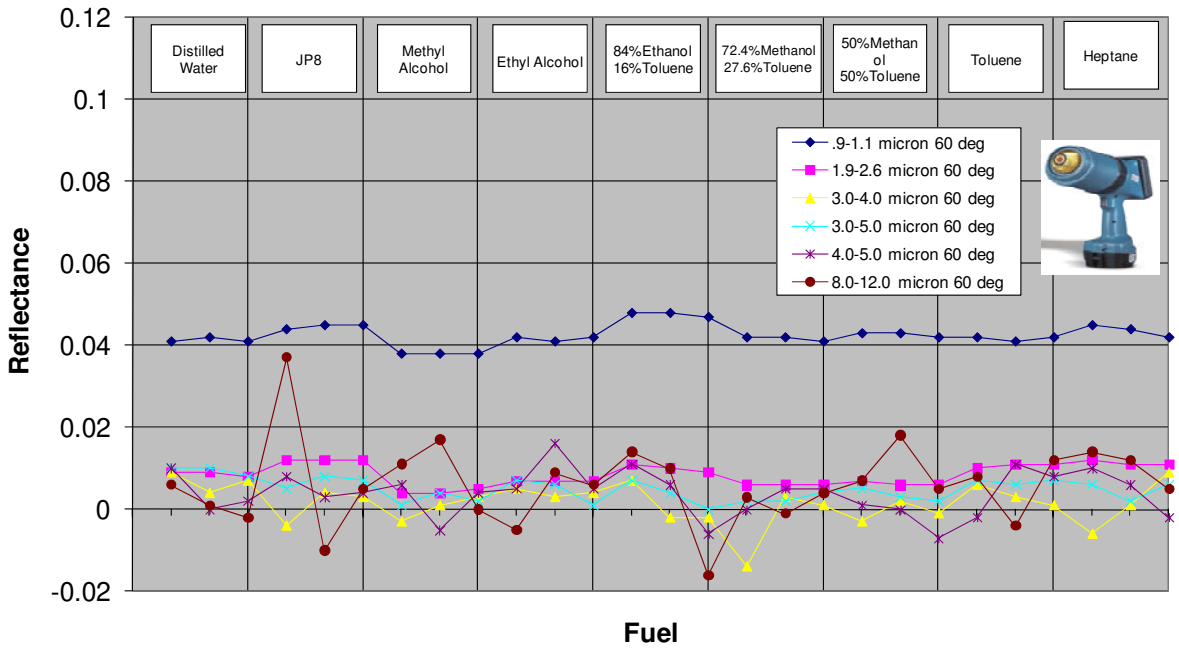

Figure 30 Reflectance of fuels at 60 degree incident angle.

4.1.6 Initial and Boundary Conditions

Air Flow Rate

The coflow air supplied to FRH was controlled to maintain a constant flow rate at the desired value. A forced-draft (FD) fan forces air into the chamber at the specified flow rate. An induced-draft (ID) fan in the exhaust duct helps to draw air and combustion products out of the chamber and maintains the pressure at ambient levels. Both fans are computer controlled and the flow rate, fan speed, and current for each fan are logged. The air temperature is measured by a thermocouple in the basement of the FRH facility.

Figure 31 shows the air flow rate profile for test #24 as measured at the FD fan and at the exhaust stack. Both fans are started and are stable at the desired flow rate at the start of the test. At t=0 min., the fire is ignited, and the stack flow momentarily see an increase in flow as the air in FLAME is heated. When the pressure in FLAME starts to increase, the ID fan increase speed to compensate and return the differential pressure across the FLAME wall to zero, and stack flow returns to the desired flow. This process reverses at the end of the fire (t=33 min.).

All tests were performed at a nominal flow rate of 57,000 scfm (Table 1).

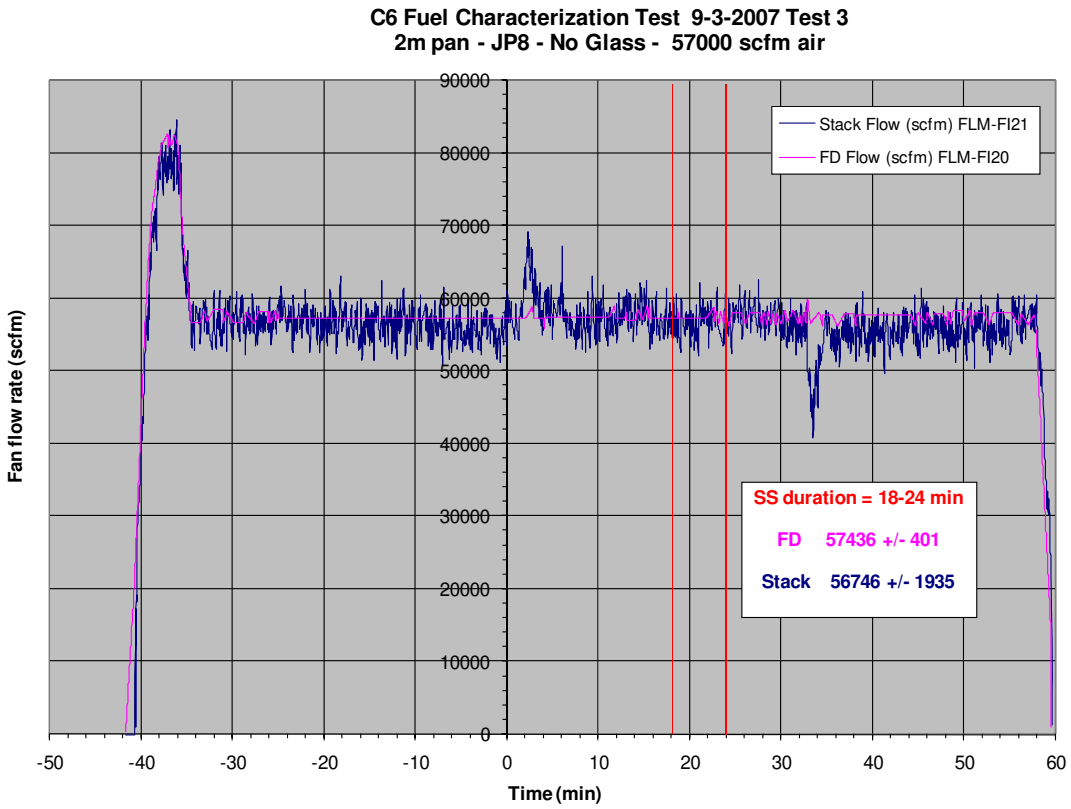

Figure 31 Facility air flow during test #24.

Pressure, Temperature, and Relative Humidity

The ambient pressure ranged from 24.52 - 24.89 inch HG. The combustion inlet air temperature ranged from 23 – 34ºC. The relative humidity ranged from 9 – 71% RH. The initial FLAME wall temperature ranged from 26 - 30ºC. The initial liquid fuel temperature ranged from 26 - 41ºC. Note Table 1 presents the initial and boundary condition values for each test.

Uncertainty - Air Flow Rate and Temperature

The air flow rate is measured by a Veltron II pressure and flow transmitter (Air Monitor Corporation, Santa Rosa, CA). The Veltron II calculates the air velocity and flow rate based on a differential pressure measurement. The differential pressure is measured to an accuracy of 0.1% of the natural span of the transmitter (10 inches of water). The uncertainty in the velocity due to the differential pressure uncertainty is approximately ±3% at the chosen flow rate of 150,000 scfm. When the uncertainties due to non-uniformity in the velocity profile, tolerances on the duct dimensions, etc. are included the total uncertainty is estimated to be approximately ±6% of the total flow rate.

Air temperature measurements are performed by thermocouples similar to those used in the liquid fuel measurements. The air temperature measurements are made inside a duct in a

relatively cool environment in which convective heat transfer from the air to the thermocouple is expected to dominate, therefore the uncertainty in the air temperature is assumed to be the same as the uncertainty in the fuel temperature measurements, ±3ºC.

The temperatures of the steel walls inside the FRH chamber (Figure 32) are measured by thermocouples mounted at heights of 1 ft (30 cm), 10 ft (3.04 m), 20 ft (6.08 m), 30 ft (9.12 m), and 39 ft (12.16 m) above the steel grating. The thermocouples are shielded from the radiation from the fire and the convective flow of the coflow air by a small piece of metal foil to minimize bias errors in the wall temperature measurement. These measurements are duplicated at four equally-spaced angular locations around the facility. The wall temperature measurements are of interest for imposed boundary conditions in validation simulations. During a test, there is no active cooling of the water-filled walls. After each test, a cooling system is activated that recirculates the water until the temperature returns to a nominal 28ºC.

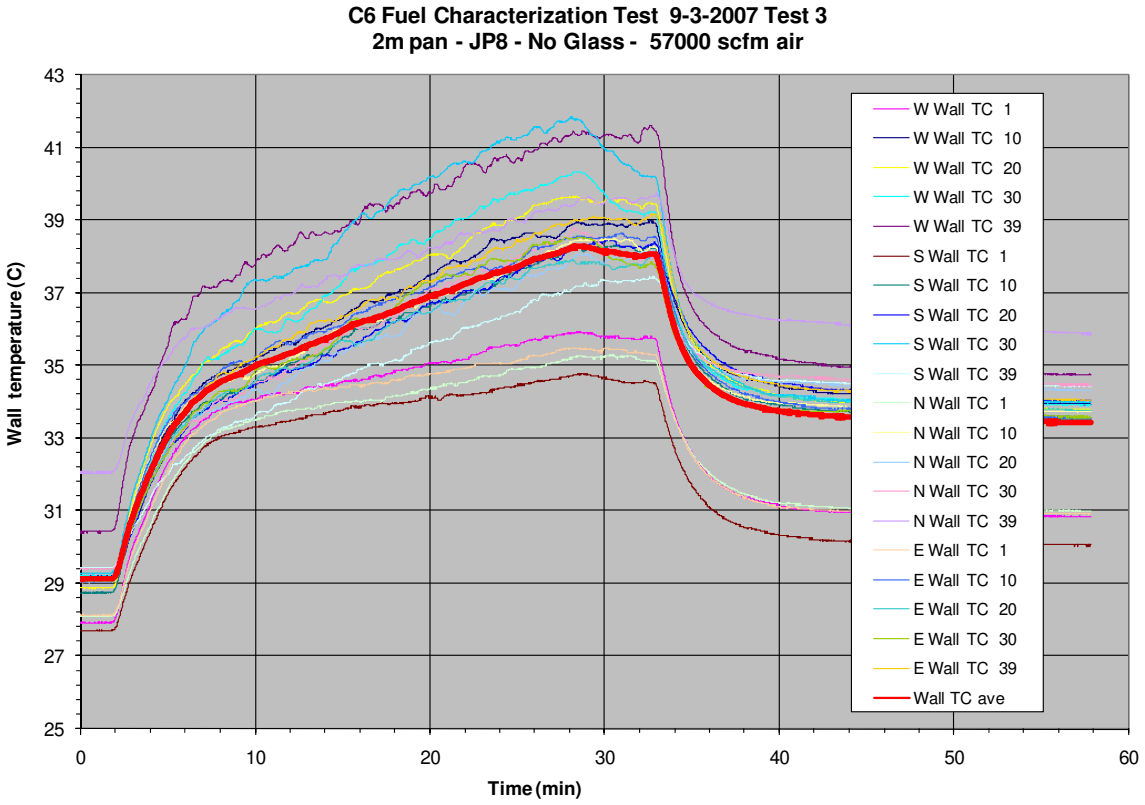

Figure 32 Wall temperatures during test #24.

Uncertainty – Wall Temperatures

Wall temperature measurements are made by thermocouples mounted to the steel walls of the FRH chamber. The thermocouples are in good thermal contact with the walls, which have a very high thermal conductivity. The thermocouples are partially shielded from the radiation of the fire and convection from the cool coflowing air. Previous experience has shown that the walls remain relatively cool during tests due to their large thermal mass. The analysis of Nakos [2004]

suggests that the maximum error is ±1% of the reading (in K) for temperatures up to 400K. An uncertainty of ±4ºC is assumed for the wall temperatures in the present tests.

4.1.7 Median Flame Height

Two video cameras, one located inside the test cell and one located inside a port of the cell, were used to view the flame height. Prior to the test series both cameras were calibrated using a stadia board located at and above the pool centerline. The board was marked with major units at 1 m intervals and minor units at 0.1 m intervals. Figure 33 shows the stadia hanging from a man lift at 2 positions to capture the full field of view for the inside camera. Figure 34 shows the curve fit and residuals for the inside camera; the largest residuals of ~0.05 m occurred at the ~10 m height. A similar method was used to calibrate the port camera. The use of the stadia provided a calibrated full field of view of 14.1 m for the inside camera and 5.8 m for the port camera.

Figure 33 Stadia frames for the inside camera view.

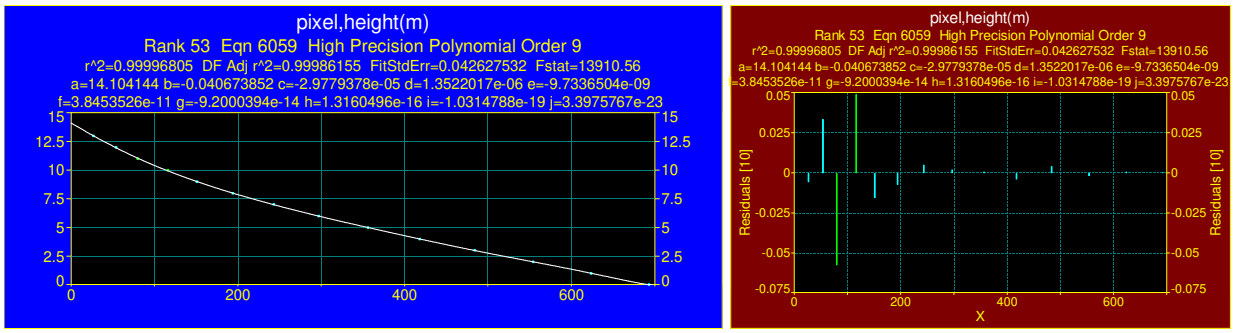

Figure 34 Curve fit and residuals for the inside camera view.

For each test, one minute of video (1800 frames), starting at the beginning of the steady-state time period listed in Table 1, was analyzed to determine the median flame height and the puffing frequency. To automate the process, imaging analyses software (ImagePro®) was used to provide the average pixel intensity for a 1/3 radius wide vertical line drawn through the pool centerline. Figure 35 illustrates the process, showing the average color pixel intensity as a function of vertical height (720 pixels tall).

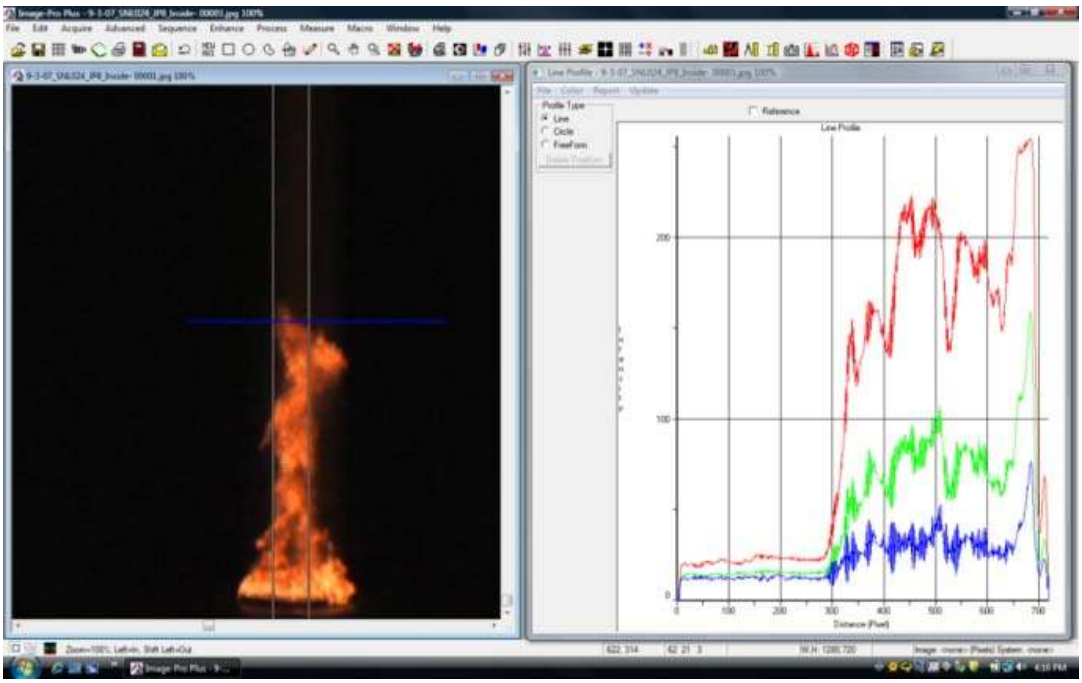

Figure 35 Intensity vs. height (line profile) for image in test#24.

It was necessary to determine the threshold intensity to be used for each test, which changed due to differences in flame color (for example, methanol yielded a blue flame) and camera settings. A Fortran routine was used to process the vertical line profile intensity of the 1800 frame dataset, varying the threshold intensity from 0 to 255. The result is shown in Figure 36 for test #24. The shape of the resulting profile is similar for the other tests. As the threshold intensity increases, a sharp drop followed by a "knee" occurs at the flame top. As the threshold intensity increases, the estimated flame height gradually decreases as the line profile progresses further down into the flame. The actual intensity used in the analysis is chosen by inspection, within ~5 units of intensity above the knee (as depicted in Figure 36). Figure 37 shows the vertical line profiles for all tests yielding the median height as a function of threshold intensity.

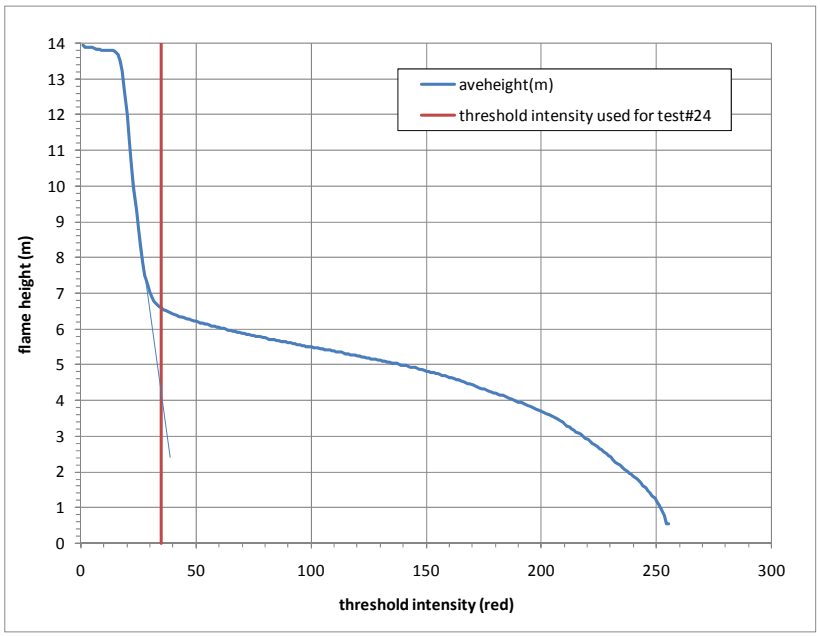

Figure 36 Test 24 dataset average flame height as a function of threshold intensity.

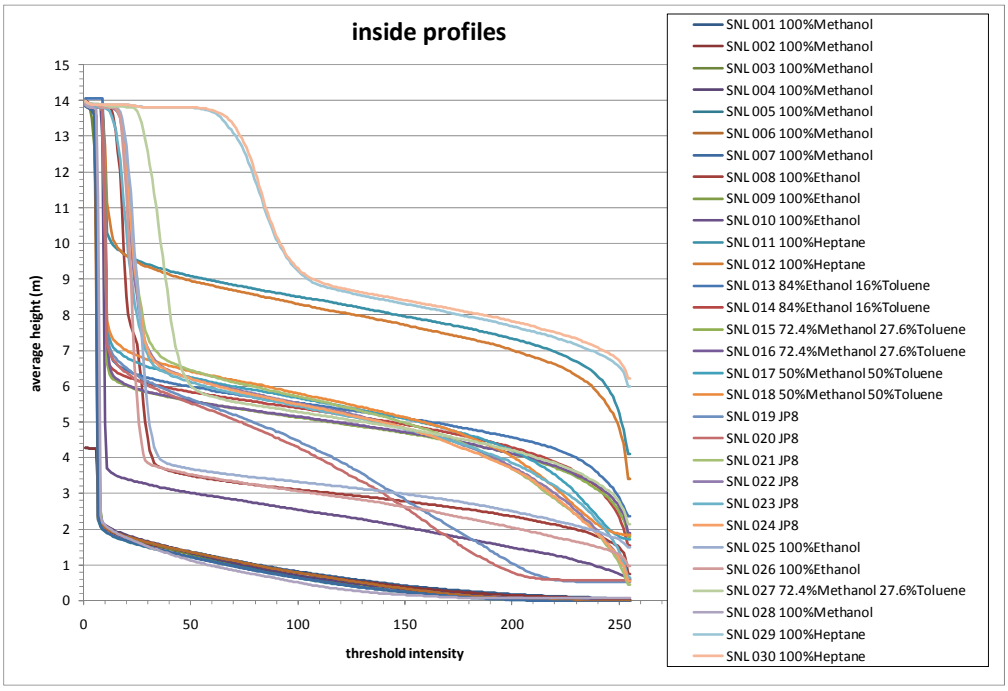

Figure 37 Average flame height as a function of threshold intensity – all datasets.

With the determination of the threshold intensity, the flame height statistics can be determined. Figure 38 shows the flame height for each frame of the test #24 dataset using a threshold intensity of 35 (red). The median flame height (where the height is above and below 50% of the time) was determined to be 6.6 m with a standard deviation of 1.1 m. Fourier analysis, with the results depicted in Figure 39, determined a puffing frequency of 1.3 Hz.

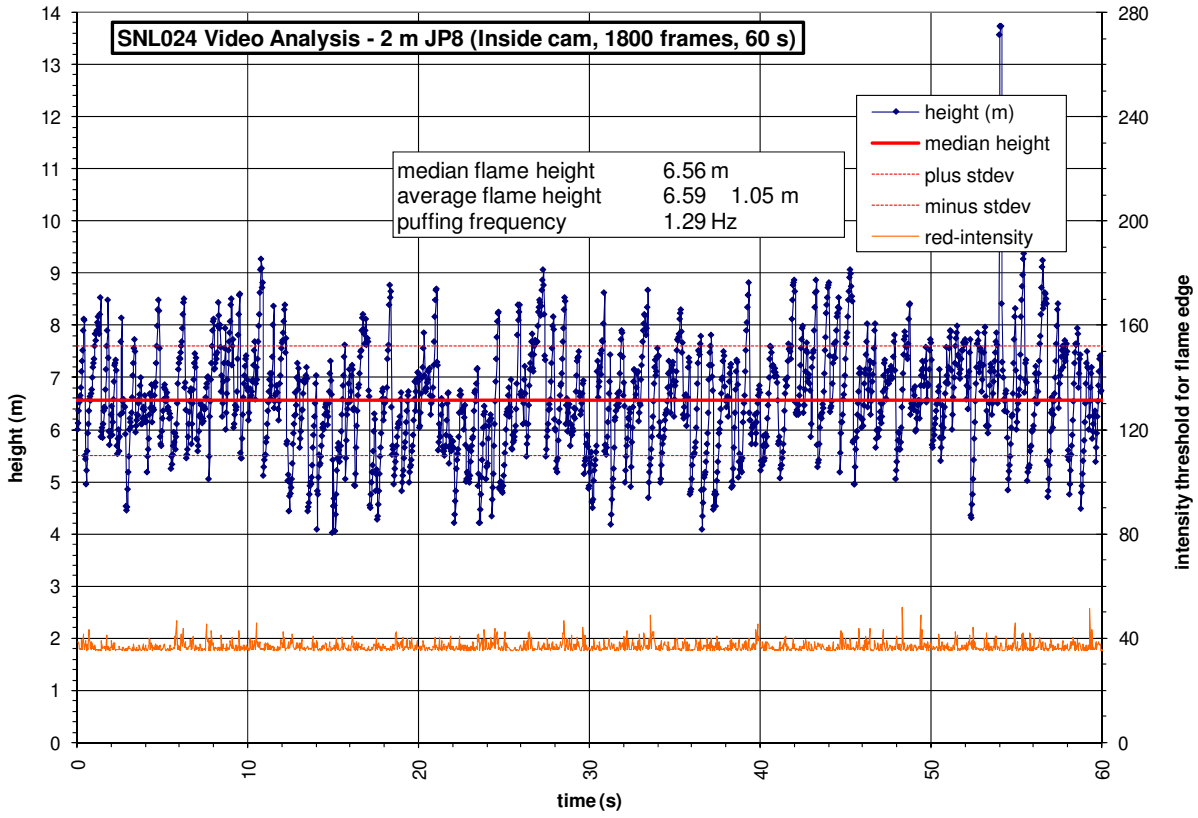

Figure 38 Test 24 median fame height (threshold intensity = 35).

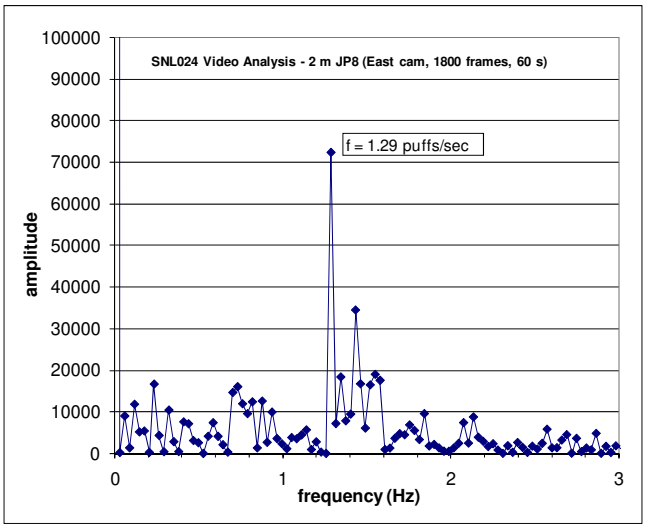

Figure 39 FFT to Determine Puffing Frequency for Test 24.

Table 9 summarizes the camera analyses for each test, providing the puff frequency, median and average flame heights and the standard deviation for the listed threshold intensity. With the smaller field of view, the port camera was over ranged for most of the fuels except for methanol and ethanol.

Table 9 Camera Analyses

Date	Test#	Fuel:	Inside Camera					Port Camera				
			Flame Threshold Intensity and color	Puffing Hz	Median Height (m)	Average Height (m)	Std. Dev. (m)	Flame Threshold Intensity and color	Puffing Hz	Median Height (m)	Average Height (m)	Std. Dev. (m)
8/3/2007	SNL **001**	100%Methanol	11, blue	0.94	1.98	2.03	0.51	na				
8/3/2007	SNL **002**	100%Methanol	11, blue	0.94	1.99	1.94	0.46	na				
8/15/2007	SNL **003**	100%Methanol	11, blue	0.97	1.98	2.02	0.50	na				
8/16/2007	SNL **004**	100%Methanol	11, blue	0.94	2.05	2.07	0.53	na				
8/19/2007	SNL **005**	100%Methanol	10, blue	0.94	1.92	1.93	0.45	10, blue	0.94	2.26	2.30	0.50
8/19/2007	SNL **006**	100%Methanol	10, blue	0.94	2.00	2.04	0.45	10, blue	0.94	2.18	2.23	0.47
8/20/2007	SNL **007**	100%Methanol	10, blue	0.94	1.90	1.94	0.48	10, blue	0.94	2.14	2.19	0.51
8/20/2007	SNL **008**	100%Ethanol	35, blue	1.00	3.61	3.74	0.76	25, blue	1.00	3.79	3.87	0.77
8/21/2007	SNL **009**	100%Ethanol	na		na	na	na	15, red	0.97	3.33	3.35	0.67
8/22/2007	SNL **010**	100%Ethanol	13, red	0.97	3.55	3.59	0.80	15, red	0.97	3.39	3.42	0.70
8/26/2007	SNL **011**	100%Heptane	13, red	1.00	10.04	10.04	1.31	120, red		over range		
8/28/2007	SNL **012**	100%Heptane	15, red	1.29	10.01	9.97	1.18	115, red		over range		
8/28/2007	SNL **013**	84%Ethanol 16%Toluene	15, red	1.29	6.58	6.65	1.12	131, red		over range		
8/29/2007	SNL **014**	84%Ethanol 16%Toluene	15, red	1.29	6.32	6.42	1.12	132, red		over range		
8/29/2007	SNL **015**	72.4%Methanol 27.6%Toluene	15, red	1.29	6.10	6.16	1.20	132, red		over range		
8/30/2007	SNL **016**	72.4%Methanol 27.6%Toluene	15, red	1.29	6.07	6.23	1.25	129, red		over range		
8/30/2007	SNL **017**	50%Methanol 50%Toluene	15, red	1.29	6.92	7.03	1.26	127, red		over range		
8/30/2007	SNL **018**	50%Methanol 50%Toluene	15, red	1.29	7.15	7.25	1.30	121, red		over range		
8/31/2007	SNL **019**	JP8	15, red	1.29	6.73	6.81	1.01	74, red		over range		
9/1/2007	SNL **020**	JP8	15, red	1.29	6.65	6.67	1.00	72, red		over range		
9/1/2007	SNL **021**	JP8	35, red	1.29	6.88	6.90	1.20	69, red		over range		
9/3/2007	SNL **022**	JP8	35, red	1.29	6.50	6.61	1.19	66, red		over range		
9/3/2007	SNL **023**	JP8	35, red	1.29	6.45	6.49	0.98	57, red		over range		
9/3/2007	SNL **024**	JP8	35, red	1.29	6.56	6.59	1.05	52, red		over range		
9/4/2007	SNL **025**	100%Ethanol	13, red	0.97	3.77	3.83	0.85	45, red	1.29	3.21	3.26	0.71
9/4/2007	SNL **026**	100%Ethanol	32, red	1.00	3.77	3.79	0.89	35, red	1.29	3.18	3.21	0.67
9/5/2007	SNL **027**	72.4%Methanol 27.6%Toluene	50, red	1.29	5.82	6.02	1.57	56, red		over range		
9/5/2007	SNL **028**	100%Methanol	10, blue	0.94	2.06	2.11	0.49	na				
9/6/2007	SNL **029**	100%Heptane	95, red	1.29	9.32	9.61	1.81	132, red		over range		
9/6/2007	SNL **030**	100%Heptane	95, red	1.29	9.40	9.66	1.75	123, red		over range		

Table 10 provides the average of the median flame height and puff frequency for each fuel type arranged in order of total HRR, which almost orders the flame height (low to high). Methanol had the lowest flame height (2.0 ± 0.1 m) and heptane the tallest ((9.7 ± 0.4 m).

The puffing frequency (Table 10) for the lightly sooting methanol and ethanol fuels ranged from 0.9 to 1.1 Hz, with the frequency increasing to 1.2-1.3 Hz for the heavier sooting fuels.

Table 10 Fuel Flame Median Height and Puffing Frequency

Fuel	Median Height (m)		Puffing HZ		Median Height (m)	% difference	Q_{total} (MW)
	Average	Std. Dev.	Average	Std. Dev.	correlation		
100%Methanol	2.0	0.1	0.9	0.0	2.0	2.3	1.2
100%Ethanol	3.5	0.2	1.1	0.1	3.2	-9.6	2.1
72.4%Methanol 27.6%Toluene	6.0	0.2	1.3	0.0	4.7	-21.5	3.8
84%Ethanol 16%Toluene	6.5	0.2	1.3	0.0	4.8	-26.5	4.4
50%Methanol 50%Toluene	7.0	0.2	1.3	0.0	5.5	-21.7	5.2
JP8	6.6	0.2	1.3	0.0	5.2	-21.6	5.4
100%Heptane	9.7	0.4	1.2	0.1	6.7	-30.5	8.7

The following flame height (in m) correlation developed by Heskestad (HRR_{m_b} in kW and D_{pool} in m) has been used for different fuels over a wide range of pool fire sizes:

$$H_{flame} = 0.235\left[HRR_{m_b}\ x1000\right]^{2/5} - 1.02D_{pool}$$

Table 10 also shows the flame height prediction and the % difference from measured values. SFPE [2002] notes that the Heskestad correlation used with spill fire data yields predicted heights that are ~17% low compared to the measured spill fire flame heights. Figure 40 plots the measured vs. correlations median flame height values.

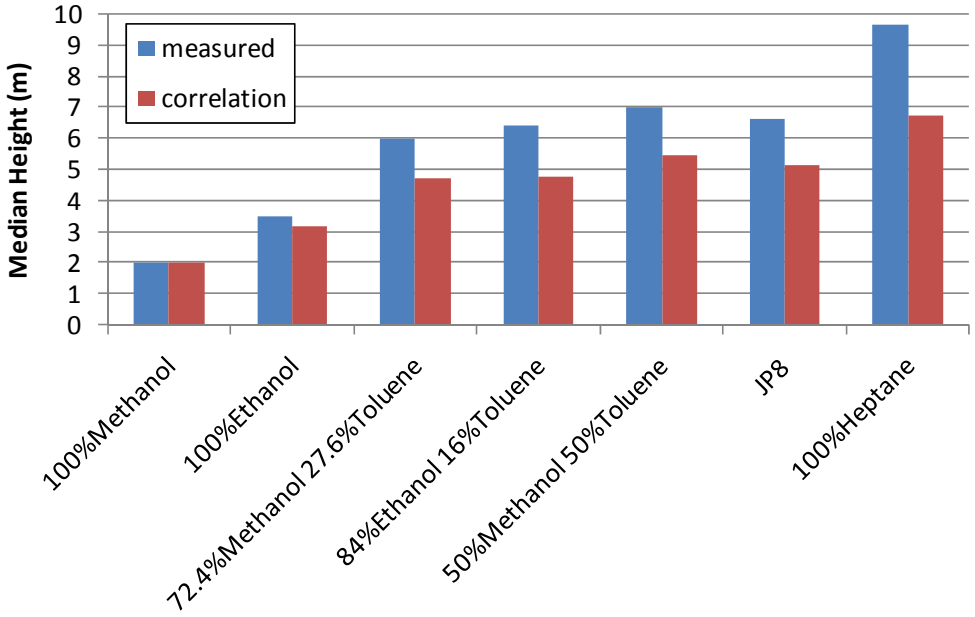

Figure 40 Flame height – measured vs. correlation values.

Uncertainty - Average Flame Height

Uncertainty in the actual height of the visible flame in an individual image is estimated to be approximately 10 cm. Uncertainty in determination of the average flame height based on a minimum of 1000 video frames is assumed to be equal to the uncertainty in determining the height of the flame within the frame.

4.1.8 Wall Heat Flux and Surface Emissive Power

Eight narrow-angle radiometers and eight total heat flux gauges measured the surface emissive power (SEP) radiation and the incident heat flux; respectively, from the flame plume as a function of height. Pairs of gauges, a narrow-angle radiometer (ZnSe window) (Medtherm model NVRW-15-5-360-2183, 5º view angle, range of 140 kW/m^2) and a total (windowless) heat flux gauge (Medtherm model 64-2-18 with a view angle of 180º, range of 15 kW/m^2), were mounted together near the FLAME wall at a distance of 28.64 ft. (8.73 m) from the center of the fire. The spot diameter for the narrow-angle gauges (at 9 m) is about 0.8 m. The gauge pairs were at heights of ~0.5 m to 4.0 m with a spacing of ~0.5 m between gauges. The line of sight for each gauge was set to pass through the centerline of the fire at the height of the gauge. All of the heat flux gauges are water-cooled.

Figures 41 and 42 present the measured wall total heat flux and flame surface emissive power, respectively, as a function of vertical height above the fuel pan in Test 24.

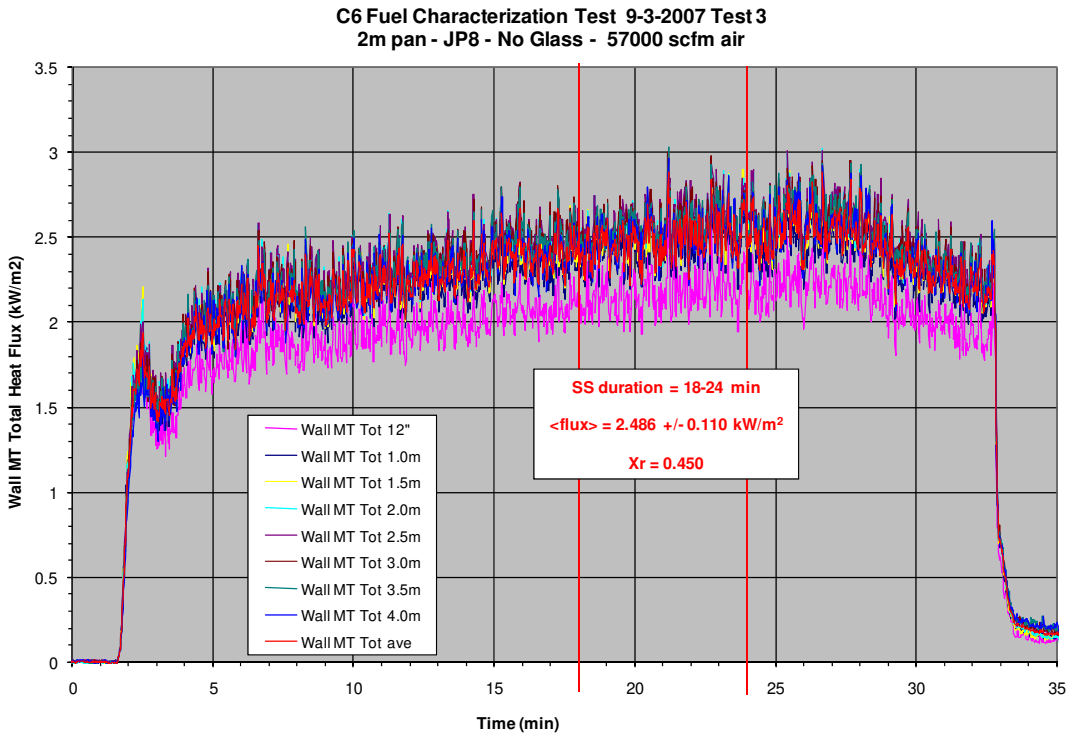

Figure 41 Measured wall heat flux in Test 24.

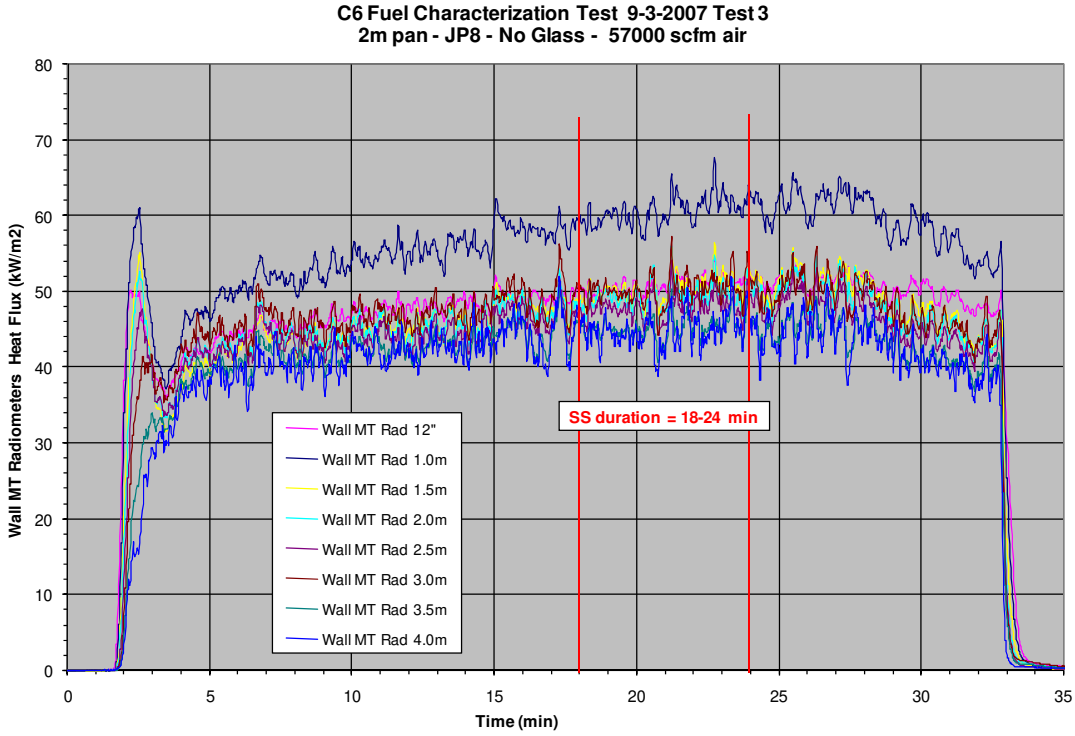

Figure 42 Measured flame surface emissive power in Test 24.

Figure 43 presents the average SEP during the SS duration for selected tests. The figure also shows the slight variation in position of the gauges from the nominal positions. Note that the lowest locations (0.32 m) may be clipping the view of the flame plume and seeing part of the fuel pan and floor, as the spot radius is ~0.4 m. Also, the SEP decreases dramatically for those gauges with a field of view above the median plume heights (in addition to those low sooting fuels), as shown for the 100% and 72% methanol and 100% ethanol tests.

Table 1 presents the average heat flux at the wall as measured by the total heat flux gauges.

Uncertainty - Incident Radiation on Objects outside the Fire

The uncertainty in the measurement is the total uncertainty in the radiometer calibration. A typical radiative heat flux calibration uncertainty of ±3% is assumed.

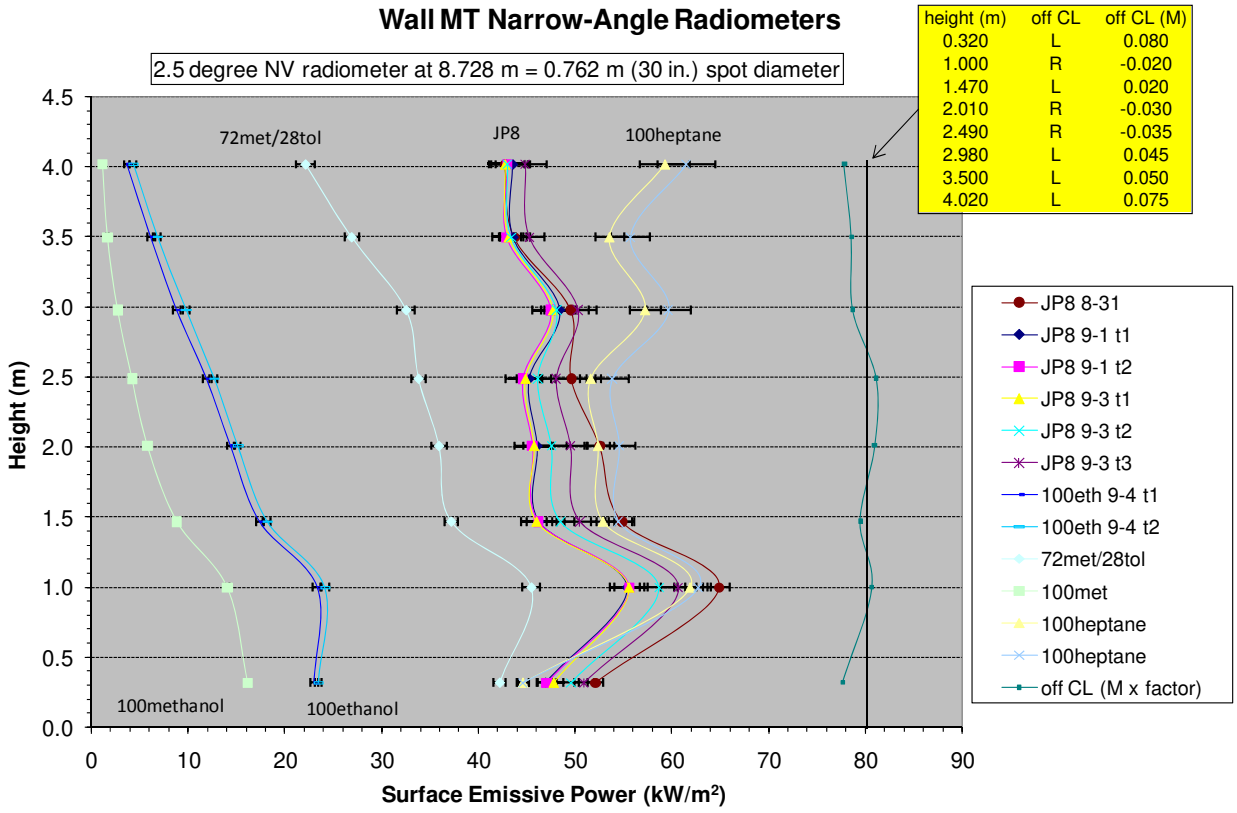

Figure 43 Surface emissive power as a function of height.

4.1.9 Composition of Combustion Gas Products in Overfire Region

The composition of the combustion products above the fire was monitored using a Combustion Gas Analyzer (CGA) sampling the exhaust duct approximately 97 ft downstream of the duct

entrance in the ceiling if the test cell. The CGA (Land Instruments International, model FGA II) measures the concentrations of CO, CO_2, O_2, NO, NO_2, NO_x, and SO_2.

Figure 44 shows the oxygen decreased from 20.8% to 19.8% during the steady-state period in test #24, resulting in a total decrease of oxygen of 9390 ± 174 ppm. Correspondingly, the carbon dioxide content increased by 7459 ± 140 ppm. Figure 45 shows the measured changes in trace gases. Similar figures (not shown) were generated for each test. Table 11 presents the measured change in O2 and CO2 for all tests. These data were used in heat release rate (HRR) analyses presented in Section 5.

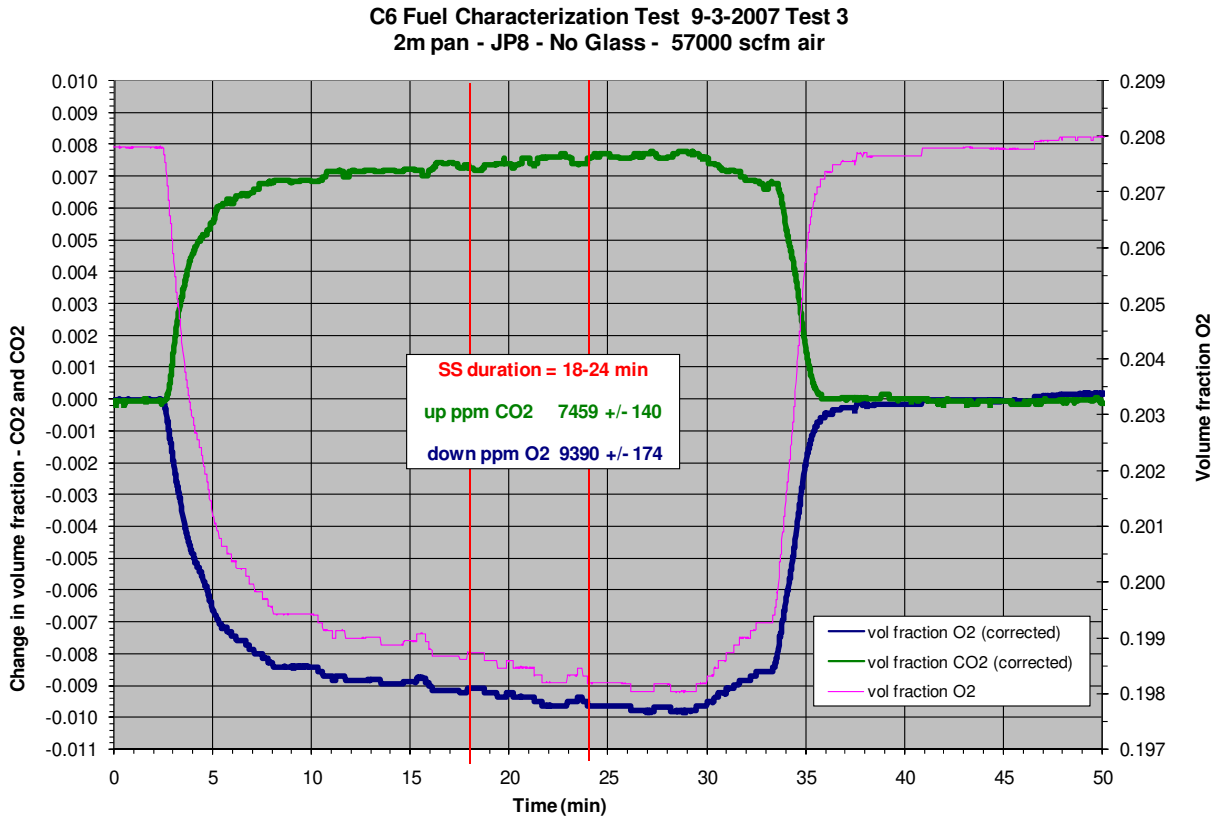

Figure 44 Measured Changes (ppm) in O2 and CO2 in Test 24.

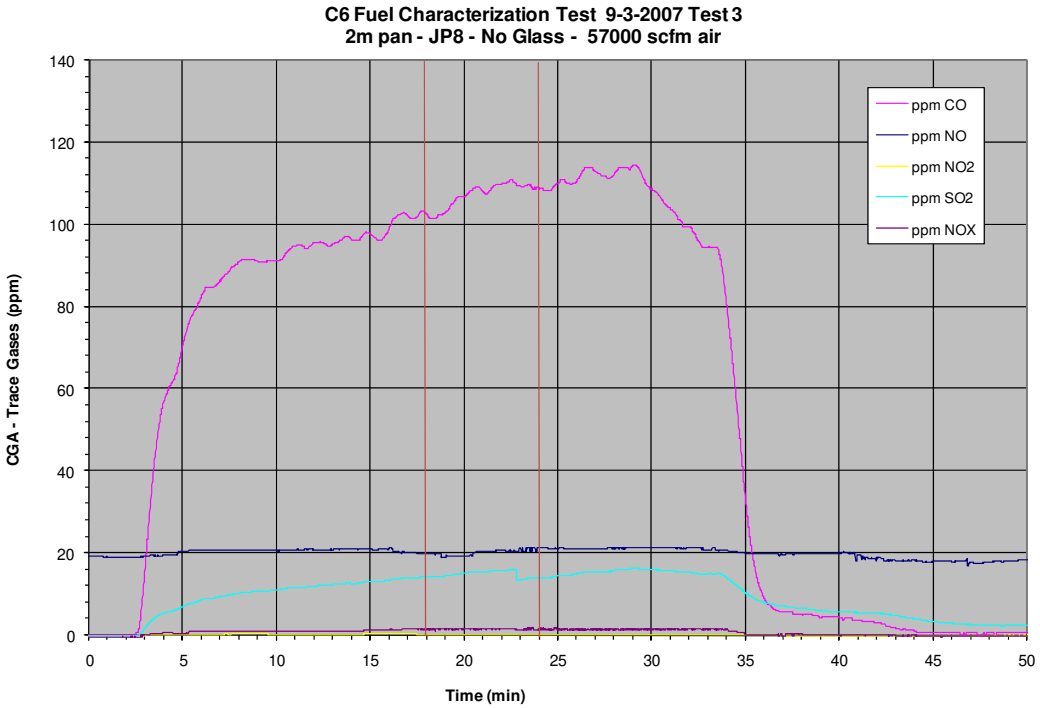

Figure 45 Trace gas concentrations in test 24.

Table 11 Measured Changes in O2 and CO2 for all tests.

SNL Hydrocarbon Fuel Fire Characterization - COMPILED RESULTS																
Date	Test	Glass Beads	Fuel:	O2 decrease (ppm)	O2 decrease (ppm)	CO2 increase (ppm)	CO2 increase (ppm)	O2 decrease (kg/s)	O2 decrease (kg/s)	CO2 increase (kg/s)	CO2 increase (kg/s)	air (kg/s)	HRR-O2	HRR-O2	HRR-CO2	HRR-CO2
-	#		-	average	std.dev.	average	std.dev.	average	std.dev.	average	std.dev.	average	average	std.dev.	average	std.dev.
8/3/2007	SNL 001	No	100%Methanol	2309	31	2326	54	0.081	0.001	0.114	0.003	32.7	1.09	0.02	1.65	0.04
8/3/2007	SNL 002	No	100%Methanol	2317	5	2628	53	0.084	0.000	0.116	0.003	32.7	1.13	0.00	1.68	0.04
8/15/2007	SNL 003	No	100%Methanol	2495	9	2352	81	0.090	0.001	0.117	0.004	32.7	1.21	0.01	1.70	0.06
8/16/2007	SNL 004	No	100%Methanol	2395	43	2483	47	0.087	0.002	0.118	0.002	32.6	1.17	0.02	1.72	0.03
8/19/2007	SNL 005	Yes	100%Methanol	2458	22	2380	47	0.089	0.001	0.118	0.003	32.6	1.19	0.02	1.71	0.04
8/19/2007	SNL 006	Yes	100%Methanol	2457	38	2398	36	0.089	0.001	0.119	0.002	32.8	1.19	0.02	1.73	0.03
8/20/2007	SNL 007	Yes	100%Methanol	2459	15	2419	54	0.089	0.001	0.120	0.000	32.7	1.19	0.01	1.74	0.04
8/20/2007	SNL 008	Yes	100%Ethanol	4251	94	3825	60	0.153	0.003	0.190	0.003	32.7	2.03	0.04	2.75	0.05
8/21/2007	SNL 009	Yes	100%Ethanol	4435	47	3877	83	0.158	0.002	0.193	0.004	32.7	2.12	0.02	2.80	0.06
8/22/2007	SNL 010	Yes	100%Ethanol	4379	86	3691	98	0.158	0.004	0.183	0.005	32.7	2.09	0.05	2.66	0.08
8/26/2007	SNL 011	Yes	100%Heptane	16485	275	12131	165	0.594	0.012	0.601	0.009	32.6	7.55	0.15	8.72	0.14
8/28/2007	SNL 012	Yes	100%Heptane	16930	505	12591	305	0.610	0.017	0.624	0.015	32.6	7.75	0.22	9.05	0.22
8/28/2007	SNL 013	Yes	84%Ethanol 16%Toluene	8424	87	7153	112	0.304	0.004	0.355	0.006	32.7	4.00	0.05	5.00	0.09
8/29/2007	SNL 014	Yes	84%Ethanol 16%Toluene	8299	63	7270	44	0.299	0.004	0.361	0.004	32.7	3.94	0.06	5.08	0.06
8/29/2007	SNL 015	Yes	72.4%Methanol 27.6%Toluene	7438	41	6507	45	0.269	0.003	0.324	0.004	32.7	3.57	0.04	4.46	0.06
8/30/2007	SNL 016	Yes	72.4%Methanol 27.6%Toluene	7294	33	6707	38	0.263	0.003	0.333	0.004	32.7	3.49	0.04	4.60	0.05
8/30/2007	SNL 017	Yes	50%Methanol 50%Toluene	9213	215	8429	157	0.332	0.009	0.409	0.010	32.7	4.37	0.12	5.42	0.13
8/30/2007	SNL 018	Yes	50%Methanol 50%Toluene	9648	67	8436	55	0.347	0.005	0.418	0.005	32.6	4.56	0.06	5.53	0.07
8/31/2007	SNL 019	Yes	JP8	10156	95	7914	99	0.366	0.006	0.392	0.007	32.6	4.65	0.07	5.53	0.09
9/1/2007	SNL 020	Yes	JP8	9411	56	7574	89	0.341	0.003	0.377	0.006	32.8	4.33	0.04	5.32	0.09
9/1/2007	SNL 021	Yes	JP8	9791	153	7686	126	0.352	0.007	0.381	0.008	32.6	4.48	0.09	5.37	0.11
9/3/2007	SNL 022	No	JP8	8839	156	7246	122	0.320	0.006	0.361	0.007	32.8	4.07	0.08	5.09	0.09
9/3/2007	SNL 023	No	JP8	9495	173	7532	136	0.344	0.006	0.375	0.008	32.8	4.37	0.08	5.29	0.11
9/3/2007	SNL 024	No	JP8	9390	174	7459	140	0.339	0.008	0.370	0.008	32.7	4.31	0.12	5.22	0.10
9/4/2007	SNL 025	No	100%Ethanol	3974	55	3754	85	0.144	0.002	0.186	0.005	32.7	1.89	0.03	2.70	0.07
9/4/2007	SNL 026	No	100%Ethanol	4057	63	3760	80	0.146	0.003	0.187	0.004	32.7	1.93	0.03	2.70	0.06
9/5/2007	SNL 027	No	72.4%Methanol 27.6%Toluene	7140	105	6567	93	0.258	0.005	0.327	0.006	32.8	3.43	0.07	4.51	0.09
9/5/2007	SNL 028	No	100%Methanol	2479	55	2388	32	0.089	0.002	0.118	0.002	32.6	1.20	0.03	1.71	0.03
9/6/2007	SNL 029	No	100%Heptane	14895	192	10989	196	0.544	0.009	0.551	0.010	33.1	6.90	0.12	8.00	0.14
9/6/2007	SNL 030	No	100%Heptane	15717	88	11770	61	0.569	0.010	0.587	0.009	32.8	7.23	0.12	8.51	0.14

Uncertainty - Combustion Gas Products Composition

Specifications of the CGA:

Measurement Ranges
CO Ranges: 0 - 10 ppm up to 0 - 40 000 ppm (4 %)
NO Ranges: 0 - 10 ppm up to 0 - 50 000 ppm (5 %)

NO2 Ranges: 0 - 10 ppm up to 0 - 1 000 ppm (0.1 %)
SO2 Ranges: 0 - 10 ppm up to 0 to 10 000 ppm (1 %)
CO2 Ranges: 0 - 3 Vol % up to 0 - 100 Vol %

Resolution: 0.1 ppm (CO, NO, NO2 & SO2); 0.1 % (CO2)

O2 Ranges: 0 - 5 Vol % to 0 - 25 Vol %
Resolution: 0.01 Vol %

The CGA resolves the concentrations of minor species CO, NO, NO_2, SO_2 to 0.1 ppm. Concentration of CO_2 is resolved to 1000 ppm and O_2 is resolved to 100 ppm. Uncertainties for all species except O_2 are a function of the user-specified total range for that species. The uncertainties are given as ±2% of the range for the calibration linearity, with additional components for zero drift and span drift over time. The uncertainty due to calibration is a fixed ±2000 ppm for O_2. The drift contributions become comparable to the linearity contributions after approximately one month between calibrations. For the present work the overall uncertainties is assumed to be ±3000 ppm for O_2 and ±3% of the full range for each of the remaining species.

4.1.10 Soot Extinction Measurements

Laser extinction measurements similar to those taken at the old FLAME facility [Jensen and Brown, 2004] were taken near the CGA and provide an estimate of the soot concentration, further extending the knowledge of the combustion products in the over-fire region. The temperature of the exhaust gases was measured by a thermocouple close to the soot probe and CGA locations in the exhaust duct.

A 2 inch diameter stainless steel tube was installed across the nine foot wide exhaust duct (north-south side), mounted in the duct in a manner that would allow it to expand as it heated to minimize the effect on the laser signals. The tube was positioned at the centerline of the 7 ft long duct (east-west side) about 1 foot below the CGA suction probe located on the north wall. The tube had a center slot (1 inch wide, 24 inches long) in line with the duct flow to allow combustion soot products to pass through the slot (note flow direction is down). A small house-air gas purge (~30 ml/min) was used at both laser and detector sides of the tube to prevent soot deposition on the optics. The purge flow rate was low enough to not have a measurable effect on the optical path length through the smoke. A 1mW HeNe laser (providing a 632.8 nm light source) was mounted to one end of the tube. The beam was split; one path went directly to a photodiode detector mounted near the laser for use as a reference signal, the other path went through the tube to for use as the soot extinction signal line. The analyses to determine the soot concentration is discussed in section 5.

5. COMPILED RESULTS AND ADDITIONAL ANALYSES

5.1 Estimates of the Heat Release Rate

The total heat release rate (in MW) can be estimated from the mass burning rate ($\dot{m}_b$ in g/s) and the heat of combustion (Δh_c in kJ/kg) for the fuel.

$$Q_{total} = HRR_{m_b} = \dot{m}_b \, \Delta h_c / 10^6 \tag{3}$$

The chemical heat release rate can also be calculated using the combustion gas measurements in the over fire region. First, the mass flow rate (in kg/s) of combustion air is estimated, based on the measured volumetric flow rate (using the FD fan data in units of scfm) and density of standard air (1.206 kg/m^3).

$$\dot{m}_{air} = \dot{V}_{air} \, \rho_{air} \frac{(0.3048 m / ft)^3}{60 s / \min} \tag{4}$$

Next, the mass flow rate (in kg/s) of oxygen consumed and carbon dioxide produced must be estimated, based on the respective molecular weights (32 g/mol oxygen, 28.97 g/mol carbon dioxide) and the respective fractional change in volume concentrations (shown in Figure 44).

$$\dot{m}_{O_2} = \frac{MW_{O_2}}{MW_{air}} \dot{m}_{air} f_{v_{O_2}} \tag{5}$$

$$\dot{m}_{CO_2} = \frac{MW_{CO_2}}{MW_{air}} \dot{m}_{air} f_{v_{CO_2}} \tag{6}$$

Finally, the *chemical* heat release rate $Q_{chemical}$ or $HRR_{chemical}$ (in MW) can be determined, estimated from the respective consumption and production of oxygen and carbon dioxide and the heats of combustion (oxygen: 12700 kJ/kg, carbon dioxide: 14100 kJ/kg).

$$HRR_{O_2} = \dot{m}_{O_2} \, \Delta h_{O_2} / 10^3 \tag{7}$$

$$HRR_{CO_2} = \dot{m}_{CO_2} \, \Delta h_{CO_2} / 10^3 \tag{8}$$

Figure 46 shows the time-dependent changes in Test #24 on oxygen consumption and carbon dioxide mass flow rates, and the combustion air, as calculated using Equations 4-6. Figure 47 presents the calculated heat release rates for Test #24. The chemical heat release rates should be less than the total heat release rates, increasingly so as the soot content increases. The calculated chemical heat release rate based on the CO_2 production in the same range as the total heat release rate indicates a suspect measurement.

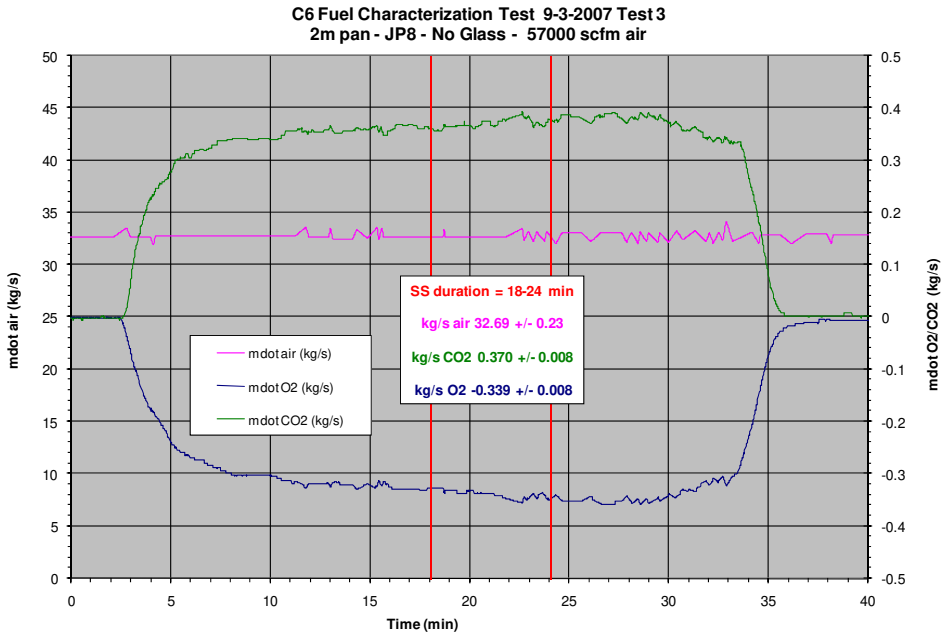

Figure 46 Calculated Changes (mass) in O2 and CO2 in Test 24.

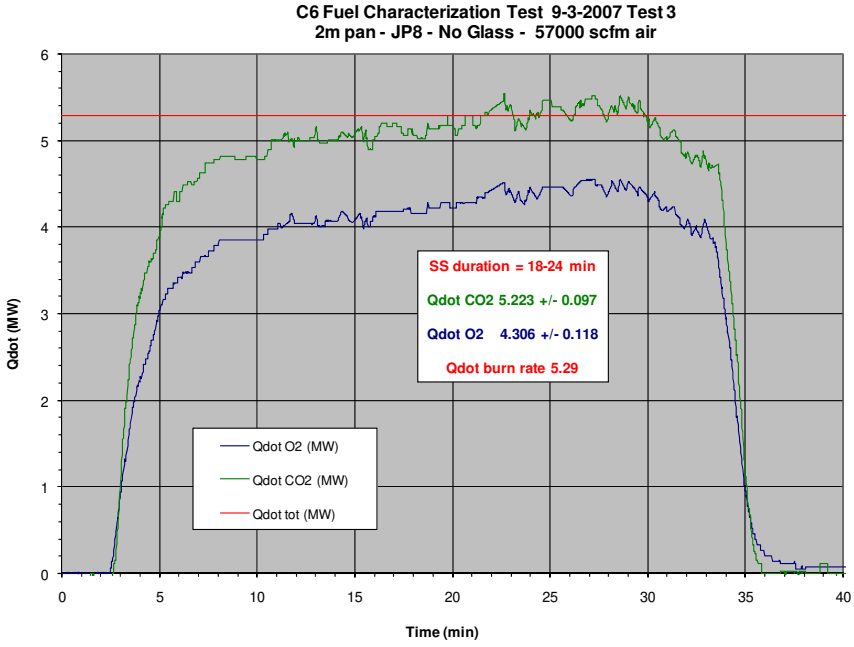

Figure 47 Calculated Heat Release Rates based on O2 and CO2 in Test 24.

5.2 Concentration of Soot Products in Overfire Region

Bouguer's law relates the laser attenuation to the volume fraction of soot in the chimney [Modest, 1993][Siegel and Howell, 1992]

$$\frac{I(\lambda)}{I_o(\lambda)} = e^{-K_e(\lambda)\frac{f_v}{\lambda}L} \tag{9}$$

where *I* and *Io* are the attenuated and incident laser intensity, *L* is the optical path length, λ is the wavelength, and *Ke* and *fv* are the dimensionless extinction coefficient and volume fraction of soot, respectively. The accuracy of the light extinction technique, therefore, depends on an appropriate value of *Ke*. A wide range of experimentally determined values of *Ke* have been reported recently18-25 for a variety of flame conditions and fuels at 632.8 nm, with the most common values in the 8-10 range. Jensen et al. [2004, 2007] measured the dimensionless extinction coefficient of soot in the flame zone and overfire regions of the JP-8 pool fires simultaneously with these soot yield experiments. They used extractive sampling combined with a portable light extinction and gravimetric sampling diagnostic that was calibrated with an aerosol of known optical properties. Their measured *Ke* value of 8.4 ± 1.2 at 635 nm (95% confidence) was used in this study when applying Equation (9) to determine *fv*. (The large 2-standard deviation uncertainty interval in *Ke* was mostly due to fluctuations in the fires.) The combined Type B (i.e., systematic) uncertainty of their diagnostic was reported as 11.9%.

Figure 48 shows the laser traces from the reference detector (soot reference trace) and receiving detector (soot signal trace) for Test #24. After the test, it was noted that there was a small change in the difference between the soot reference signal and the soot signal. For the analysis, this small difference was corrected (simple interpolation between pretest and posttest values) when adjusting the reference signal to soot value seen just prior to ignition. For analysis purposes, the background laser intensity, *Io*, was the trace labeled as soot ref bias and the attenuated laser intensity, *I*, was the trace labeled as soot signal. For each fire, Equation 9 was solved to yield a time-dependent soot volume fraction (in ppm units) as shown in Figure 48. The constants *Ke* = 8.4, λ (m) = 6.35E-07, and *L* (m) = 0.6096 was used for all tests.

Soot production rate (g/s), was calculated from the experimentally determined parameters,

$$\dot{m}_s = \rho_s f_v \dot{V}_{air} = \frac{\rho_s f_v \dot{m}_{air}}{\rho_{air}} x10^3 \tag{10}$$

where $\dot{V}_{air}$ is volumetric flow rate of air in the exhaust duct, $\dot{m}_{air}$ is volumetric flow rate of air in the exhaust duct, ρ_s is the density of soot, *fv* is the volume fraction of soot, $\dot{V}_{air}$ is the volumetric flow rate of air in the chimney, and ρ_{air} is the density of air at standard condition (1.206 kg/m^3).

Soot yield, defined as the ratio of mass of smoke emitted to the mass of fuel burned, was calculated from the experimentally determined parameters,

$$EIs = \frac{\dot{m}_s}{\dot{m}_b} \qquad (11)$$

where *EIs* is the soot yield, $\dot{m}_s$ is mass flow rate of soot in the chimney and $\dot{m}_b$ is the fuel mass burning rate. The notation '*EI'* chosen for yield is based on the terminology of an "emission index" used for yields of species emitted during combustion [Turns, 1996] and to avoid confusion with mass fraction commonly denoted by the letter *Y*. The commonly accepted value [Choi, 1995] of 1.74 g/cm3 was chosen for the density of soot.

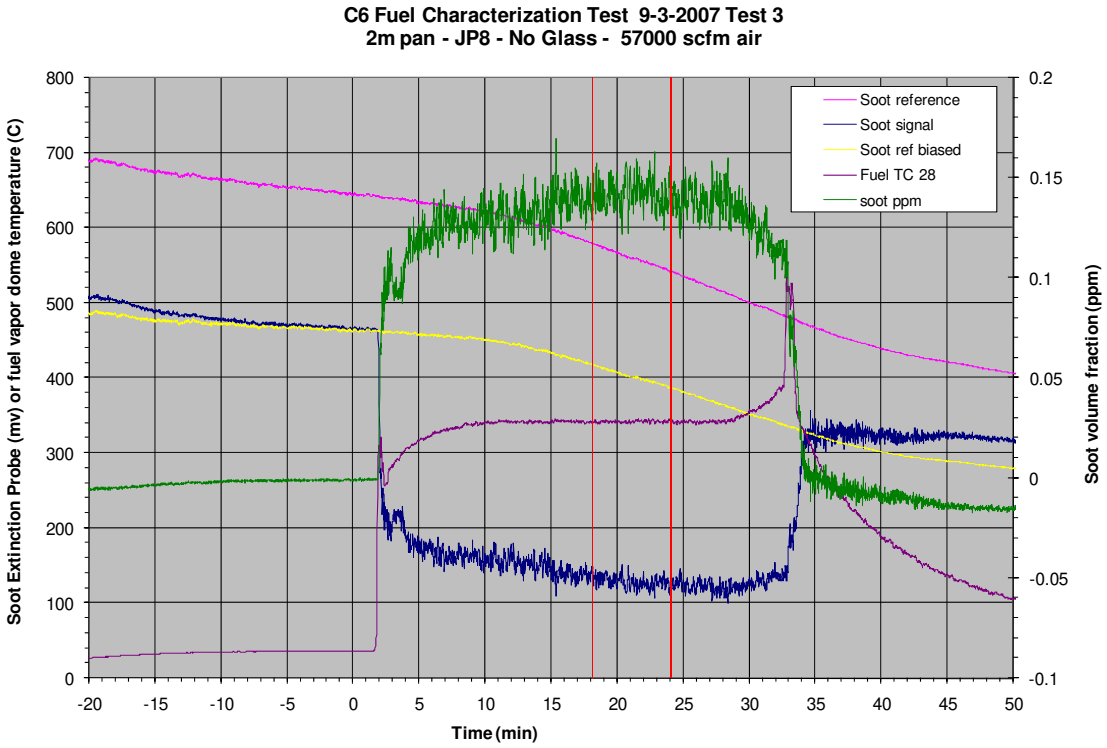

Figure 48 Soot extinction measurements in Test 24.

In Equation 11, the mass flow rate of soot is calculated with the assumption that the volume of soot and gas products is negligible compared to the air flow, which is a reasonable since it was estimated to be 3 orders of magnitude less than the air flow rate. Heating of the air flow was assumed negligible (the measured peak air temperatures at the CGA ranged from 60-120°C, depending on the fuel type).

Figure 49 presents the soot production as calculated using Equation 10 for Test #24, averaging ~7 g/s during the steady state burn duration. A wall heat flux measurement is also presented to provide reference to the fire duration.

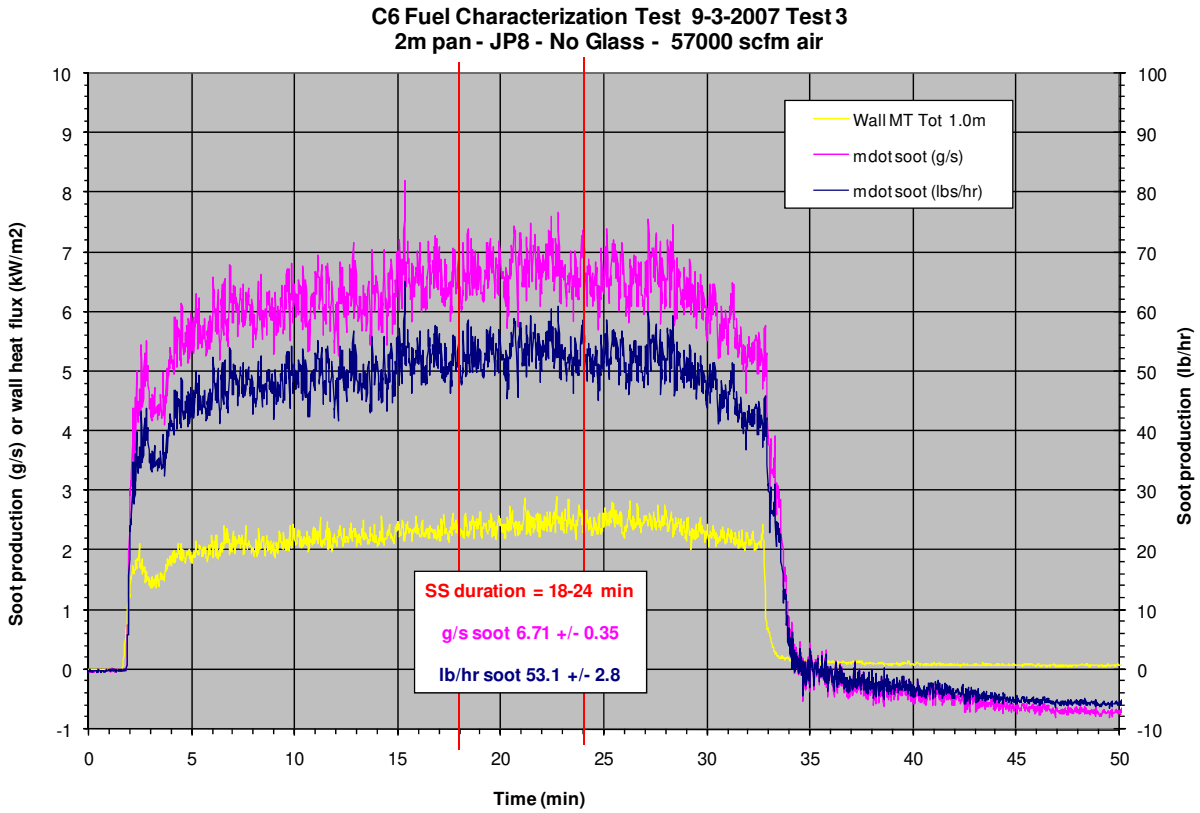

Figure 49 Soot production in Test #24.

Uncertainty – Soot Concentration

Jensen and Brown [2004] estimated the total uncertainty in soot yield fraction for a soot probe similar to the one used in the present test series to be ±26.0% of the measurement. The largest single contributor to the uncertainty was the uncertainty in the fuel regression rates, which was limited by low resolution in the regression measurements of ±0.5 mm/min (~20%) in their application. As previously discussed, uncertainty in fuel regression rates for the present test series will decrease as the averaging time increases and become small (~2%) over ten minute intervals. The total uncertainty in the present experiments based on an uncertainty of ±5% in the fuel regression rate but otherwise with the same uncertainties as reported by Jensen and Brown [2004], is ±17.4% of the measurement.

Temperatures in the exhaust duct are measured by a thermocouple located near the CGA and soot probe. At this location the flow can be assumed to be relatively uniform and to vary slowly compared to the time response of the thermocouple. Furthermore, the heat transfer is expected to be dominated by convection due to the large flow rate and the assumed uniformity in temperatures throughout the duct. The uncertainty of temperature measurements in the duct is assumed to be the same as the uncertainty of the coflow air temperature measurements.

5.3 Completeness of Combustion

In fires, the chemical heat release rate $Q_{chemical}$ should always be less than the heat release rate for complete combustion Q_{total}. The ratio of the two is defined as the combustion efficiency Ψch:

$$\Psi ch = \frac{Q_{chemical}}{Q_{total}} = \frac{\dot{m}_{ch}\,\Delta H_{ch}}{\dot{m}_{b}\,\Delta H_{mb}} \qquad (12)$$

The *chemical* heat release rate (subscript *ch*) has already been defined in Equations 7 and 8 and the total heat release rate defined in equation 3, with values tabulated in Table 11. All of the fuel average heat release rates and combustion efficiencies are tabulated in summary Table 14. Plots are provided in Figures 50 and 51.

Reasonable results are obtained when calculation Ψch based on oxygen consumption; however, values of ≥ 1 for Ψch based on carbon dioxide production indicate problems with the CO_2 measurement.

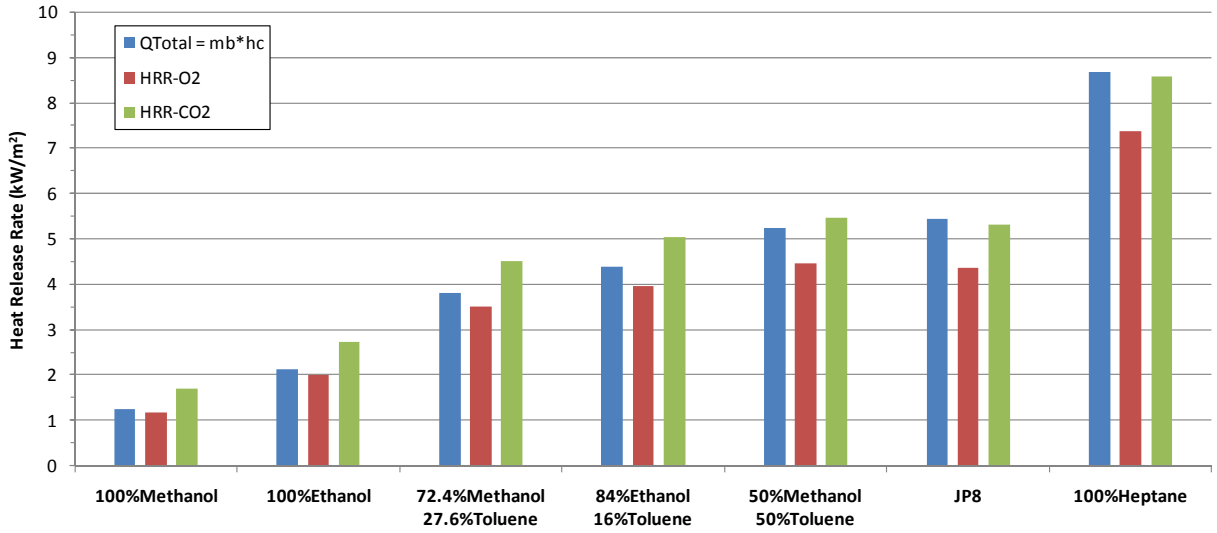

Figure 50 HRR comparisons: burn rate vs. combustion gas measurements.

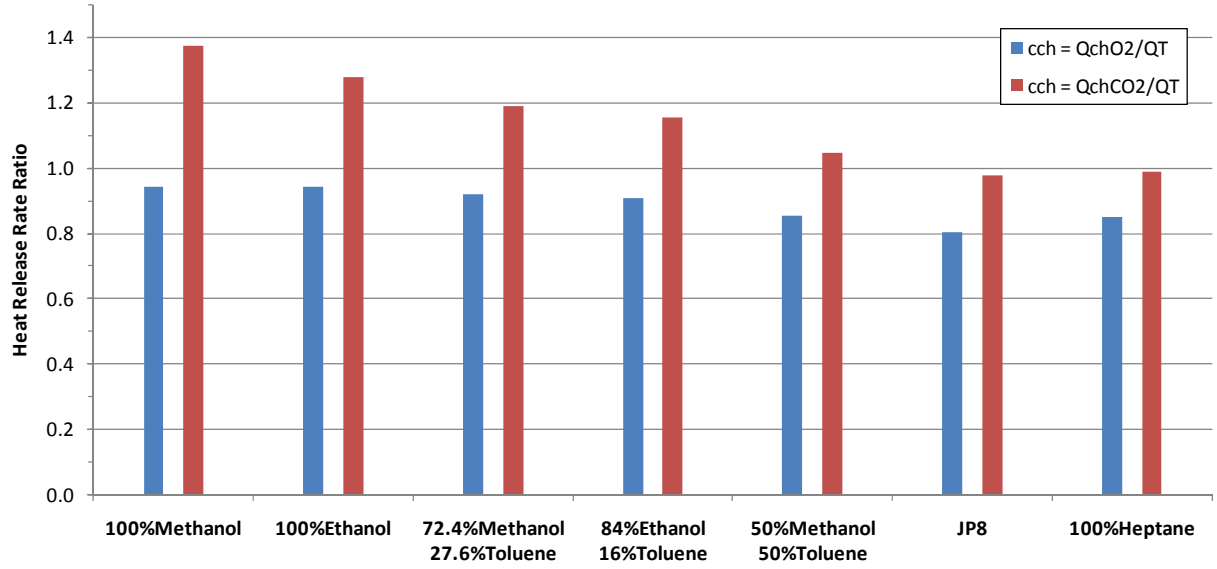

Figure 51 Ratio of chemical HRR to burn rate HRR.

5.4 Radiant Fraction Analyses

The radiative fraction χ_r, can be estimated knowing the radiative heat flux $\dot{q}''_{rad}$ at distance r (8.73 m from the center of the fire) and the heat release rate of the fuel ($HRR_{m_b} = \dot{m}_b \, \Delta h_c$)

$$\chi_r = \frac{4\pi r^2 \dot{q}''_{rad}}{\dot{m}_b \, \Delta h_c} \qquad (13)$$

The total heat flux thermopile gauge (Table 1 provides the data from each test) mounted near the FLAME wall was used for the measurement as the convective component (likely cooling) was assumed to be negligible. Radiative fractions for each test are tabulated in Table 2. Fuel average radiative fractions are tabulated in Table 13. Figure 52 presents the fuel average radiative fraction and compares that to the soot yield.

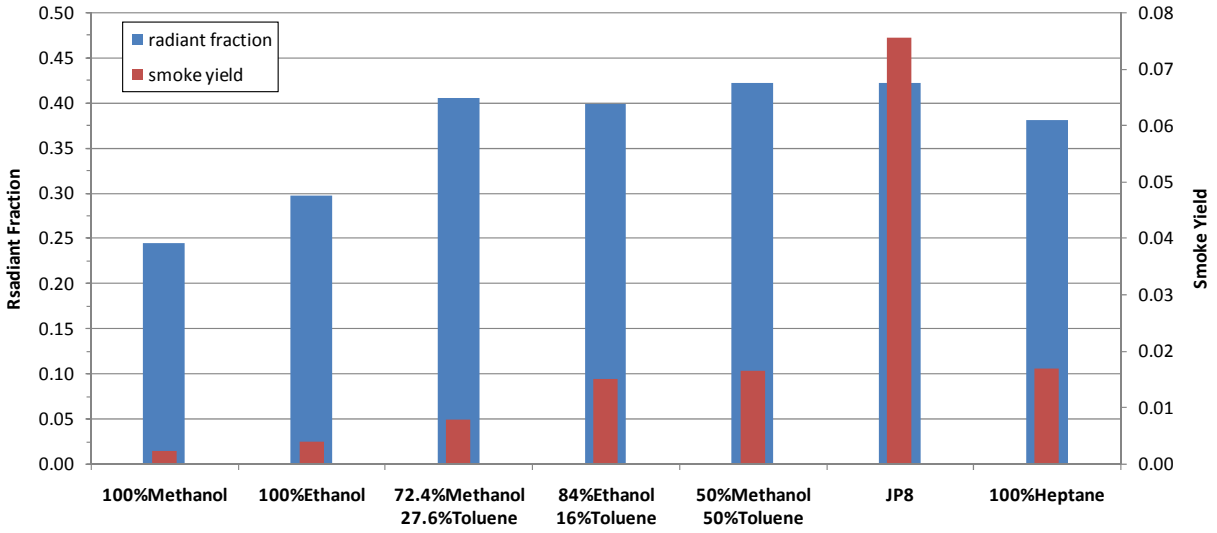

Figure 52 Fuel average radiant fraction compared to the soot yield.

Figure 53 compares the burn rate to the pan average heat flux. Note that all the plots are arranged for the data to be plotted in order of increasing total heat release rate (Equation 3), also plotted in Figure 53.

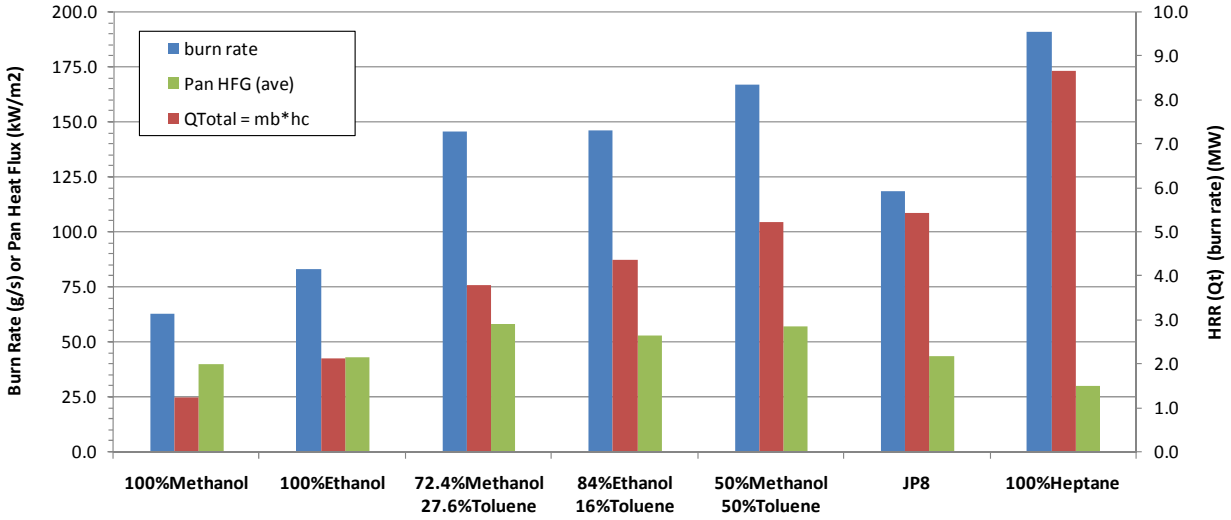

Figure 53 Burn rate compared to pan average heat flux.

5.5 Effect of Convection in the Bulk Liquid

Figures 54-60 plot the average temperature of each pan rake thermocouple versus its locations in the pan during the steady-state interval of each fire. The interface between the fuel vapor dome and the liquid pool occurs at the highest thermocouple on the rake measuring the boiling point and the "jump" to the next thermocouple measuring a significantly higher temperature.

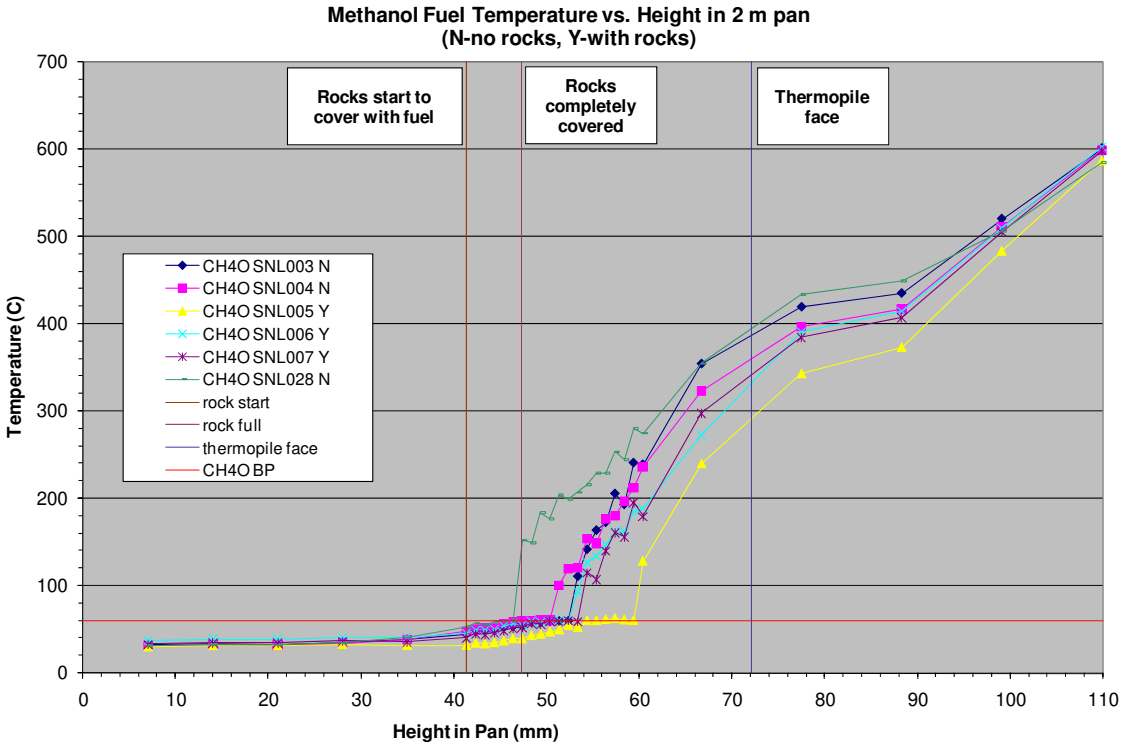

Figure 54 Location of liquid-vapor interface for methanol tests.

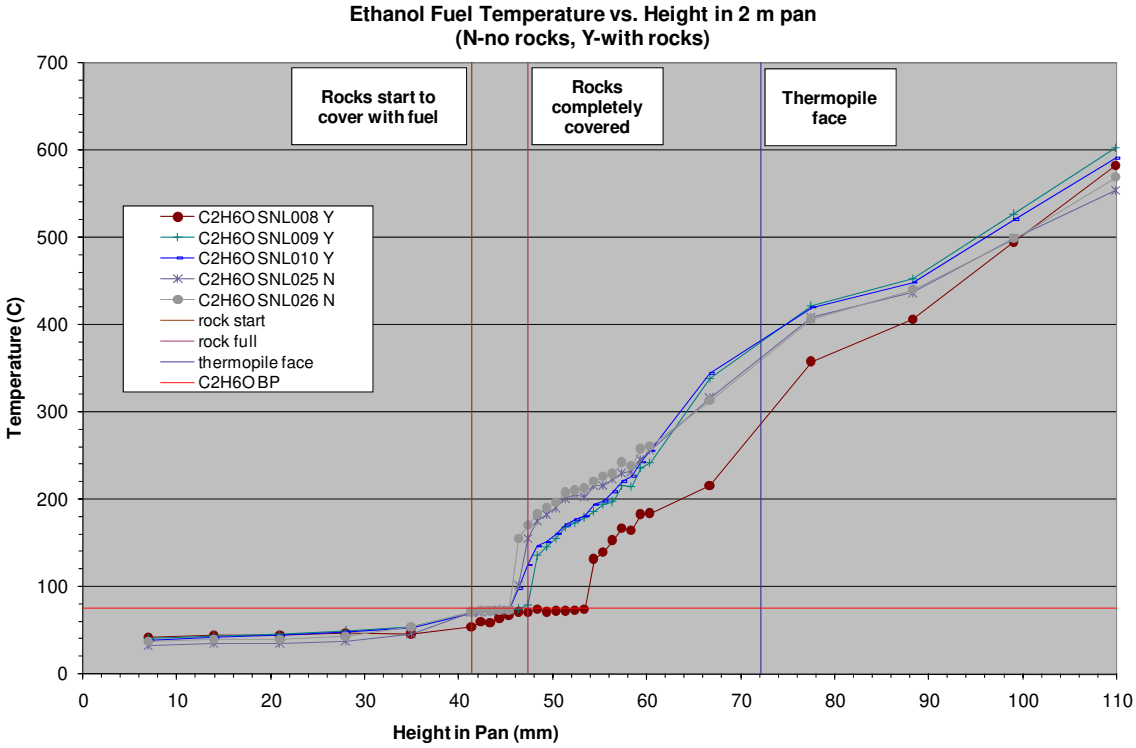

Figure 55 Location of liquid-vapor interface for ethanol tests.

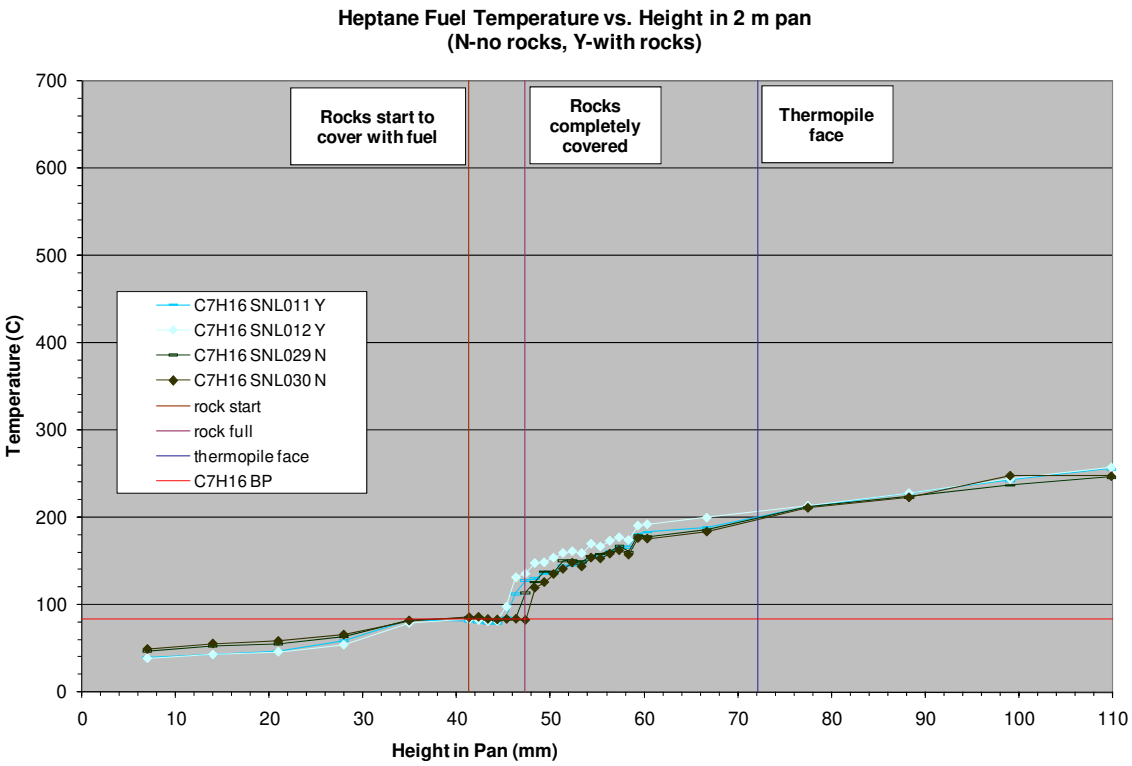

Figure 56 Location of liquid-vapor interface for heptane tests.

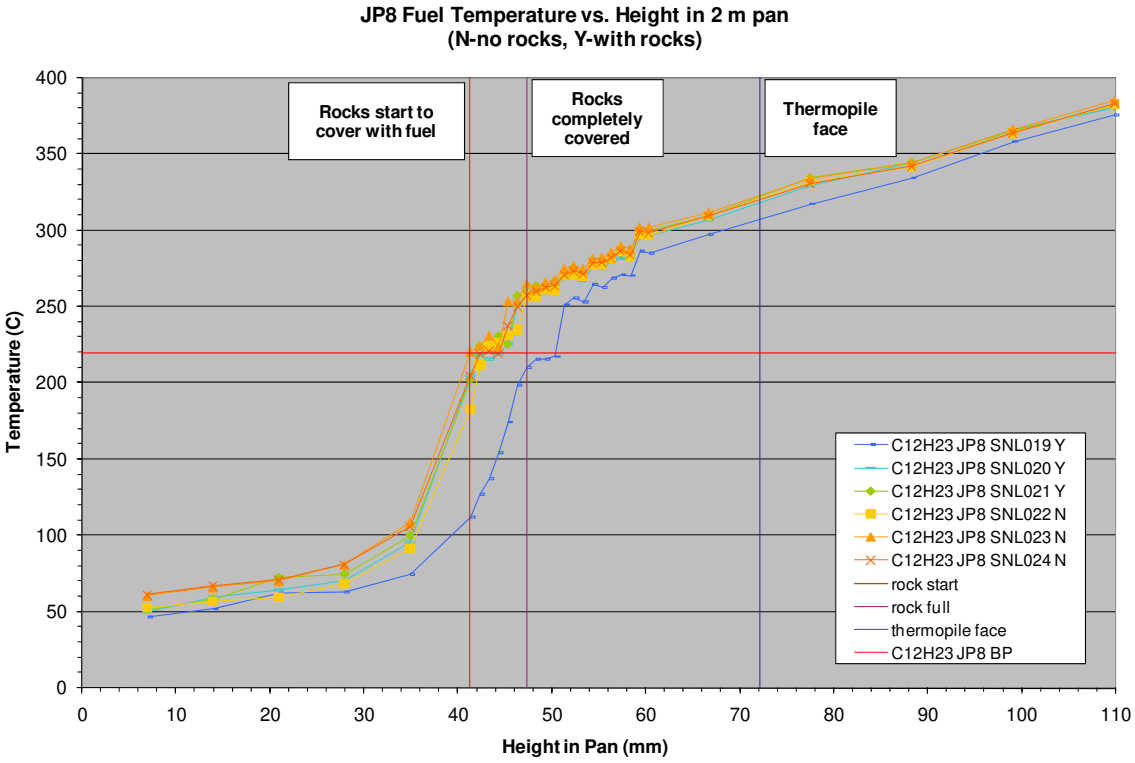

Figure 57 Location of liquid-vapor interface for JP8 tests.

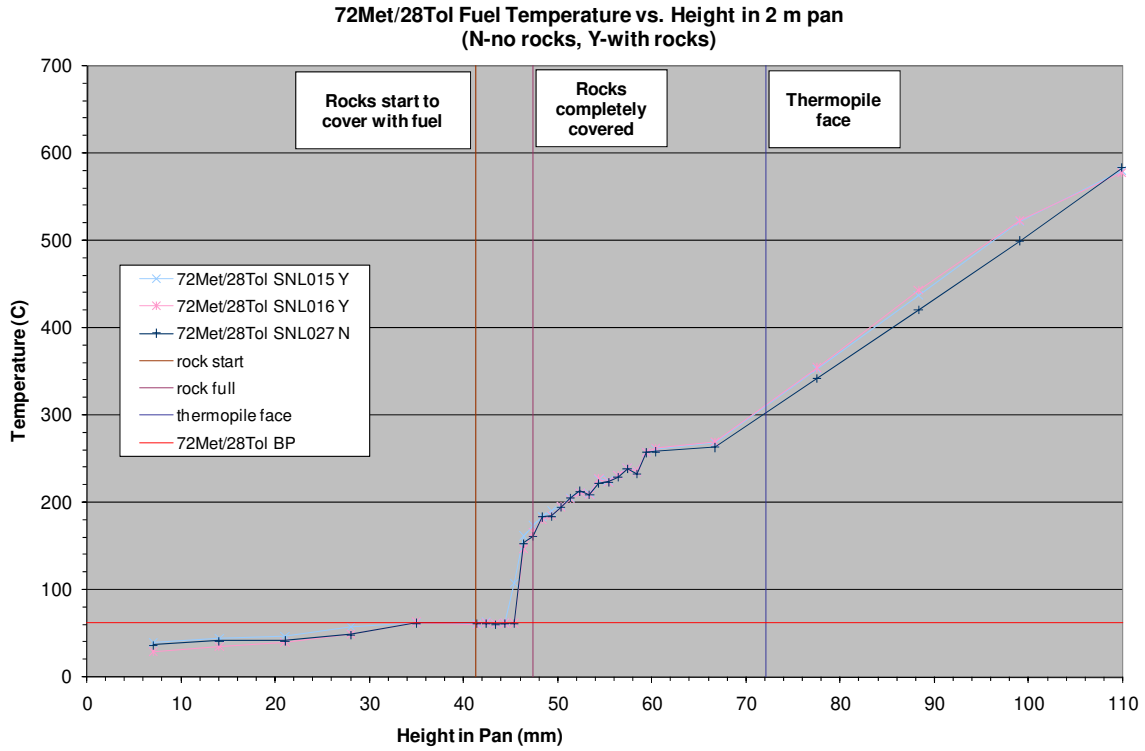

Figure 58 Location of liquid-vapor interface for 72/28 methanol/toluene tests.

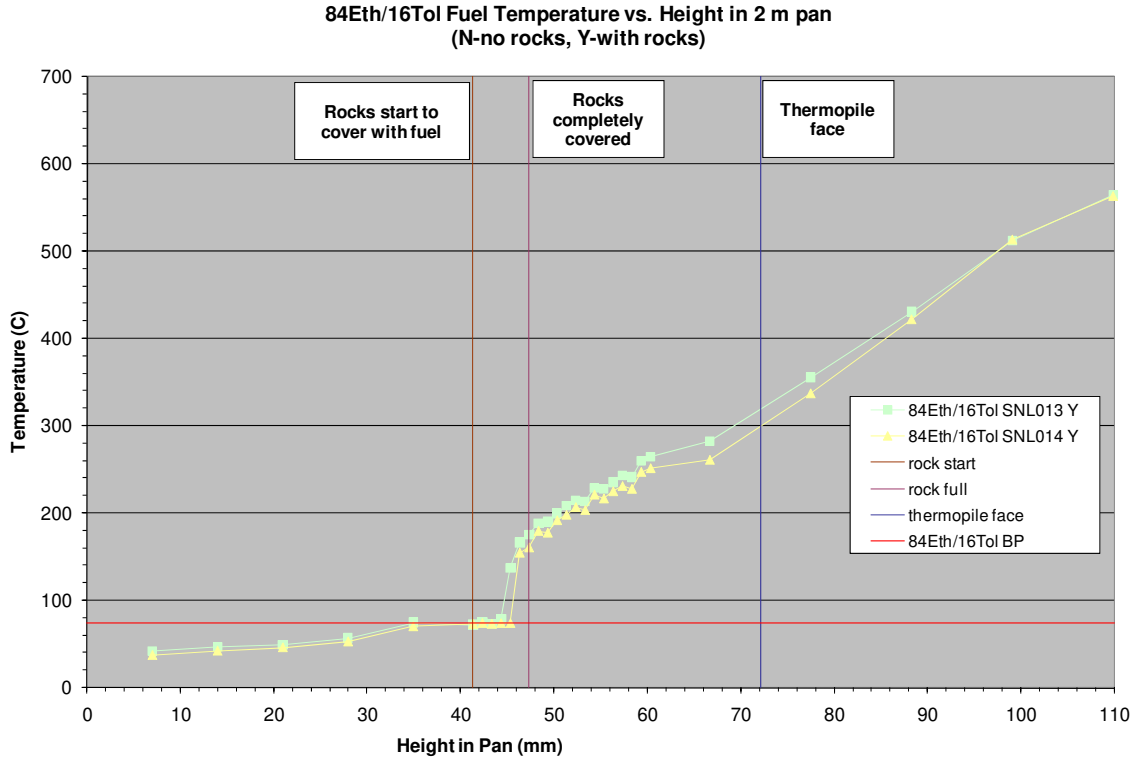

Figure 59 Location of liquid-vapor interface for 86/16 ethanol/toluene tests.

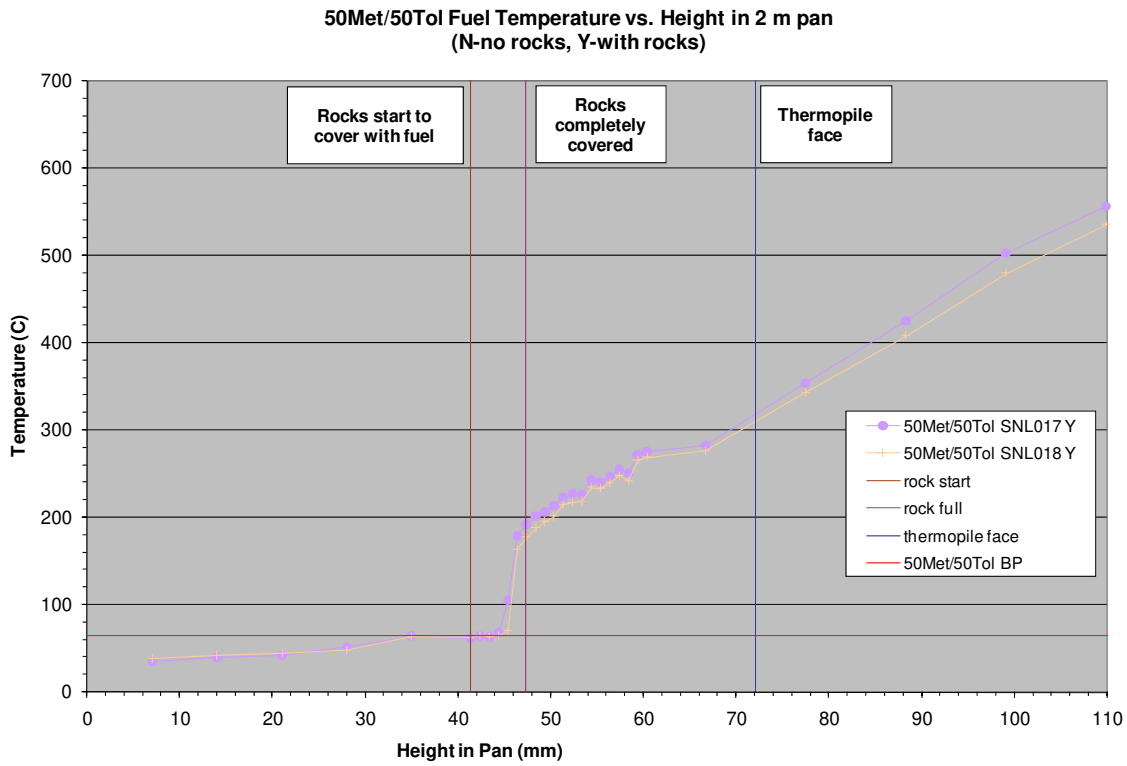

Figure 60 Location of liquid-vapor interface for 50/50 methanol/toluene tests.

The above figures show that the jump occurs either just above or below where the rocks are completely covered. Note that the measured boiling temperature is also indicated on each figure. Table 12 gives the burn rates for those tests with and without the glass rocks (average and one standard deviation). Convection does not appear to have a significant effect on the burn rate, as the data indicates the burn rates fall within the uncertainty error. Table 12 also shows the percent difference between the two cases ((with-without)/without) in addition to the measured boiling temperature.

Table 12 Effect of Convection In the Bulk Fluid

Fuel		m_b	m_b	m_b	T_{boil}
		g/s	g/s	%	C
		rocks	**no rocks**	**% diff to no rock case**	
100%Methanol	average	62.7	63.4	-1.1	61
	std. dev.	0.2	2.3		
100%Ethanol	average	83.8	82.7	1.3	75
	std. dev.	1.4	2.5		
72.4%Methanol 27.6%Toluene	average	146.6	144.8	1.2	62
	std. dev.	2.9	n/a		
84%Ethanol 16%Toluene	average	146.2	n/a	n/a	74
	std. dev.	0.3	n/a		
50%Methanol 50%Toluene	average	167.4	n/a	n/a	65
	std. dev.	1.0	n/a		
JP8	average	120.5	116.5	3.4	220
	std. dev.	5.7	4.0		
100%Heptane	average	193.3	185.1	4.4	84
	std. dev.	5.3	5.4		

Table 13 Fuel-Averaged BCs and Results Summary

Fuel		Patm (ABQ at t0)	Tatm (inlet air at t_0)	Tfuel (TC1-10 ave at t_0)	Twall (ave at t_0)	ABQ RH (at t_0)	Fan Flow	Pan HFG (ave)	Wall HFG (ave)	Burn Rate Loadcell	Soot
units		in. HG	C	C	C	%	scfm	kW/m^2	kW/m^2	g/s	g/s
100%Methanol	average	24.6	30	30	28	32	57262	40.0	0.3	63.1	0.1
	std. dev.	0.1	3	2	1	12	255	1.5	0.0	1.8	-
100%Ethanol	average	24.6	31	33	29	24	57435	43.3	0.7	83.4	0.3
	std. dev.	0.0	3	4	1	11	62	2.2	0.0	1.7	0.2
72.4%Methanol 27.6%Toluene	average	24.7	25	29	28	45	57480	58.6	1.6	146.0	1.1
	std. dev.	0.2	5	5	2	23	34	0.8	0.0	2.3	0.5
84%Ethanol 16%Toluene	average	24.6	29	34	29	31	57394	53.3	1.8	146.2	2.2
	std. dev.	0.1	5	1	1	11	30	0.1	0.1	0.3	0.3
50%Methanol 50%Toluene	average	24.8	27	34	28	43	57314	57.2	2.3	167.4	2.8
	std. dev.	0.1	2	4	0	5	90	2.6	0.1	1.0	0.2
JP8	average	24.7	27	37	28	34	57481	43.6	2.4	118.5	8.9
	std. dev.	0.1	2	4	1	10	163	2.9	0.1	4.9	1.7
100%Heptane	average	24.6	26	31	29	43	57587	30.1	3.5	191.2	3.3
	std. dev.	0.0	3	4	1	4	346	1.0	0.1	8.3	0.5

Table 14 Fuel-Averaged Compiled Analyses Summary

Fuel		m_b	Regression Rate	$Q_{Total} = m_b * h_c$	HRR-O2	HRR-CO2	$\chi_{ch} = Q_{chO2}/Q_T$	$\chi_{ch} = Q_{chCO2}/Q_T$	$\chi_r = 4\pi r^2 q''/m_b h_c$ (wall hfg)	Ψ_{smoke} (smoke yield)
units		g/s	g/m^{2}s	MW	MW	MW	-	-	-	g/g
100%Methanol	average	63.1	20.1	1.2	1.2	1.7	0.94	1.37	0.24	0.002
	std. dev.	1.8	0.6	0.0	0.0	0.0	0.03	0.04	0.01	-
100%Ethanol	average	83.4	26.5	2.1	2.0	2.7	0.94	1.28	0.30	0.004
	std. dev.	1.7	0.5	0.0	0.1	0.1	0.04	0.03	0.01	0.002
72.4%Methanol 27.6%Toluene	average	146.0	46.5	3.8	3.5	4.5	0.92	1.19	0.40	0.008
	std. dev.	2.3	0.7	0.1	0.1	0.1	0.02	0.01	0.00	0.003
84%Ethanol 16%Toluene	average	146.2	46.5	4.4	4.0	5.0	0.91	1.15	0.40	0.015
	std. dev.	0.3	0.1	0.0	0.0	0.1	0.01	0.01	0.01	0.002
50%Methanol 50%Toluene	average	167.4	53.3	5.2	4.5	5.5	0.85	1.05	0.42	0.016
	std. dev.	1.0	0.3	0.0	0.1	0.1	0.02	0.01	0.01	0.001
JP8	average	118.5	37.7	5.4	4.4	5.3	0.80	0.98	0.42	0.076
	std. dev.	4.9	1.6	0.2	0.2	0.1	0.02	0.02	0.01	0.017
100%Heptane	average	191.2	60.8	8.7	7.4	8.6	0.85	0.99	0.38	0.017
	std. dev.	8.3	2.6	0.4	0.4	0.4	0.01	0.01	0.01	0.002

6. CONCLUSIONS

Validation quality data sets are the standard by which modeling and simulation uncertainty can be quantified. An extensive fire test suite of various fuels yielding key fire parameters (burn rate, heat flux to fuel pool surface, etc.) at large scale (2 m diameter) has been performed with well-controlled and well-characterized boundary conditions to produce archival datasets. A negligible data loss rate (over 30 tests) in notoriously harsh environments was achieved. These datasets include the most comprehensive experimental uncertainty of large-scale fires to date. Emissivity of the object surface, determined pretest to be the source of the largest experimental uncertainty, was very well characterized.

The relationship between burn rate, total heat release rate, and fuel regression rate was determined for a wide variety of fuels, specifically varying the sooting propensity and the heat of vaporization.

Thermal radiation spectra from 1.3 - 4.8 μm were measured within the flame zone of 2m pool fires from the fuel surface to a height of 1m and the dominant emission was determined to be from soot, CO_2, and H_2O. Intensity of thermal radiation incident upon the fuel surface for sooting fuels was impacted by absorption due to cold soot, CO2, and H2O and fuel vapor (absorption by the C-H bond stretching). Transmission of thermal radiation through liquid fuel layers revealed a significant fraction is absorbed within the first 3 mm (75% for JP-8 and 90% for ethanol). Heptane and JP-8 were quite transparent at wavelengths less that 1.6 μm and from 1.85 - 2.1 μm, where a significant amount of incident thermal radiation exists

This data set is the 7th data set funded by Campaign 6 and ESRF in support of fire model validation. The published datasets include:

- Study of a Turbulent Buoyant Helium Plume (O'Hern et al., 2005)
- Study of a 1Meter Diameter Methane Fire (Tieszen et al., 2002)
- Study of Soot and Species in a JP8 Fire (Jensen et al., 2007)
- Study of Mixed Convection from a Horizontal Cylinder in Crossflow (Laskowskia et al., 2007)
- Study of Radiation/Convection Partitioning (Blanchat et al., 2009)
- Study of Heat Flux to Objects (Blanchat et al., 2010)

REFERENCES

Babrauskas, V., "Estimating large pool fire burning rates," *Fire Technology* 19:251-261, 1983.

Beaulieu, P., FM Global Research, Informal communication to Tom Blanchat, Sandia National Laboratories, May 2005.

Blanchat, T., O'Hern, T., Kearney, S., Ricks, A., and Jernigan, D., "Validation Experiments to Determine Radiation Partitioning of Heat Flux to an Object in a Fully Turbulent Fire," Proceedings of the Combustion Institute, 32, 2, 2511-2518, 2009.

Blanchat, T. K., and Jernigan, D., "Temperature and Heat Flux Datasets of a Complex Object in a Fire Plume for the Validation of Fire and Thermal Response Codes," SAND2009-6944 Sandia National Laboratories, Albuquerque, NM (in printing).

Brown, A. L., Gill, W., and Lopez, C., "Predictive evolution of fuel from a liquid pool fire: phenomenology identification and ranking exercise," paper IMECE2006-15157, *Proceedings of International Mechanical Engineering Congress and Exposition*, November 5-10, 2006, Chicago, IL

Chatris, J. M., Quintely, J., Folch, J., Planas, E., Arnaldos, J., and Casal, J., "Experimental study of burning rate in hydrocarbon pool fires," *Combust. Flame* 126:1373-1383, 2001.

Choi, M.Y., Mulholland, G.W., Hamins, A., and Kashiwagi, T., *Combustion and Flame*, Vol. 102, pp. 161-169, 1995.

Coleman and Steele. *Experimentation and Uncertainty Analysis for Engineers*, Wiley & Sons, 1999.

Hamins, A.; Fischer, S. J.; Kashiwagi, T.; Klassen, M. E.; Gore, J. P., "Heat Feedback to the Fuel Surface in Pool Fires," Combustion Science and Technology, Vol. 97, No. 1-3, 37-62, 1994.

Hottel, H. C., "Certain laws governing diffusive burning of liquids," *Fire Research Abstracts Reviews* 1:41-43, 1959.

Jensen, K. A., and Brown, A. L., "Measurement of soot yield from JP-8 pool fires using light extinction," *INTERFLAM04*, Edinburgh, Scotland, July 5-7, 2004.

Jensen, K.A., Suo-Anttila, and Blevins, L.G., "Measurement of Soot Morphology, Chemistry, and Optical Properties in the Visible and Near-Infrared Spectrum in the Flame Zone and Overfire Region of Large JP-8 Pool Fires," *Combustion Science and Technology*, Volume 179, Issue 12, December 2007, pages 2453 – 2487.

Kearney, S. P., "Temporally resolved radiation spectra from a sooting, turbulent pool fire," *Proceedings of International Mechanical Engineering Congress and Exposition*, November 11-16, 2001, New York, NY.

Koseki, H., "Combustion properties of large liquid pool fires," *Fire Technology* 25(3):241-251, 1989.

Koseki, H., and Mulholland, G. W., "The effect of diameter on the burning of crude oil pool fires," *Fire Technology* 27(1):54-65, 1991.

Koseki, H., and Iwata, Y., "Tomakomai large scale crude oil fire experiments," *Fire Technology* 36(1):24-38, 2000.

Laskowski, G.M., Kearney, S.P., Evan, G., and Greif, R., "Mixed Convection Heat Transfer To and From a Horizontal Cylinder in Cross-flow with Heating from Below," International Journal of Heat and Fluid Flow, Volume 28, Issue 3, June 2007, Pages 454-468, 2007.

Modest, M.F., Radiative Heat Transfer, McGraw-Hill, New York, 1993.

Muñoz, M., Arnaldos, J., Casal, J., and Planas, E., "Analysis of the geometric and radiative characteristics of hydrocarbon pool fires," *Combust. Flame* 139:263-277, 2004.

Nakos, J. T., "Uncertainty analysis of thermocouple measurements used in normal and abnormal thermal environment experiments at Sandia's Radiant Heat facility and Lurance Canyon burn site," SAND2004-1023, April 2004, Sandia National Laboratories, Albuquerque, NM.

Nakos, J. T., "Uncertainty analysis of steady state incident heat flux measurements in hydrocarbon fuel fires," SAND2005-7144, December 2005, Sandia National Laboratories, Albuquerque, NM.

Novozhilov, V., and Koseki, H., "CFD prediction of pool fire burning rates and flame feedback," *Combust. Sci. and Tech.* 176:1283-1307, 2004.

O'Hern, T. J., Weckman, E. J., Gerhart, A. L., Tieszen, S. R., and Schefer, R. W., "Experimental Study of a Turbulent Buoyant Helium Plume", Journal of Fluid Mechanics, 544, pp 143-171, 2005.

Orloff, L., and de Ris, J., "Froude modeling of pool fires," *Proceedings of the 19th Symposium (International) on Combustion*, 1982, pp. 885 – 895.

Pouchert, C. J., *The Aldrich library of FT-IR spectra*, Volumes 1 through 3, Aldrich Chemical Company, Milwaukee, WI, 1985.

Prasad, K., Li, C., Kailasanath, K., Ndubizu, C., Ananth, R., and Tatem, P. A., "Numerical modeling of methanol liquid pool fires," *Combust. Theory Modeling* 3:743-768 (1999).

Ricks, A. J., "Characterization of air flow in New FLAME / Radiant Heat," Sandia internal memo to T. Blanchat, March 20, 2006.

Romero, V. J., Sherman, M. P., Johnson, J. D., Dempsey, J. F., Edwards, L. R., Chen, K. C., Baron, R. V., and King, C. F., "Development and validation of a component failure model,"

paper AIAA2005-2141, *46th AIAA/ASME/AHS/ASC Structures, Structural Dynamics, and Materials Conference*, April 18-21, 2005, Austin, TX.

SFPE handbook of Fire Protection Engineering, 3rd Edition, 2002, National Fire Protection Association

Siegel, R., and Howell, J.R., *Thermal Radiation Heat Transfer*, 3rd Edition, Hemisphere Publishing Corporation, Washington, 1992.

Suo-Anttila, J. M., Blanchat, T. K., Ricks, A. J., and Brown, A. L., "Characterization of Thermal Radiation Spectra in 2m Pool Fires," *Proceedings of the 32nd Symposium (International) on Combustion*, Montreal, Canada, August 3-8, 2008.

Turns, S.R., *An Introduction to Combustion*, McGraw-Hill, New York, p. 475, 1996.

Tieszen, S.R., O'Hern, T.J., Schefer, R.O., Weckman, E.J., and Blanchat, T.K., "Experimental Study of the Flow Field In and Around a One Meter Diameter Methane Fire," Combustion and Flame, 129:378-391, 2002

DISTRIBUTION

External

1 John L. de Ris
FM Global Research
1151 Boston-Providence Hwy.
Norwood, MA 02062

1 Benjamin Ditch
FM Global Research
1151 Boston-Providence Hwy.
Norwood, MA 02062

Internal

1	MS0384	D.B. Dimos	1500
1	MS1139	D.L. Miller	1530
1	MS1135	R.D. Watkins	1532
1	MS0836	S.R. Tiezsen	1532
3	MS1135	T.K. Blanchat	1532
1	MS1135	A.J. Ricks	1532
1	MS0821	A. Luketa	1532
1	MS0826	W. Gill	1532
1	MS1135	J.T. Nakos	1532
1	MS1135	J.M. Suo-Anttila	1532
1	MS1135	A.L. Brown	1532
1	MS1135	D.A. Jernigan	1532
1	MS0828	V.J. Romero	1544
1	MS0828	A.R. Black	1544
1	MS0826	S.P. Kearney	1512
1	MS0836	S.P. Domino	1541
1	MS9001	C. Moen	8005
1	MS0899	Technical Library	9536 (electronic copy)

Sandia National Laboratories